RIT

Rochester Institute of Technology
Golisano Institute for Sustainability
190 Lomb Memorial Drive
Rochester, NY 14623
585-475-4696
http://www.rit.edu/gis/

October 28, 2022

G. William Nickerson
ONR Program Officer CBM+
PEO USC S&T HM&E/CBM+ Technical Lead
Office of Naval Research
875 North Randolph Street
Arlington, VA 22203-1995

RE: N00014-18-1-2339 Final Report

Dear Mr. Nickerson:

The Golisano Institute for Sustainability at Rochester Institute of Technology is pleased to submit the Final Technical Report with SF298 for the "Impacts of Technology Advancements on CBM+" project under award number N00014-18-1-2339.

If you have any technical questions regarding this report, the Principal Investigator, Dr. Michael Thurston, can be reached at (585) 475-6550 or via email at mgtasp@rit.edu. For administrative or contracting inquiries, I can be reached at (585) 475-4325 or kxkasp@rit.edu

Sincerely,

Kathleen Kosciolek

Kathleen Kosciolek
Assistant Director for Program Administration

cc: Administrative Office - ONR REG BOSTON (transmittal letter only)
Defense Technical Information Center
Naval Research Laboratory
File

Enclosures: RIT N00014-18-1-2339 Final Technical Report with SF298

RIT | Golisano Institute for Sustainability

Impacts of Technology Advancement on CBM+

Final Report

28 October 2022

This research was conducted under Office of Naval Research Grant N00014-18-1-2339.

Report Generated by:

Golisano Institute for Sustainability
Rochester Institute of Technology
190 Lomb Memorial Drive
Rochester, NY 14623
(585) 475-5101

Table of Contents

1 Introduction

Fleet maintenance is a priority for all military, industrial, and commercial equipment and vehicles. Until the late 1960's, the dominant maintenance philosophies were reactive maintenance (i.e. fix upon failure), or scheduled maintenance for critical systems. The aerospace industry moved toward condition based maintenance (CBM) after recognizing that scheduled maintenance was leading to unwarranted early component replacement and sometimes even damaging inspection processes. Early CBM practices were typically based around physical inspections of components to look for wear or cracking. However, CBM has evolved to include digital data collection, computerized data analysis, and off-board communications, leading to real-time condition monitoring.

The U.S. Department of Defense (DoD) has recognized the opportunity associated with increased deployment of CBM, driven in part by increasing costs of sustainment and the associated goal to reduce operations and maintenance staff levels. DoD policy now requires that Condition Based Maintenance Plus (CBM+) be implemented wherever cost effective for maintenance and logistics support of service weapon systems[1]. The CBM+ Guidebook[2] describes the relationship of CBM+ to the total Life-Cycle System Management of an asset. Throughout this report, CBM and CBM+ may be used interchangeably.

The research performed under this project has direct implications to the maintenance strategies required by the DoD directive on CBM+, as well as the total life-cycle management of DoD assets. The research work was broken down into three areas: 1) Vehicle CBM Research, 2) Gear Prognostics Research, and 3) Additive Manufacturing Research. Vehicle CBM research focused on the impacts of new technologies on CBM+ capabilities for fleets of vehicles. Gear prognostic research focused on the fusion of vibration and oil quality monitoring data to enhance the detection horizon of existing gear prognostics. The additive manufacturing research program focused on closing the knowledge gaps relating to additive repair material properties and advancing the state of technology to facilitate the adoption of additive manufacturing repair processes.

2 Vehicle CBM Research

2.1 Research Goals and Objectives

The Vehicle CBM subproject focused on the impacts that advancements in technology will have on the future implementations of CBM+. The goal of this subproject was to provide a forward looking projection of new CBM capabilities, with three major objectives. First, the project was aimed at researching CBM solutions that are impacted by technology changes, with particular focus on cases studies of technologies that may reach adoption in CBM over the next few years. Second, the project was to perform demonstrations of the technologies selected for case studies. Finally, research was conducted on how to evaluate the Return on Investment (ROI) of new CBM technologies.

2.1.1 Selecting CBM Solutions

RIT researched specific CBM system solutions that are likely to be impacted by technology change (e.g. advances in sensors, processing hardware, model and analysis structures, and architectural options). Additional consideration was given to technologies that will have a near term impact on CBM+. A finite number of technologies was selected for case studies. Case studies focused on capability development and evaluation of the technologies in a selected application.

2.1.2 Case Study Demonstrations

RIT selected a set of case studies that have a near term impact on CBM+. These cases studies evaluate the technology maturity, the enhanced capability provided by the technology, and discuss where the technology may have the greatest impacts.

2.1.3 Return on Investment of New CBM+ Technologies

RIT developed a methodology for evaluating the ROI of new technologies based on the enhanced capabilities that they provide. Utilizing knowledge gleaned from the case studies, the ROI methodology was evaluated. Included in the evaluation, is a discussion of cost factors that may be difficult to estimate, but should be considered when evaluating the impact of the technologies.

2.2 Research Accomplishments

2.2.1 CBM Technology Selection

Condition monitoring was initially applied to the aerospace industry, because the cost could be justified based on the value of the asset, crew, and cargo (material and lives). For example, an Airbus A220-300 has a list price of $91.5M[3], whereas a ground vehicle, such as a Kenworth T680 sleeper truck, has a price of around $210,000[4]. So, the price of the Airbus is 435x the price of the truck. Additionally, assuming failures are not monitored, the risk of complete loss of the asset due to failure during operation is higher in the airborne platform. Thus, it is easy to justify expensive sensors for an aircraft - specific examples are discussed in the Return on Investment section.

The initial focus of Condition Based Monitoring solutions for this project focused on the application of CBM to ground vehicles.

Typical monitoring of ground platforms is performed with lower cost, commodity pressure, temperature and digital pulse counters. Research studies have been done on vibration monitoring for various engine and transmission faults, but the application to mobile platforms is generally considered cost prohibitive. Typical piezo sensors require a charge amplifier, in addition to the data acquisitions system. For similar reasons, acoustic emissions monitoring has been utilized in research but not generally adopted on mobile platforms. Recent advances in micro-electromechanical systems (MEMS) sensor technology have potentially lowered the cost threshold for vibration and acoustic sensing by removing the charge amplifier and providing a standard voltage output, which requires a less expensive data acquisition system.

Furthermore, vibration and acoustic sensing in ground vehicles require high frequency data acquisition. Typical Central Processing Unit (CPU) based systems may struggle to keep up with a real-time processing requirements of high frequency data. Graphical Processing Units (GPUs), however, are becoming the gold standard of machine learning and data mining. For example, mobile GPUs, such as the NVidia Jetson series[5], have been utilized in autonomous vehicles[6][7], and Peeters, et al. examined the use of the Jetson TX2 GPU for vibration monitoring of wind turbines utilizing 10 second intermittently collected data samples[8][9]. An evaluation of real-time processing of continuous vibration data is of specific interest to ground assets as they experience rapidly changing conditions. This project explored several monitoring technologies as potential solutions for ground vehicle CBM application.

2.2.1.1 Low Cost MEMS Accelerometers

The most commonly used accelerometers for monitoring modern machinery are piezoelectric sensors. For the purpose of vehicle monitoring, specifically engine or transmission monitoring, the sensors must

be capable of withstanding engine temperatures of up to 250° Fahrenheit (121° Celsius) , capable of measuring a minimum of ± 50g, and measuring up to 10 kHz with a low noise density.

MEMS accelerometers are miniscule and quite affordable. However, initial MEMS accelerometers were limited in their bandwidth, noise performance, and measurement range. In general, high measurement range sensors typically suffered from poor bandwidth and noise performance. Low noise sensors historically had limited bandwidth and low measurement ranges. These sensors gained popularity in applications such as impact detection (automotive), tilt and motion detection (handheld electronics), but still struggled with the requirements of a vibration monitoring solution for condition assessment. Gradually, manufacturers are improving performance of MEMS sensors to remove these shortcomings.

The Analog Devices ADXL1002 is a low cost, low noise, high frequency accelerometer that has the potential for condition based monitoring applications. The sensor is capable of measuring ±50 with a noise density of 25 µg/√Hz. For comparison purposes, the ADXL1002 (shown in Figure 1) is compared to a PCB 603C01 ICP accelerometer (shown in Figure 2) below (Table 1).

Table 1. Comparison of Two MEMS Accelerometers

	Analog Devices ADXL1002	PCB 603C01
Sensitivity (mV/g)	40	100
Measurement Range (g)	±50	±50
Frequency Range (Hz)	C-11,000	0.5-10,000
Resonant Frequency (kHz)	21	25
Broadband Resolution (µg)		350
Non-Linearity (%)	±0.1	±1
Transverse Sensitivity (%)	±1	≤7
Overload Limit (g peak)	10,000	5,000
Temperature Range (°C)	-40 to 125	-54 to 121
Current (mA)	1 to 1.15	2 to 20
Spectral Noise @ 10 Hz (µg/√Hz)	25	8
Spectral Noise @ 100 Hz (µg/√Hz)	25	5
Spectral Noise @ 1 kHz (µg/√Hz)	25	4

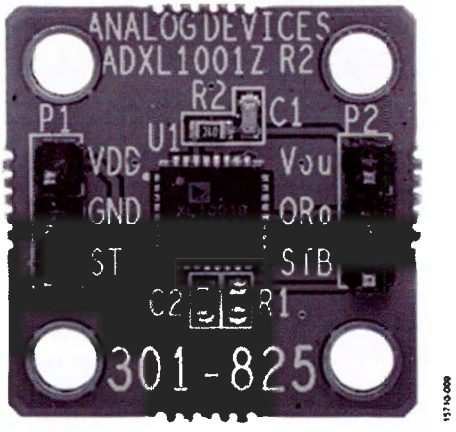

Figure 1 - Analog Devices ADXL1002 Evaluation Board

Figure 2 – PCB 603C01 Accelerometer

The spectral noise is still slightly higher than the PCB accelerometer. However, if the MEMS accelerometer may be proven effective for CBM purposes, there is a significant cost savings over traditional piezo accelerometers. Traditional piezo devices require charge amplifiers, which increase the cost of each vibration channel. However, MEMS accelerometers are low impedance devices that need a simple power supply and analog data acquisition hardware. The cost savings for a single accelerometer application can be as much as 50% and the savings only increases as the number of sensors increases, because the data acquisition and power supply hardware typically provide capability for more than one sensor.

2.2.1.2 Low Cost MEMS Microphones

Microphones have been demonstrated for various engine monitoring techniques[10]–[12]. Similar to accelerometers, MEMS microphones have the same benefits of decreased cost per channel being collected and simplicity of integration and monitoring. A comparison of a laboratory grade, free-field microphone (shown in Figure 3) and a MEMS omnidirectional microphone (shown in Figure 4) is provided below in Table 2. Similar to accelerometers, the effectiveness of MEMS microphones for CBM needs to be demonstrated.

Table 2. Comparison of Two MEMS Microphones

	TDK Invensense ICS-40618	PCB 130A23
Frequency Response (Hz)	50 to 20,000	20 to 20,000
Sensitivity (mV/Pa)	12.59	14
Dynamic Range (dB)	140	150
Dynamic Range, 3% distortion limit (dB)	132	>143
Temperature Range (°C)	-40 to 85	-10 to 50
Temperature effect on output, in range (dB)	N/A	<0.7

Figure 3 - TDK Invensense EV_ICS-40618 Evaluation Board

Figure 4 – PCB 130A23 Electret Microphone

Similar to accelerometers, the cost savings of MEMS sensors is directly related to the hardware costs. The savings are similar, but the lab grade microphones actually cost more than accelerometers, thus the savings start closer to 60% for a single sensor and, again, increases as more sensors are added.

2.2.1.3 Low Cost Mobile Graphical Processing Units

Machine learning has made significant strides since the acoption of GPUs for deep learning in the late 2000's. Initial GPU computing adapted computing problems by reformulating them in terms of graphical primitives. By 2007, Nvidia released their CUDA-enabled GPUs, which allow for ease of access to the GPU for general purpose processing. In 2008, Microsoft followed with their DirectCompute API for utilizing general purpose GPUs, followed shortly thereafter by OpenCL from the Khronos Group. The parallelization of processing has a significant impact on deep learning, which has been exploited through deep learning frameworks like TensorFlow or PyTorch. These advancements have allowed significant strides to be made in the development of machine learning models for CBM.

Until the mid-2010's, the majority of deep learning with GPUs was being done with traditional computers or servers equipped with GPU cards. However, with the advent of System on Chip (SoC) processors with integrated GPUs that are capable of breaking the 1 teraFLOP barrier, mobile platforms now have significant computation power to perform computing at the edge. Nvidia has been leading the way with their Jetson family of portable GPUs designed for efficiency and edge computing. The first Jetson development kit, the Jetson TK1, was released in 2014 with new members of the Jetson family being added regularly with major performance improvements. Artificial Intelligence (AI) performance is measured in floating point operations per second (FLOPS) The lowest cost version of the Jetson, the Nano, has a stated performance of 472 gigaFLOPS (10^9) for the 128 CUDA cores. The highest end Jetson AGX Orin 64GB is capable of performing approximately 5.3 teraFLOPS (10^{12}) [5], [13].

Current applications of the Jetson SoC hardware have been used in tablets, phones, and AI-powered self-driving vehicles, including their Nvidia Drive Platform[6]. The mobile GPUs enable processing of large quantities of sensor data, including video processing to identify objects, calculating optimal paths, and guiding the vehicle to its destination. The next logical application of mobile GPUs is for processing large quantities of CBM data at the edge.

Traditionally, CBM systems have employed an onboard computer that simply captures data from the sensors, does limited processing on the Central Processing Unit (CPU) to provide status to the crew, and stores the data to be transferred to a backend for further analysis. Systems like the eDAQ-lite are being used by Army Materiel Systems Analysis Activity (AMSAA) to collect CBM data from both the vehicle databus and added sensors. However, some platforms, such as helicopters, utilize vibration analysis for detecting failures in flight critical systems, i.e. gearboxes. Vibration signals consist of high frequency data that cannot be reported over a wireless communication system. Instead, these systems utilize on-board

feature extraction of condition indicators. Gearboxes are inherently noisy; therefore, these condition indicators typically consist of Time Synchronous Average (TSA), residual and difference signals[14], [15]. These indicators are then sent off-platform and analyzed by subject matter experts to determine if a problem exists.

With the advancement of machine learning, autoencoders have been shown to be extremely adept at learning signal characteristics and identifying changes in the signal data from those characteristics. Significant research has been performed in applying autoencoders to rotating machinery, i.e. motors and gearboxes[16]–[24]. As mobile SoC GPU computers have become available, limited research has been done on utilizing them in a CBM environment. Mittal provides a good overview of the capabilities of the Nvidia Jetson relative to video or image processing[25].

Lin et al. utilize a Jetson TX2 for performing anomaly detection on machine tools[26]. Specifically, the paper investigated the performance of a Jetson GPU vs. traditional CPU computers for running Recurrent Neural Network (RNN) inference models that were trained on a server. In this scenario, RNNs cannot be computed in parallel and therefore do not provide a performance improvement over CPUs. However, the results showed that the model results can still provide reasonable response time for real-time monitoring of machine tools.

Alternatively, Verstraeten et al. attempt to balance processing between the edge and cloud while performing analysis of vibration signals from wind turbines[9]. Once again, models are trained in the cloud; however, a Jetson TX2 is utilized for edge processing. Sensor data is processed through a series of pipelines (speed compensation, Cepstrum filtering, additional filtering, and Cyclic spectral coherence) prior to modeling with Bayesian ridge regression. The trained models are run on the Jetson and outliers beyond three standard deviations are classified as anomalies. The GPU is utilized to efficiently run the matrix multiplications required by the Bayesian ridge regression for prediction. Peeters et al. also published on the wind turbine research utilizing Jetson for edge computing[8], acknowledging that the next step is to utilize the Jetson for neural network learning.

Lipnicki et al. investigated utilizing the Jetson platform for monitoring compressors on a test stand. Multilayer perceptrons (MLP), convolutional neural networks (CNN), long short term memory (LSTM) networks, and Support Vector Machines (SVM) were all studied and compared for performance[27]. The results show that certain algorithms are feasible to implement on GPU based edge devices, but that additional enhancements and research can improve performance.

The Nvidia Jetson Nano, which has less processing power than the TX2, is of particular interest due to the low cost of hardware. At the time of the initial research into the Jetson Nano, the 4GB evaluation board had a cost of $89, thereby representing a limited additional investment to add GPU processing capabilities. The specifications on the Jetson Nano developer kit (shown in Figure 5) are provided in Table 3 below.

Table 3. Nvidia Jetson Nano Specifications

GPU	128-Core NVIDIA Maxwell
CPU	Quad-core ARM A57 @ 1.43 GHz
Memory	4GB 64-bit LPDDR4 25.6 GB/s
Storage	microSD
Video Encoder	4Kp30 | 4x 1080p30 | 9x 720p30 (H.264/H.265)
Video Decoder	4Kp60 | 2x 4Kp30 | 8x 1080p30 | 18x 720p30 (H.264/H.265)
Connectivity	Gigabit Ethernet, M.2 Key E
Camera	2x MIPI CSI-2 connectors
Display	HDMI and DisplayPort
USB	4x USB 3.0, 1x USB 2.0 Micro-B
Others	40-pin header (GPIO, I2C, I2S, SPI, UART) 12-pin header (Power and related signals, UART) 4-pin fan header
Mechanical	100 mm x 80 mm x 29 mm

Figure 5 - The Nvidia Jetson Nano

2.2.2 Selecting Technology Applications

Before demonstration of the potential technologies could begin, an application needed to be identified. As most military ground vehicles utilize diesel powered engines, and Golisano Institute for Sustainability had access to engine dyno and a Cummins ISC diesel engine, it was selected as the platform of interest. The next step was to determine which failure modes would be pursued in the research. High value failure modes are modes that result in significant degradation or complete loss of the vehicle's ability to complete its designated mission, or result in a high probability of further damage to additional components on the vehicle, incurring greater costs of failure. Additionally, modes of failure that occur either suddenly, or randomly, such as the case with a piece of debris causing a sudden failure, were of less value to pursue for this project as there is no progression of the failure to track.

To determine which engine components would be monitored, a combination of methods was used, the first of which was a Reliability Centered Maintenance (RCM) analysis of the engine. RCM is a structured process used to identify maintenance requirements of an asset under its operating context[28]. A typical

RCM analysis has a facilitator leading a group of stakeholders through the RCM process. Typical stakeholders consist of operators, maintainers, and subject matter experts, such as engineers or decision makers. For the RCM analysis of the Cummins engine, a team was formed that consisted of mechanical and industrial engineers, engineering co-ops, and a technician with significant experience in building and maintaining engines and vehicles.

The RCM analysis consisted of the engine block, internal components, and all major components mounted onto the engine, including the oil system (pump, cooler, filters), fuel system (filters, pump, injectors, fuel rail), the air intake and exhaust systems (intercooler, turbo, air filter, etc.), and belts. The results of the full engine RCM analysis can be found in Appendix A. The top candidates for on-condition maintenance from the RCM analysis were the mechanical fuel pump due to a gear/injection pump failure, fuel injector failures, worn piston rings, and head gasket failure.

As an additional justification, the outcomes of RIT's 2017 Office of Naval Research-sponsored research project titled, "Feasibility of Diagnostics, Prognostics and Hybrid Prognostics across Multiple Platforms" were used[29]. Under that project, one of the assets that was evaluated was a Family of Medium Tactical Vehicles (FMTV) platform. The research evaluated the maintenance data for the platform over a year and a half for approximately 500 assets. The maintenance data analysis also identified fuel injector replacements as area of interest due to the quantity that had been replaced.

Fuel injectors lend themselves to on-condition monitoring as the primary modes of failure progress over time, and component failure eventually leads to engine shutdown. The failure modes for injectors in common rail diesel fuel systems are failure of the solenoid, leakage from the solenoid valve, leakage from the injector needle valve, erosion of the injector jets, carbon buildup clogging the injector jets, and stiction in the injector piston or needle valve. Each of these modes of failure result in altering the flow of diesel fuel by either reducing the flow (failure of the solenoid, clogging jets, and stiction of the moving components), or by increasing the flow (solenoid valve leakage, injector nozzle leakage, erosion of the jets, and stiction of the moving components), while all of the failure modes have the potential to degrade the spray pattern of the injectors.

Of the identified failure modes within the fuel injectors, the decision was made to focus on failures that increased fuel flow, specifically leakage of the injector needle valve shown in Figure 6 below as component 11. This failure results in fuel leakage throughout the engine cycle, allowing fuel to enter the cylinder during the intake stroke, and when increased to a sufficient level, results in detonation, or combustion before the cylinder reaches top dead center. This specific case is of particular concern, because the increased load on the piston, connecting rod, and journal bearings that results from detonation will ultimately result in the failure of one or more of those components, which can often lead to further damage to the engine requiring either a complete rebuild of the engine, or its total loss.

Much of the published literature also focused on injector failures with increased fuel flow as well as altered injector flow patterns. Albarbar used accelerometers and acoustic monitoring to detect faults in mechanical diesel injectors where fuel system pressures were reduced resulting in early fuel injection and poor spray patterns, but limited the analysis to single engine cycles [10], [11]. More recent research from Taghizadeh used a combination of analysis methods, including short term Fourier transforms[30], to detect injector faults, identifying increases in energy from 10-25 kHz as well as increased levels of energy measured early in the combustion cycle. A more controlled study was done by Carlucci, who controlled the fuel injection process by altering the pressures in the fuel system and timing and length of the fuel

injection events [31]. His work also utilized vibration monitoring to detect the changes made to the injection events, resulting in the detection of vibration energy much earlier in the engine cycle once a critical amount of fuel had been injected into the engine before top dead center. Other research groups utilized thermocouples to track exhaust gas temperature (EGT) to detect fuel related issues [32], [33], noting that EGTs increased with increasing quantities of fuel injected into the cylinders. These studies utilized the thermal measurements on their own, as well as in conjunction with vibration monitoring to improve performance of the sensor array in its ability to successfully detect fuel injector issues without seeing false positives.

This literature made it evident that a combination of microphones, accelerometers, and thermocouples could be used to successfully monitor an engine and track the degradation of the fuel injector's performance as the seeded fault mode progresses. In addition to the fuel system faults, the RCM analysis determined that the engine's valve train was also of value to investigate. The published literature had several studies where vibration and acoustics had again been used to detect changes in valve train timing [34], [35]. This further led the RIT research team to look at valve train timing changes, as the same sensor array could be used to potentially detect faults in this second component system, and could be used to determine if the two different sub-system faults could be isolated from one another.

RIT also evaluated the fuel pump failures identified by the RCM analysis. Fuel pumps are of interest because the fuel pump could result in the engine shutting down, and the vehicle platform losing its ability to complete its assigned mission. The specific failure modes identified were failure of the high or low pressure check valves, wear of the high pressure pistons, wear of the tappets, wear of the camshaft lobes, failure of the solenoid, and cracking of the ceramic high pressure piston. Several of these failure modes would typically happen suddenly, specifically the check valves typically fail as the result of debris preventing their closure. Others are specific to the fuel pump installed on the engine (cracking of the ceramic piston), and largely eliminated the ability to seed the fault of another (wear of the high pressure pistons due to the nature of the ceramic pistons on our pump).

This left wear of the camshaft lobes, or the tappet assemblies, and failure of the solenoid. The nature of this pump is that solenoid failure results in the pump running at full displacement at all times. This would result in excess engine power wasted, pressurizing excessive amounts of fuel, but the result of this would be the opening of the pressure relief valve in the high pressure fuel rail that supplies all of the injectors. This would limit fuel pressure to the injectors to 1000 Bar, which the engine's control unit would detect through the fuel rail pressure and would simply adjust the injection pulse width to account for this. This renders solenoid failures a minor issue, which leaves the wear of the camshaft lobes and tappet assemblies.

These failure modes were not pursued over concern of debris from the fuel pump, which is lubricated with the engine's oil supply, entering the remaining portions of the engine and causing greater damage to the engine as a whole. Similarly, the piston ring wear and head gasket failures were avoided to prevent more catastrophic damage to the test platform (engine).

2.2.3 Case Study Demonstrations

2.2.3.1 Low Cost Sensing Technologies

Once the failure modes of interest were identified and the background research for the sensor applications was complete, the next steps consisted of setting up the full test system on the engine dynamometer and identifying methods of seeding the faults.

The engine test system consists of a Cummins ISC engine rated at 240 HP and 660 Ft-lb of torque placed on an eddy current dynamometer capable of absorbing 600 HP. A National Instruments data acquisition system was assembled that included 1) piezoelectric accelerometers (PCB 603C01) connected to a NI-9231 vibration module with integrated charge amplifier, 2) MEMS accelerometers (Analog Devices ADXL1002) connected to a NI-9220 voltage module, 3) Piezoelectric (PCB 130a23) microphones connected to a NI-9234 vibration module with integrated charge amplifier and a NI9220 module, 4) MEMS (Invensense 40618) microphones connected to the NI-9220 voltage module, 5) a Dynapar Nexgen 221440B12E rotary encoder connected to an NI-9401 Digital module, and 6) Watlow K type thermocouples connected to an NI-9213 thermocouple module.

2.2.3.2 Fault Seeding

The fuel injector was evaluated and five major failure modes were identified, as seen in Figure 6: (A) Weakening or failure of the solenoid valve spring, (B) Failure or shorting of the solenoid, (C) Erosion of the solenoid valve seat, (D) failure of the injector nozzle needle valve spring, and (E) eros on of the injector nozzle needle valve.

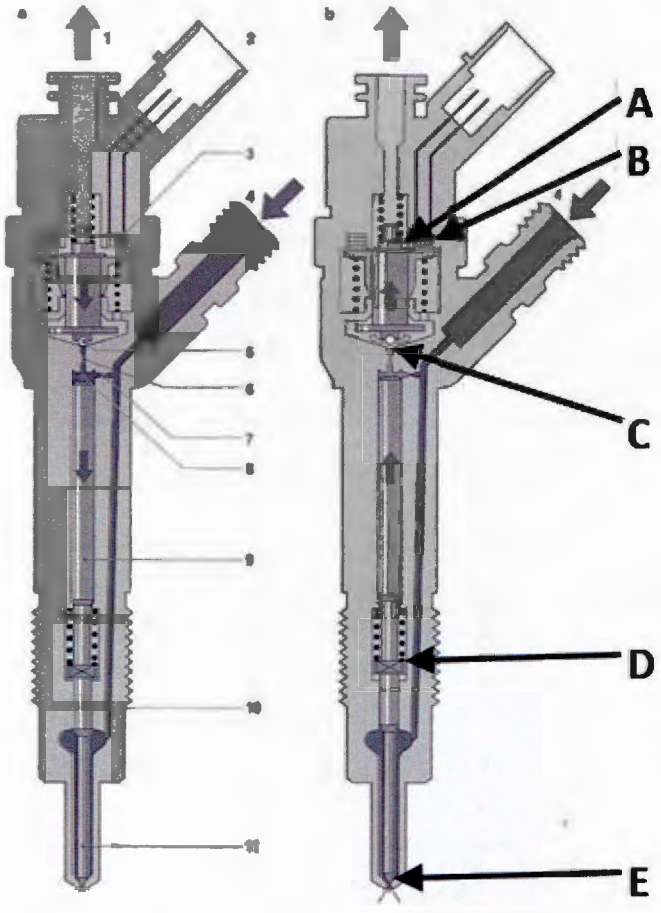

Figure 6 - Fuel Injector Failure Mode Locations

The two erosion failure modes were selected for this study, as they can be seeded with different levels of failure.

Solenoid Valve Seat Erosion

The valve area opening and closing over the course of the component's life causes rapid changes in flow velocity to occur in the narrow flow path and results in erosion the material. This fluid stream may also carry small pieces of debris that are not filtered out. The high pressure filter is a 2 micron filter that is effective at filtering out particles larger than 5 micron, so particles between 2 and 5 micron should be targeted as the size to create simulated wear on the part. The sealing mechanism is made of a removable rod/platform with the flow port in the middle of its face, and a tiny ball bearing (~0.5 mm in diameter) that is pressed into its face.

Erosion of the solenoid valve seat (B) was simulated by scratching the surface of the ball seat with a spring loaded diamond scribe. The cross sectional area of the leak path was measured and a leakage rate was estimated. The estimate was utilized to set the various fault levels, with subsequently worse levels having more gouges, Figure 7.

Figure 7 - Scratches in the solenoid valve ball seat allowing leakage

Injector Needle Valve Erosion

As this sealing interface progresses through its failure, the leakage flow will increase, and the pressure behind the control piston will reduce. As that pressure reduces, the balance of forces that keeps the injector nozzle closed is altered, allowing the injector to open and seep fuel into the engine. With enough fuel injected into the engine before reaching top dead center, pre-detonation in the accelerometer signal is expected, as well as an elongated combustion event, or a combustion event with two peaks. This would also result in increased exhaust gas temperatures. This behavior is clearly shown in research from Carlucci *et al.*[31]. The magnitude of these changes will progress as the failure mode progresses, starting with earlier combustion events and elevated exhaust gas temperatures, and progressing into pre-detonation and the potential of two distinct peaks in the acceleration data for each combustion event. These signatures would be similarly shared with a leaking injector nozzle, but could be isolated from one another through an elevated return flow pressure potentially.

Figure 8 – Precision ground flat spots on the side of the injector valve nozzle

The erosion of the valve nozzle was seeded by precision grinding a flat spot on to the side of the injector nozzle needle valve, Figure 8. The size of the grinding mark, determined by the duration of grinding, controls the amount of leakage of fuel into the engine cylinder. For each failure mode, multiple levels of failure were created and validated through flow testing at D&W Diesel[36], thus allowing for quantification of each level of fault, as shown in Table 4 and Table 5.

Flow Specification For Needle Valve Leak	220.4±9.9mm^3/H
Level 1 Damage	229.45mm^3/H
Level 2 Damage	230.15mm^3/H
Level 3 Damage	245.15mm^3/H
Level 4 Damage	317.99mm^3/H

Table 4 --- Flow values and specification for nozzle valve seeded failures

Flow Specification For Ball seat Leak	48.5±43.5mm^3/H
Level 1 Damage	68.5mm^3/H
Level 2 Damage	74.3mm^3/H
Level 3 Damage	78.45mm^3/H
Level 4 Damage	95.43mm^3/H
Level 5 Damage	97.36mm^3/H

Table 5 - - Flow values and specification for ball seat valve failures

2.2.3.3 Experimental Set-up and Design

The experimental system consisted of the Cummins engine on the eddy current dynamometer with a programmed engine cycle consisting of 1) an idle warm-up, 2) a highway cycle based on a modified EPA highway cycle, 3) another idle cycle, 4) a series of static test points, and 5) an idle cool down period. The modified EPA cycle was utilized to allow for analysis of dynamic data. The static test points were selected to provide some steady state data for analysis, and were designed to include a point representative of steady state highway driving, 1700 RPM and 330 Ft-lbs of torque. The steady state test points are defined in Table 6. All changes between states consisted of 200 RPM/sec and 75 Ft-lb/sec ramp rates.

Table 6 - Steady State Test Points

Step	Time	Engine Speed	Torque
1	240	700	0
2	180	1100	165
2	180	1700	165
4	180	2200	165
5	180	1100	330
6	180	1100	495
7	180	1700	330
8	180	2200	330
9	180	1700	495
10	180	2200	495
11	180	1900	400
12	180	1700	400
13	180	1900	330
14	180	1500	400
15	180	1500	330
16	180	1900	250
17	180	1700	250
18	180	1500	250
19	180	1100	80
20	180	700	75
21	180	700	50
22	180	800	0
23	10	700	0

Testing consisted of a set of known good, baseline injectors, as well as the multiple damage levels defined in Table 4 and Table 5. The damaged injectors were typically placed in Cylinder 2 or Cylinder 5, where accelerometers were mounted. Finally, the worst needle valve injector was moved across the other cylinder locations to determine effectiveness of the approaches on cylinders away from the accelerometers. The testing was randomized with individual tests typically performed twice per day. Replication was performed to determine if there was any noticeable impact from hysteresis. Additionally, testing of valve adjustments were completed in an attempt to gather data for analysis of feature similarities to the failed injectors. The order of testing is provided in Table 7.

Table 7 - Engine Dyno Testing Order

Injector set-up	Location of Fault	Number of Runs Collected
Needle Valve Damage Level 3	Cylinder 2	4
Needle Valve Damage Level 4	Cylinder 2	4
Baseline	N/A	2
Needle Valve Damage Level 4	Cylinder 5	4
Ball Seat Damage Level 1	Cylinder 2	4
Ball Seat Damage Level 2	Cylinder 2	4
Ball Seat Damage Level 4	Cylinder 2	4
Ball Seat Damage Level 3	Cylinder 2	2
Baseline	N/A	4
Needle Valve Damage Level 1	Cylinder 2	5
Ball Seat Damage Level 5	Cylinder 2	4
Baseline	N/A	6
Needle Valve Damage Level 1	Cylinder 2	2
Needle Valve Damage Level 2	Cylinder 2	4
Ball Seat Damage Level 3	Cylinder 2	1
Intake Valve Lash set to 0.022"	Cylinder 2	4
Intake Valve Lash set to 0.006"	Cylinder 2	4
Exhaust Valve Lash set to 0.0015"	Cylinder 2	4
Exhaust Valve Lash set to 0.0032"	Cylinder 2	2
Baseline	N/A	8
Needle Valve Damage Level 4	Cylinder 2	2
Needle Valve Damage Level 3	Cylinder 2	2
Needle Valve Damage Level 3	Cylinder 5	2
Needle Valve Damage Level 4	Cylinder 5	2
Needle Valve Damage Level 1	Cylinder 5	1
Needle Valve Damage Level 2	Cylinder 5	1
Baseline	N/A	3
Needle Valve Damage Level 1	Cylinder 2	1
Needle Valve Damage Level 2	Cylinder 2	1
Needle Valve Damage Level 4	Cylinder 1	2
Needle Valve Damage Level 4	Cylinder 6	2
Needle Valve Damage Level 4	Cylinder 3	2
Needle Valve Damage Level 4	Cylinder 4	2

2.2.3.4 Modeling Approaches

The initial intent of testing was to evaluate the shift in the timing of combustion events, as well as changes in magnitude, similar to what was found in Albarbar. However, as the data was reviewed, it was

determined that the magnitude and timing changes existed across individual engine cycles on the same test set-up. Therefore, more effort was spent attempting to select the proper features for identifying injector faults. Multiple approaches were taken for feature identification: 1) engineered vibration features, 2) machine learned vibration features, and 3) exhaust thermal models.

2.2.3.4.1 Engineered and Machine Learned Features

The major results of this research will be presented at the 14th Annual Conference of the Prognostics and Health Management Society being held from November 1-4, 2022. A journal publication will follow the conclusion of conference. The expected reference is:

A. Islam *et al.*, "Feasibility of Low-cost Vibration Monitoring for Ground Vehicles," *Annu. Conf. PHM Soc.*, vol. 14, no. 1, Nov. 2022.

The abstract for the research is as follows:

"This paper reports empirical investigation for the feasibility of *micro-electromechanical systems* (MEMS) sensors, accelerometers and microphones, for *prognostic health management* (PHM) application in monitoring of ground vehicles on the use case of diesel engine monitoring. The failure mode was injector leakage with four seeded levels of damage. MEMS and piezoelectric accelerometers were mounted in close proximity, following the usual good practices of sensor placement to enable fair comparisons. The process of computing both engineered and data-driven condition indicators was repeated for the data captured by the type of sensors. In addition to the empirical study, the article includes elementary economic analysis to compare the cost of the MEMS-based solution to that of the traditional vibration data acquisition channel. The results suggest that data-driven models seem to be agnostic to the sensor source, but feature engineering may require additional tuning. Also, economic analysis will show that MEMS-based sensing could cheaper than piezo-based sensing for low-cost *health and usage monitoring systems*(HUMS)."

2.2.3.4.2 Exhaust Thermal Models

The major results of this research have been documented in a research paper titled, "Exhaust-gas Temperature Model and Condition Indicator for Diesel Engines," which is being submitted to *Applied Thermal Engineering*.

The abstract for the research is as follows:

"This article presents the development of a prognostic feature for fuel injector faults in diesel engines based on individual cylinder exhaust gas temperatures (EGT) as part of a low cost health and usage monitoring system (HUMS). Faults were seeded at multiple damage levels in the fuel injectors to demonstrate the ability of the tool to monitor the progression of the mode of failure by monitoring the EGT levels with thermocouples, while modeling the predicted EGTs for a healthy engine using the data communicated over the CANBUS from the engines control unit.

This feature is shown capable of tracking the level of damage to the injector through multiple independent sets of data collected using two different forms of diesel fuel, taken at stable operating points, and from transient data collected on an engine dyno. A second tool was developed and discussed to determine what sections of data in the transient case could be considered stable to ensure model accuracy. Further, results from seeded faults in the timing of the valve train, and thus air-flow into the cylinder were shown not to interfere with the accuracy of the feature."

2.2.3.4.3 Feature Fusion

The major results of this research have been documented in a research paper titled, "Prognostics Health Monitoring of Diesel Fuel Injectors," which is in preparation for submission to *Mechanical Systems and Signal Processing*.

The abstract of the research is as follows:

"A detector was developed for monitoring injector leaks in truck diesel engines at four levels of damage, starting with leaks that pass the existing test during maintenance and progressing to relatively large leaks. Two distinct detectors, based on statistically-independent information sources, were developed separately, evaluated and finally integrated using statistical sensor fusion. A physics-based detector employed measurements of exhaust temperature and produced inferences on the state of health during both transients and steady-state intervals. The second detector was data-driven, employing an autoencoder with fully-connected layers to learn compact representation of vibration data, after time-synchronous averaging. The models integrated to further improve their performance using three different methods: sequential probability ratio test, Bayesian beta fusion, and Bayesian Dirichlet fusion. The advantages and limitations of fusion methods were discussed."

2.2.3.5 Mobile GPU Processing for CBM

To study the capability of the Nvidia Jetson Nano, a system was set-up with access to data provided by Navair as part of the gear prognostics research subproject under this award. The goal of the research was to determine if high speed vibration data could be computed at the edge, thus decreasing bandwidth requirements.

The major results of this research will be presented at the 14th Annual Conference of the Prognostics and Health Management Society being held from November 1-4, 2022. A journal publication will follow the conclusion of conference. The expected reference is:

C. Valant *et al.*, "Evaluation of NVIDIA Jetson System for Vibration HUMS," *Annu. Conf. PHM Soc.*, vol. 14, no. 1, Nov. 2022.

The abstract for the research is as follows:

"An NVIDIA Jetson graphical processing unit (GPU) was evaluated for utilization in a health and usage monitoring system by computing vibration-based condition indicators (CIs) and evaluating autoencoders for anomaly detectors. The GPU performance was subsequently compared to a central processing unit (CPU) performing the same computations, included signal preprocessing. Two distinct cases of interest were considered with neural network autoencoders: model evaluation and model adaptation with limited training. The experiments found that computations associated with signal preprocessing and condition indicators performed faster on the CPU, but neural network model evaluation and adaptation were faster on the GPU. Utilizing the GPU capability of the Jetson Nano, it was estimated that 42 accelerometer signals could be evaluated through autoencoders in real time, when data was processed in one second batches."

2.2.4 Return on Investment

Traditionally, maintenance in the military has been performed on a usage (hours or mi es) or time based schedule. Alternatively, CBM is a maintenance approach by which the actual condition of a system is assessed and maintenance applied on an as needed basis. Adoption of CBM orig nated in railroad applications in the late 1940's[37]. In the subsequent decades, CBM has been embraced in the automotive, aerospace, military, and manufacturing industries. Recently, the military has made a strategic push for the implementation of CBM across all platforms[2].

CBM assessments are typically performed by a Health and Usage Monitoring System (HUMS) that will collect data, assess usage, and perform diagnostic or prognostic processes. A typical CBM system implementation begins with an RCM activity. The outcome of the RCM process is a series of actions: 1) failure finding, 2) redesign, 3) run to failure, 4) scheduled restoration or discard, or 5) on-condition tasks. This final category, on-condition tasks, identifies the systems that require condition monitoring on the platform, informing the design of the HUMS. Additionally, the HUMS may track the scheduled restoration or discard tasks.

CBM, however, goes beyond just the on-platform HUMS. The DoD breaks down health assessment processing into an on-system component, which has an automated data processing element on embedded processors, and an off-system element consisting of longer term data storage and management, as well as health assessment software applications designed for ente-prise level CBM+ capabilites, particularly analytics[2]. This overall CBM+ system design covers on-system (sensors and an embedded processor), at-system (portable maintenance aids), and off-system (enterprise systems) components.

The value of a CBM system is derived from its ability to proactively apply maintenance to impending failures, extend maintenance cycles through timely repair, and increase asset availability, ultimately decreasing life-cycle costs of the asset[38]. Value, however, does not provide economic justification for the implementation of CBM+. Instead, Return on Investment (ROI), a standard business metric for economic investment, may be utilized by decision makers to detemine if the CBM− system is worth undertaking. ROI may be utilized for comparing varying approaches to CBM, and more importantly, for comparison of CBM+ against more traditional maintenance approaches. Conceptual y, ROI is a simple formula:

$$ROI = \frac{Final\ value\ of\ the\ investment - Initial\ cost\ of\ the\ investment}{Initial\ cost\ of\ the\ investment} \quad (1)$$

However, in practice, calculating the actual ROI for a product may be much more complex, with a large number of factors impacting the final value of the investment. The ROI of a CBM+ system can be a complex calculation due to the potential for savings in areas aside from just maintenance. Even the estimation of maintenance savings can be a difficult task. Therefore, many early applications of CBM+ have been focused on implementation with the knowledge that there will be maintenance savings. The ROI of these applications were then evaluated after implementation, such as the Joint Strike Fighter[39], the CH-47, UH-60 and AH-64 helicopters[40]–[42], and an Airbus A320[43].

Many ROI analyses have been performed to estimate the benefits of CBM on military vehicles[44], LED lighting[45], electronics[46][47][48], telecom applications[49], offshore windfarms[50] and aerospace applications[46][51][52]. To estimate benefits, simulations are typically performed with various time to failure distributions, estimates of prognostic distance, false alarm rates, and costs of achieving the varying levels of CBM+ capability. Stochastic modeling is then used to assess the ROI of the CBM+ capability. Alternatively, other programs have utilized historical maintenance data to assess the impacts of the CBM+ system, but these often ignore additional factors such as field recovery costs or risk to vehicle and crew.

2.2.4.1 Previous ROI Analysis Based on Historical Data

The application of CBM+ to several platforms has enabled a historical review of system benefits, including the ROI. Analysis has typically been focused on the cost avoidance of the systems with little attention paid to the investment as it was considered a sunk cost.

Zaman et al.[40] utilize over 14 years of data on the AH-64 aircraft, including two distinct periods of time, FY2000 to FY2006 and FY2007 to FY2013, where, respectively, the vibration monitoring unit (VMU) and the modernized signal processing unit (MSPU) were implemented. Costs were calculated for maintenance utilizing replacement part and labor data from FED LOG (the Federal Logistics Database) and the Global Combat Support System – Army (GCSS-Army). Operating costs were estimated from maintenance test flights, "partial mission capable" maintenance costs, and "non-mission capable" supply costs. Partial mission capable maintenance costs account for a percentage of a day that an aircraft is inoperable. Non-mission capable costs consider entire days when the aircraft is inoperable. After considering inflation rates, and normalizing data by active aircraft and flight hours, it was shown that the ROI per aircraft over the combined 14 year period was 742%. Furthermore, the addition of the MSPU created a significant reduction in replacement part costs and maintenance test flight costs. Another significant finding is that the partial mission capable maintenance costs significantly increased while the non-mission capable supply costs decreased by more than half. These two numbers are related because implementation of CBM+ identified additional partially mission capable aircraft, thus reducing non-mission capable aircraft.

Blechertas et al.[41] performed a cost benefit analysis on the UH-60 and CH-47 helicopters, in addition to the AH-64. The focus of the cost benefit analysis was on tangible benefits through reduced maintenance flights hours, reduced maintenance man hours and parts cost, and increasing time between overhauls. However, non-tangible benefits were also considered. In this scenario, the non-tangible benefits include operational readiness, morale, performance, and safety. These benefits were evaluated through interviews and discussions with crew chiefs and operators and were rated on a Likert scale.

2.2.4.2 Previous ROI Analysis Based on Modeling

Another option for performing an ROI analysis is to perform stochastic modeling of the failures and predict the performance improvements facilitated by an enhanced maintenance regime utilizing CBM. This has been done across many industries and applications, including military vehicles[44], LED lighting[45], electronics[46][47][48], telecom applications[49], offshore windfarms[50] and aerospace applications[46][51][52]. In order to perform this type of modeling, an understanding of the exact type of failure and component reliability is necessary. For the evaluation of the low cost sensing technologies, a more pragmatic approach is presented below.

2.2.4.3 Evaluating ROI of a CBM+ System

2.2.4.3.1 Defining Return on Investment

The focus of the efforts for this project was on identifying the parameters that can impact the ROI of a potential CBM+ system capability. Return on investment is an economic measure for evaluating the efficiency of an investment, previously shown as:

$$ROI = \frac{Final\ value\ of\ the\ investment - Initial\ cost\ of\ the\ investment}{Initial\ cost\ of\ the\ investment} \quad (1)$$

A positive ROI represents a cost benefit for the investment and is typically calculated over a period of time after the investment, with 1 to 5 years often being utilized as a period to achieve a pos tive ROI. Another method for calculating ROI utilizes cost avoidance[47], defined as the reduction of costs paid in the future. The cost avoided is given by:

$$\Delta C_A = C_{wo} - C_w \quad (2)$$

where:

C_{wo} = the total lifecycle cost of supporting the system without CBM+

C_w = the total lifecycle approach of supporting the system with CBM+

Therefore, the return on investment is defined as:

$$ROI = \frac{\Delta C_A}{I} \quad (3)$$

where:

I = investment cost of CBM+

Utilizing the cost avoidance approach simplifies the ROI calculation by ignoring all of the costs that remain the same between the two approaches. To expand the equations and cancel out terms that exist across the lifecycle costs, we initially evaluate the lifecycle and investment costs separately. To achieve the return portion of the ROI equation, the lifecycle cost of the vehicle must be evaluated under an unscheduled maintenance policy and then compared to the lifecycle cost of the vehicle under a CBM+ maintenance policy. In both scenarios, the basic categories of lifecycle costs are: acquisition, operating, maintenance, and preventative maintenance costs. Each of these categories will be looked at separately and then the factors will be brought together to show the overall return based on implementation of the CBM+ capability.

2.2.4.3.2 Components of the ROI Equation

Acquisition Costs

Relative to the total lifecycle cost of the platform, the acquisition costs consist of the acquisition of the platform, Acq^P and the acquisition costs of the CBM+ system, Acq^{CBM}. These costs are simply the cost to purchase each asset and do not include the investment costs of developing the systems.

Operating Costs

The operating costs of a platform, O^P, typically consist of operational manpower, energy necessary to operate a platform, training munitions, operational support services, and transportation services. Operational manpower typically consists of the crew necessary to operate the platform. For example, an armored vehicle's operational manpower may consist of a crew chief, commander, gunner, driver, loader, etc. Additionally operational manpower may include staff, security, logistics and ordnance support costs that are required to support the platform. These costs are typically estimated at a unit level. Energy costs consist of those forms of energy necessary to operate the platform, typically fuel and fuel additives costs. The cost of training munitions consists of the cost of all expendable munitions that must be removed from stock, and may include munitions that have reached the end of their shelf life.

Operational support services costs consist of field service representatives who support non-maintenance activities, as well as additional rental and lease costs that are necessary for land, facilities, communications, etc. that are not part of the base operating support costs. Transportation services costs include the moving equipment, personnel and supplies for training or remote operational sites. However, transportation services does not include the cost of relocating the platform for depot maintenance, which is included in the maintenance budget.

Maintenance Costs

The maintenance costs of the platform consist of all costs of labor and materials necessary to maintain the operational capability of the platform. These maintenance costs consist of consumables, depot level reparables (DLRs), intermediate maintenance, and depot maintenance.

Consumable items consist of "throw-away" items that are replaced at the unit level. These items will be replaced and will not be sent to another location for repair, e.g. batteries or filters. The costs should also include any incurred costs for transportation, warehousing, inventory management, etc.

DLR items are removed from the platform, replaced with an item from inventory, and are then sent to a depot to be repaired and then placed back in inventory. The DLR costs consist of the labor and material costs necessary to repair the item at the depot, the transportation and storage costs of the item, as well as replacement costs for condemned (unrepairable) DLR items.

Intermediate maintenance (IM) costs consist of the costs of labor, material and other costs associated with maintenance performed at an intermediate maintenance location. This category essentially covers maintenance that is not performed at the unit-level or depot.

Depot maintenance consists of the costs of labor, materials and overhead incurred with major overhauls of the platform or with repair of DLRs. Depot maintenance costs should consider the different schedules necessary for overhaul cycles, for example engine overhau may occur on a different schedule than hull or frame overhaul.

Ideally, for the purposes of analysis, each of these categories may be evaluated on the basis of a platform under an unscheduled maintenance regime versus a CBM+ based maintenance regime. The cost of the maintenance of the CBM+ system is an added cost that will only be applied to the CBM+ regime costs. Therefore, the costs for an unscheduled maintenance regime are:

$$M_{US}^{P} = M(C)_{US}^{P} + M(DLR)_{US}^{P} + M(IM)_{US}^{P} + M(D)_{US}^{P} \quad (4)$$

Where:

$M(C)^P_{US}$ = Maintenance cost of consumables for the platform under unscheduled maintenance

$M(DLR)^P_{US}$ = Maintenance cost of DLRs for the platform under unscheduled maintenance

$M(IM)^P_{US}$ = Maintenance cost of IM for the platform under unscheduled maintenance

$M(D)^P_{US}$ = Depot Maintenance costs for the platform under unscheduled maintenance

Similarly, the maintenance costs for the CBM+ regime are:

$$M^P_{CBM} = M(C)^P_{CBM} + M(DLR)^P_{CBM} + M(IM)^P_{CBM} + M(D)^P_{CBM} \quad (5)$$

Where:

$M(C)^P_{CBM}$ = Maintenance cost of consumables for the platform under CBM+ maintenance

$M(DLR)^P_{CBM}$ = Maintenance cost of DLRs for the platform under CBM+ maintenance

$M(IM)^P_{CBM}$ = Maintenance cost of IM for the platform under CBM+ maintenance

$M(D)^P_{CBM}$ = Depot Maintenance costs for the platform under CBM+ maintenance

Another method of analysis of maintenance costs is to determine the savings from detection of a failure prior to secondary damage. The component will need to be replaced either way, but if it prevents secondary damage requiring additional maintenance, this secondary damage savings can be quantified and the remainder of the cost for the damaged component can be assumed to be the same under either maintenance regime.

Preventative Maintenance Costs

A further consideration in maintenance cost, not evaluated in this project, is preventative maintenance (PM) costs. In the military, preventative maintenance consists of preventative maintenance checks and services (PMCS) for a platform. This is a defined schedule of checks performed before during, and after operation, as well as a set of scheduled services, e.g. oil and filter changes. Although the addition of a CBM system may have some impact on PMCS, for this study, we assume that an operator will still need to verify any PMCS performed by the CBM system and that the scheduled services will remain the same. Therefore, cost implications are negligible. However, it should be noted that if a full RCM analysis is performed to inform the CBM+ system, there may be changes to PMCS that are identified that could impact costs.

Additional Cost Considerations

The goal of a CBM+ program is to decrease maintenance costs, improve maintenance logistics responsiveness, increase operational availability and readiness, and ultimately decrease unscheduled failures. Although the basic lifecycle costs have been identified above, a major impact of a CBM+ system relates to the unscheduled failures. Unscheduled failures may have several cost implications ranging from loss of mission objective to loss of platform and crew. The ability to prevent an unscheduled failure during

operations will reduce both costs and risks to personnel. The additional costs of failure during operations may consist of:

$C_{MO} = Cost\ of\ loss\ of\ mission/objective$
$C_R = Cost\ of\ vehicle\ recovery$
$C_C = Cost\ of\ the\ loss\ of\ life\ or\ crew$
$C_V = Cost\ of\ the\ loss\ of\ the\ vehicle, replacement\ cost = Acq^P$
$C_D = Cost\ of\ collateral\ damage$

The most obvious cost, yet one of the hardest to estimate, is the cost associated with the loss of the mission if the platform fails. This cost will be highly dependent on the platform. For example, the failure of a B-2A bomber that prevents carrying out a bombing mission may be significantly different than a failure of a Medium Tactical Vehicle Replacement (MTVR) moving supplies between bases. Although an MTVR moving a howitzer into position may be just as critical as a bombing mission. An analysis of prior mission losses may be able to provide some costs associated with mission loss by platform.

The cost of recovery of the platform again has a wide range of costs, which may consist of bringing unit level maintenance and parts to the platform for repair to sending a recovery vehicle to tow or carry a platform back to the unit for maintenance. Again, this cost will be very platform dependent. For example, recovery of a UH-1Y helicopter will be significantly more expensive than towing an MTVR back to base.

The cost of the loss of crew can be from either injury or death. Injury costs may consist of medical costs and survivor benefits. In the unfortunate event of death, costs will include death benefits. In addition, any loss of crew will require additional crew members as replacements which should include the cost of training the crew. Many of these benefits are explained on the Army website[53] and articles designed to help people understand the benefits[54]. These costs will vary slightly due to the salary of the soldier[55].

The cost of the loss of the platform may be considered as the replacement or acquisition cost of the platform. Even if it is determined that a vehicle will not be replaced, the cost of the replacement should be considered. In this case, the cost of the replacement was applied at the beginning of the program by buying spares, i.e. buying 20 vehicles when only 15 are necessary. However, the cost of a replacement platform should still be considered when discussing the impacts of preventing such failures applied to a single asset lifecycle cost.

Another difficult to estimate cost of failure is collateral damage. In some cases, there may not be any collateral damage, e.g. an engine quits and the vehicle is able to pull over and wait for repair. In other cases, damage may be minimal, e.g. property damage to a farm field caused by recovery of a helicopter after an emergency landing. Alternatively, collateral damage may be high, e.g. a plane crashing into a residential neighborhood.

Failure Probabilities

In order to evaluate the ROI, each failure mode that the system is capable of capturing must be considered. Mean time between failures (MTBF) is a common measure of the frequency of failures. MTBF may be turned into a failure rate expressed for a period of time.

Where:

$$\text{MTBF} = \frac{\text{Total Uptime}}{\text{Number of Failures}} \quad (6)$$

Then:

$$\text{Failure Rate} = \frac{\text{Number of Failures}}{\text{Total Uptime}} \quad (7)$$

For example, if an industrial gearbox has two bearing failures over three years with 40 hours of operation per week, the uptime for that period is 6,240 hours (3 years x 52 weeks x 40 hours). Therefore, the MTBF is 3,120 hours. The failure rate can be expressed as 0.00032051 failures per hour. The failure rate can be extrapolated out to longer timeframes by simply multiplying by the number of hours, but maintaining the number based on hours of operation allows for easier calculation should the number of operating hours per year change.

This failure rate only considers the failure of the component due to the specific failure mode of interest. An additional consideration is the probability that the failure causes loss of the asset. For example, an engine oil leak may lead to a total loss of lubrication in an engine and potential engine seizure. Not all oil leaks may lead to this failure, a small enough leak may not lose enough oil to have this catastrophic of an impact between oil changes. This is often referred to as a "hazard rate". However, when speaking of a specific component, the hazard rate would be the probability that the component would die based on the age of the component. For our analysis, we need to understand the probability of the loss of the platform due to the loss of a component. This can either be calculated from existing data or can be estimated as a probability of catastrophic failure, P_C, applied to the failure rate. Using the above gearbox example, assume an engineering analysis estimates that 13% of bearing failures lead to catastrophic failure and loss of the gearbox. Then the modified hazard rate of an asset, HR_{Asset}, given a specific failure mode (FM_x) could be expressed as:

$$HR_{Asset}^{FM_X} = failure\ rate * P_C \quad (8)$$

For the bearing example, this translates into an HR_{Asset} = 0.000041667 catastrophic failures per hour, or one catastrophic failure every 24,000 operating hours (11.54 years). The addition of a CBM system should increase MTBF and lower the modified hazard rate due to the number of failures decreasing.

The goal of a CBM system is to predict failures so that components are replaced prior to failure. However, there is a trade-off in any system between catching all failures and prematurely replacing components with significant remaining life available in the component. The time between prediction and failure, often times referred to as the P-F interval, needs to be long enough to order parts and perform the repair. Too early and life of the component is lost when it is replaced early. Too late and the asset may be out of commission waiting on parts, or worse, break down in the field. Generally, the cost of the PHM algorithm development increases significantly as the "perfect" window of opportunity is honed in on. Additionally, no prediction is going to be perfect, so it should be assumed that some failures will be missed and some components may be replaced early. For the purposes of this analysis, we are most concerned with the

cost of missing a prediction. Although false alarms will occur, in some cases, these are intentional as the subject matter experts (SMEs) want to validate the outputs with a "man-in-the-loop".

Application of Failure Probabilities to Additional Cost Considerations

The failure rate and hazard rate are critical to determining the added costs of failure. First, the hazard rate must be applied to the costs of loss of vehicle and crew. As the hazard rate is the likelihood of failure, it should be applied across the planned life of the vehicle. Therefore, the lifecycle costs of a platform from the loss of crew is:

$$C_C = HR_{Asset}^{FM_X^Y} * T_{SL} * C_C^x \quad (9)$$

Where:

$HR_{Asset}^{FM_X^{US}} = Hazard\ rate\ for\ the\ asset\ for\ the\ given\ failure\ mode, X, under\ maintenance\ regime\ Y$
$T_{SL} = Planned\ service\ life$
$C_C^x = Cost\ of\ the\ loss\ of\ life\ or\ crew\ for\ platform\ x$

Similarly, the lifecycle costs of a platform from the loss of the vehicle is:

$$C_V = HR_{Asset}^{FM_X^{US}} * T_{SL} * Acq^P \quad (10)$$

Where:

$Acq^P = Acquisition\ Cost\ of\ the\ Platform$

The cost of vehicle recovery is an expense that only exists when the vehicle suffers a failure, but does not suffer from a catastrophic failure. Therefore, recovering the asset makes sense. The cost of vehicle recovery is:

$$C_R = (FR^{FM_X^{US}} - HR_{Asset}^{FM_X^{US}}) * T_{SL} * C_R^x \quad (11)$$

Where:

$C_R = Cost\ of\ vehicle\ recovery$
$HR_{Asset}^{FM_X^{US}} = Hazard\ rate\ for\ the\ asset\ for\ the\ given\ failure\ mode, X, under\ maintenance\ regime\ Y$
$FR^{FM_X^{US}} = failure\ rate\ for\ the\ given\ failure\ mode, X, under\ unscheduled\ maintenance$
$T_{SL} = Planned\ service\ life$
$C_R^x = Cost\ of\ vehicle\ recovery for\ a\ given\ failure\ mode, X$

Finally, the cost of collateral damage and loss of mission can be applied to all failures. Therefore, the equation for those are:

$$C_{MO} = (FR^{FM_X^{US}} - HR_{Asset}^{FM_X^{US}}) * T_{SL} * C_{MO}^X \quad (12)$$

Where:

$C_{MO} = Cost\ of\ loss\ of\ mission/objective$
$HR_{Asset}^{FM_X^{US}} = Hazard\ rate\ for\ the\ asset\ for\ the\ given\ failure\ mode, X, under\ maintenance\ regime\ Y$
$FR^{FM_X^{US}} = failure\ rate\ for\ the\ given\ failure\ mode, X, under\ unscheduled\ maintenance$

$T_{SL} = Planned\ service\ life$
$C_{MO}^{X} = Cost\ of\ loss\ of\ mission\ or\ objective\ due\ to\ failure\ X$

$$C_D = (FR^{FM_X^{US}} - HR_{Asset}^{FM_X^{US}}) * T_{SL} * C_D^X \quad (13)$$

Where:

$C_{MO} = Cost\ of\ collateral\ damage$
$HR_{Asset}^{FM_X^{US}} = Hazard\ rate\ for\ the\ asset\ for\ the\ given\ failure\ mode, X, under\ maintenance\ regime\ Y$
$FR^{FM_X^{US}} = failure\ rate\ for\ the\ given\ failure\ mode, X, under\ unscheduled\ maintenance$
$T_{SL} = Planned\ service\ life$
$C_{MO}^{X} = Cost\ of\ collateral\ d\ due\ to\ failure\ X$

Other Factors Impacting ROI of a CBM+ System

The application of a CBM+ system may happen at two distinct points in time for a platform: 1) during the development of the platform or 2) after the platform has been placed into service. Although the systems may be capable of performing relatively similar CBM+ tasks, the costs and benefits of the systems may vary. For example, if a platform has a CBM+ system that improves reliability and availability of a platform, then it may be possible to decrease the number of vehicles being procured. Additionally, if the addition of a CBM+ system during the vehicle lifecycle increases availability of the platform, it may not translate into additional missions as the platform was designed for a specific life, usually based around a number of years or number of hours.

Therefore, the analysis of ROI provided in this section will focus on the more direct cost impacts of the implementation, such as maintenance costs, secondary failure costs, and implementation costs, as opposed to potential procurement savings.

2.2.4.3.3 Avoided Costs Equation

Optimally, the actual cost of all of the above factors would be known and the equation for cost avoidance would be broken down as follows:

$$\Delta C_A = C_{wo} - C_w \quad (2)$$

Where the lifecycle cost of the platform without a CBM system is defined as:

$$C_{wo} = Acq^P + O^P + M(C)_{US}^P + M(DLR)_{US}^P + M(IM)_{US}^P + M(D)_{US}^P + C_C + C_V + C_{MO} + C_R + C_D) \quad (14)$$

Where:
$Acq^P = Acquisition\ Cost\ of\ the\ Platform$
$O^P = Lifetime\ cost\ of\ operating\ the\ platform$
$M(C)_{US}^P = Lifetime\ maintenance\ cost\ of\ consumables\ for\ the\ platform\ under\ unscheduled\ maintenance$
$M(DLR)_{US}^P = Lifetime\ maintenance\ cost\ of\ DLRs\ for\ the\ platform\ under\ unscheduled\ maintenance$
$M(IM)_{US}^P = Lifetime\ maintenance\ cost\ of\ IM\ for\ the\ platform\ under\ unscheduled\ maintenance$
$M(D)_{US}^P = Lifetime\ depot\ maintenance\ costs\ for\ the\ platform\ under\ unscheduled\ maintenance$

$C_C = Cost\ of\ the\ loss\ of\ life\ or\ crew$
$C_V = Cost\ of\ the\ loss\ of\ the\ vehicle$
$C_{MO} = Cost\ of\ loss\ of\ mission/objective$
$C_R = Cost\ of\ vehicle\ recovery$
$C_D = Cost\ of\ collateral\ damage$

And the lifecycle cost of the platform with a CBM system is defined as:

$$C_W = Acq^P + O^P + M(C)^P_{CBM} + M(DLR)^P_{CBM} + M(IM)^P_{CBM} + M(D)^P_{CBM} + C_C + C_V + C_{MO} + C_R + C_D) \quad (15)$$

Where:
$C_W = lifecycle\ cost\ in\ the\ case\ of\ CBM\ policy\ implementation$
$Acq^P = acquisition\ cost\ of\ platform$
$Acq^{PHM} = acquisition\ cost\ of\ the\ PHM\ system$
$O^P = Lifetime\ cost\ of\ operating\ the\ platform$
$M(C)^P_{CBM}$ = *Lifetime maintenance cost of consumables for the platform under CBM*
$M(DLR)^P_{CBM}$ = *Lifetime maintenance cost of DLRs for the platform under CBM*
$M(IM)^P_{CBM}$ = *Lifetime maintenance cost of IM for the platform under CBM*
$M(D)^P_{CBM}$ = *Lifetime depot maintenance costs for the platform under CBM*
$C_C = Cost\ of\ the\ loss\ of\ life\ or\ crew$
$C_V = Cost\ of\ the\ loss\ of\ the\ vehicle$
$C_{MO} = Cost\ of\ loss\ of\ mission/objective$
$C_R = Cost\ of\ vehicle\ recovery$
$C_D = Cost\ of\ collateral\ damage$

There are common terms across the equations that should be considered to cancel each other out. While the initial platform acquisition cost cancels out, the cost of the loss of the vehicle is based on a hazard ratio that is different across maintenance regimes. Similarly, operating costs will be considered to be the same between the maintenance regimes. In general, the platforms will perform the same amount of work necessary to complete the missions, with differences being accounted for in maintenance costs. Therefore, a combined and reduced equation for avoided cost is:

$$\Delta C_A = \Delta M^{CBM}_{US} + \Delta C_C + \Delta C_V + \Delta C_{MO} + \Delta C_R + \Delta C_D - Acq^{PHM} \quad (16)$$

Where:

$$\Delta M^{CBM}_{US} = (M(C)^P_{US} + M(DLR)^P_{US} + M(IM)^P_{US} + M(D)^P_{US}) - (M(C)^P_{CBM} + M(DLR)^P_{CBM} + M(IM)^P_{CBM} + M(D)^P_{CBM}) \quad (17)$$

ΔC_C = *the difference in costs of loss of life of the crew between unscheduled and condition based maintenance regimes*
ΔC_V = *The difference in costs of loss of vehicle between unscheduled and condition based maintenance regimes*
ΔC_{MO} = *the difference in costs of loss of mission objective between unscheduled and condition based maintenance regimes*
ΔC_R = *the difference in costs of recovery between unscheduled and condition based maintenance regimes*
ΔC_D = *the difference in costs of collateral damage between unscheduled and condition based maintenance regimes*

The differences in the simplified cost equation are associated with two factors: 1) the costs associated with different hazard and failure ratios, and 2) the change in maintenance costs between regimes.

2.2.4.3.4 CBM Investment Costs

Investment costs consist of non-recurring, recurring, and annual infrastructure costs. Non-recurring costs are one-time costs typically associated with the development of hardware and software, as well as documentation and training. These costs are usually incurred at the front end of the PHM timeline and can be spread across the number of assets being deployed. Those costs can be calculated as follows:

$$C_{NRE}^{PHM} = C_{devH}^{PHM} + C_{devS}^{PHM} + C_{dev\_A}^{PHM} + C_{tr}^{PHM} + C_{doc}^{PHM} + C_{int}^{PHM} + C_{qual}^{PHM} \quad (18)$$

Where:

$C_{devH}^{PHM} = cost\ of\ hardware\ development\ for\ the\ PHM\ system$

$C_{devS}^{PHM} = cost\ of\ software\ development\ for\ the\ PHM\ system$

$C_{dev_A}^{PHM} = cost\ of\ the\ initial\ development\ of\ PHM\ algorithms\ in\ the\ system$

$C_{tr}^{PHM} = cost\ of\ training\ the\ initial\ algorithms$

$C_{doc}^{PHM} = cost\ of\ documentation$

$C_{int}^{PHM} = cost\ of\ integration$

$C_{qual}^{PHM} = cost\ of\ testing\ and\ qualification$

Recurring costs are those costs that continuously occur throughout the PHM program. These cost typically include the cost of hardware, assembly and installation for the PHM system on each asset, including the repair and replacement upon failure of the system. Therefore, recurring costs may be calculated as follows:

$$C_{REC}^{PHM_i} = HW_i^{PHM} + Assy_i^{PHM} + Test_i^{PHM} + Inst_i^{PHM} \quad (19)$$

Where:

$HW_i^{PHM} = cost\ of\ the\ PHM\ hardware\ for\ platform\ i$

$Assy_i^{PHM} = cost\ of\ the\ assembly\ of\ the\ PHM\ hardware\ for\ platform\ i$

$Test_i^{PHM} = cost\ of\ recurring\ tests\ on\ the\ PHM\ hardware\ on\ platform\ i$

$Inst_i^{PHM} = cost\ of\ the\ installation\ of\ the\ PHM\ hardware\ on\ platform\ i$

Finally, infrastructure costs consist of all supporting costs necessary to sustain the PHM system over its intended life. Those costs may be calculated as follows:

$$C_{INF}^{PHM} = \sum_{i=0}^{N} M_{P_i}^{PHM} + DS_P^{PHM} + RTR_P^{PHM} + \sum_{i=0}^{N} D_{P_i}^{PHM} \quad (20)$$

Where:

$M_{P_i}^{PHM} = cost\ of\ maintenance\ of\ the\ prognostic\ devices\ on\ platform\ i$

$DS_P^{PHM} = cost\ of\ decision\ support\ tools\ provided\ by\ PHM\ for\ all\ platforms\ of\ type\ P$

$RTR_P^{PHM} = cost\ of\ retrianing\ personnel\ in\ the\ utilization\ of\ PHM\ for\ all\ platforms\ of\ type\ P$

$D_{P_i}^{PHM} = cost\ of\ PHM\ data\ management\ (collection, archiving, analysis\ and\ reporting)\ for\ platform$

2.2.4.4 ROI Examples

The equations defined in the previous sections are an ideal version of the information necessary to get a full picture of the ROI of a system. However, in many cases, all of the data will not be readily available and assumptions will need to be made. Three examples of the application of ROI are provided to show the types of information and assumptions necessary for ROI evaluation. The first example will evaluate the ROI of an existing vibration monitoring system utilized for a gearbox on the H-1 series of helicopters. The second example will evaluate the ROI of a CBM system for monitoring a transmission (gearbox) on an Army FMTV. The third example will consider the monitoring of the FMTV transmission (gearbox) as an added capability to an existing CBM system. For each example, as much publicly available data was gathered as possible, and assumptions were stated as necessary.

2.2.4.4.1 H-1 Helicopter Gearbox ROI Example

The AH1-Z Viper and the UH-1Y Venom are helicopters utilized by the United States Marine Corps. The helicopters were developed to share approximately 85% of their components to reduce lifecycle costs and increase maintainability[56]. Part of the program that upgraded the platforms from the AH-1W and UH-1N included vibration monitoring of the main rotor gearbox, as well as the tail rotor gearbox. One of the common failure modes in these gearboxes is from cracked spur gears. A cracked spur gear while airborne is an event with catastrophic consequences. Vibration monitoring is one of the common methods of detection for spur gear failures. Below, we calculate the ROI of a vibration monitoring system as applied specifically to the main rotor gearbox (MRGB).

The analysis in this section focuses on the AH-1Z Viper. To calculate lifecycle costs for the platform, background information on platform was collected. The AH-1Z fleet consists of 61 helicopters[57] with a planned service life of 30 years or 10,000 hours. Assuming even usage, each platform should operate 333 hours per year.

The collection of maintenance costs as outlined in the cost avoidance calculation was not possible as much of that information is not published. Instead, the information that could be gathered from budget reports, presentations, standard cost methodologies, etc. was brought together and the equation was modified to fit the available data. The data that was identified and derived is listed in Table 8. Further discussion of how those numbers were calculated is provided below.

Table 8 - AH-1Z Table of Cost Information

Cost Component	***Abbreviation***	***Cost***	***Notes***
Platform Cost	Acq^P	*$31M*	*AH-1Z Viper Cost*[58]
CBM System Cost	Acq^{CBM}	*$252,885*	*Simmonds Precision IMD-HUMS Kit*[59]
Operating and Maintenance Costs (Calculated below)	$O^P + M_{US}^P$	*$47,980,000*	*Calculated below*
CBM+ Maintenance Cost Savings	ΔM_{US}^{CBM}	*$1.45M*	*Calculated below, Savings estimated from Navair Data*[57]
Cost of Mission objective	ΔC_{MO}	*$4,429*	*Calculated below*

Cost Component	Abbreviation	Cost	Notes
Cost of Recovery	ΔC_R	*$3,676*	*Calculated below*
Cost of Crew Loss	ΔC_C	*$20,111*	*Calculated below*
Cost of Vehicle Loss	ΔC_V	*$253,239*	*Calculated below*

Operating and Maintenance Costs

The actual operating and maintenance (O&M) costs for the AH-1Z are not published. Instead, the reimbursement rates for utilization of the assets are published rates. The rate for DoD customers represents the actual cost per flight hour for all operating and maintenance costs. The AH-1Z has a published O&M rate of $4,798 per flight hour. Assuming the platform is operated for the full planned service life, the total cost of operations and maintenance can be calculated as:

$$O^P + M_{US}^P = \$4{,}798 * 10{,}000 = \$47{,}980{,}000 \quad (21)$$

Estimated Maintenance Cost Savings from CBM+

Without the ability to separate maintenance costs from operating costs, and further identify the costs before and after installation of the CBM system, an alternative approach to cost savings was needed. Navair has presented on the savings from their implementation of CBM on the MRGB[57]. The application of CBM practices to the (MRGB) of the H-1 have prevented 22 gearbox removals over four years (May 2016 – May 2020). Repair costs of the MRGB if a failure occurs resulting in downstream damage are estimated to be upwards of $1.2M per repair. This maintenance savings can be assumed to be shared across the fleet. Assuming the 22 prevented failures are across the full fleet of H-1 platforms (61 AH-1Z and 141 UH-1Y) over four years, this equates to 0.02723 failures per year per aircraft. This equates to 0.8169 failures over the life of a single platform. According to Navair, $39M has been saved across the avoided 22 MRGB failures, which is actually $1.77M per event[57]. Therefore maintenance savings for a single aircraft across its lifecycle is estimated to be:

$$M_{US}^P - M_{CBM}^P = 0.8169 * \$1.77M = \sim\$1.45M \quad (22)$$

Additional Cost Consideration

As previously discussed, each prevented failure also has additional cost implications (loss of platform, crew, etc.). Based on the Navair data, each successful identification of a MRGB failure through CBM, likely prevented a precautionary emergency landing (PEL). The cost of the loss of mission objective is difficult to estimate, but a simple view of the cost is to assume the mission needs to be carried out again to obtain the objective. The AH-1Z has an estimated combat range (radius) of 144 miles or overall range of 430 miles, along with a cruise speed of 180 mph[60]. Let's assume a typical military mission plans to utilize 50% of that range, or 144 miles total (out and back). At a cruise speed of 180 mph, and an additional 20 minutes to obtain a specific objective, this equates to 1.13 hours of flight time. So, a minimum cost of the loss of the mission is:

$$C_{MO} = Mission\ flight\ hours * Hourly\ Rate * Number\ of\ failures = 1.13 * \$4{,}798 * 0.8169 = \$4{,}429 \quad (23)$$

The cost of the recovery of the helicopter can vary greatly, from no cost due to failure occurring over the base, to extremely expensive and hazardous when the vehicle fails on a combat mission in hostile territory. For the purpose of this exercise, let's assume that 50% of failures occur outside of the range of the base. Additionally, the cost to recover the helicopter can be assumed to include a truck with crane capabilities and a number of hours to travel to the site, load the helicopter, secure the helicopter, return to base and unload the helicopter. Assuming the need for a heavy equipment transporter and a crew of 2 to 3 people, and a roughly 10 hour recovery time (driving, load and unload). That is 30 man hours, plus the truck operating costs. Assume the truck costs (fuel, maintenance, etc.) are approximately $300/hr.

The total cost of recovery is assumed to be:

$$C_R = (personnel\ hours * pay\ rate + truck\ hours * truck\ rate) * number\ of\ failures \quad (24)$$

$$C_R = (30 * \$50 + 10 * \$300) * 0.8169 = \$4{,}500 * 0.8169 = \$3{,}676$$

The cost of loss of life and vehicle will be assumed to occur if the platform fails to detect the failure, and the crew does not notice a problem in time to land the aircraft. This estimation is performed with the following assumptions: 1) the CBM+ system captures 95% of the potential failures and 2) only 20% of the remaining failures would result in the loss of an aircraft and crew. Based on the earlier equation:

$$HR_{Asset} = failure\ rate * P_C \quad (8)$$

Where:

$$P_C = CBM\ Miss\ Rate * Rate\ of\ loss \quad (25)$$

Therefore:

$$HR_{Asset} = 0.8169 * 0.05 * 0.2 = 0.008169$$

This is the rate at which the aircraft may be lost, which can be applied to the cost of the helicopter and crew. The cost of the loss of crew include death gratuity, survivor benefits, insurance (service members group life insurance maximum assumed), and the cost of training new personnel[53][54][61]. The survivor benefits are based on 55% of expected retirement salary with an estimated 20 year payout. That is crew pay * 50% retirement income * 55% survivor benefit * 20 years, which is $97,644[62] * 50% * 55% * 20 years = $537, 042.

$$C_C = (death\ gratuity + life\ insurance + survivor\ benefit\ plan + Cost\ of\ training) * HR_{Asset} \quad (26)$$

$$C_C = (2 * (\$12{,}410 + \$400{,}000) + \$537{,}042 + \$1{,}100{,}000) * 0.008169$$

$$C_C = \$20{,}111$$

The cost of the replacement helicopter is estimated as follows:

$$C_V = Acq^P * HR_{Asset} \quad (27)$$

$$C_V = \$31M * 0.008169 = \$253,239$$

Based on the previous discussion, the cost of collateral damage is difficult to estimate and will be left out of the calculation of ROI.

Avoided Costs

Bringing the above estimates back to the cost avoidance equation, the total avoided costs may be calculated as:

$$\Delta C_A = \Delta M_{US}^{CBM} + \Delta C_C + \Delta C_V + \Delta C_{MO} + \Delta C_R + \Delta C_D - Acq^{CBM} \quad (28)$$

$$\Delta C_A = \$1.45M + \$20,111 + \$253,239 + \$4,429 + \$3,676 - \$252,885$$

$$\Delta C_A = \$1,475,570$$

Investment Costs

In 2015, Simmonds Precision Products (dba Goodrich Sensors and Integrated Systems) was awarded a DoD contract for $8,092,320 for the procurement of 32 Integrated Mechanical Diagnostics and Health Usage Monitoring System (IMD-HUMS) kits. This equates to a cost of $252,885 per kit. The development cost for the IMD-HUMS system is difficult to determine as this technology was first developed under a DoD Commercial Operations and Support Savings Initiative (COSSI) award, whereby an existing commercially available system (Goodrich's IMD-HUMS) was proven to work on two defense articles, the CH-53E and SH-60B. After this initial program, Goodrich performed a follow-on program to adapt the existing IMD-HUMS platform to the H-1 drivetrain. Therefore, trying to determine actual development costs of the IMD-HUMS system is not feasible. However, it can be assumed that some of the non-recurring costs, as well as the recurring costs are included in the cost of the kits. Therefore, the kit cost can be applied to a single vehicle with an estimated failure and replacement rate to finalize the non-recurring and recurring costs, as follows:

$$C_{NRE}^{PHM} + C_{REC}^{PHM} = Acq^{CBM} * (1 + FR_{CBM}) \quad (29)$$

Furthermore, information relating to the reliability of the IMD-HUMS system is not readily found through a web research. However, for the sake of the analysis, we will assume that 80% of the system has to be replaced during the course of the platform service life. This would equate to replacing some sensors, 1 to 2 harnesses and the IMD-HUMS main processing unit. So the above equation becomes:

$$C_{NRE}^{PHM} + C_{REC}^{PHM} = \$252,885 * (1.8) = \$455,193 \quad (29)$$

For the infrastructure costs to maintain the data warehouse, continuously evaluate and update CBM algorithms, etc., the costs are estimated based on commercial rates for data storage and two engineers working halftime to support the CBM program. In order to estimate costs, the data was assumed to include the entire fleet of H-1 aircraft (approximately 330). averaging 28 hours of flight time per month, and collecting data at a rate of 1 GB per hour. Further, it was assumed that data would be kept for no more than 10 years. Therefore, the necessary storage requirement was calculated to be approximately 1 Petabyte (PB) of data. Utilizing published rates for the Amazon S3 storage[63], the average monthly cost for 1 PB of storage is approximately $492/month. Therefore, for a single vehicle, across 30 years, the cost equates to $537. Assuming reports are run once daily on the previous day's data and it takes roughly 1 hour on a virtual machine with 1 Nvidia Tesla V100 GPU, and SMEs run other reports and analysis for another 2 hours per day, then the total usage is 3 hours per day for 21 work days in the month. An Amazon EC2 P3 instance with the single Nvidia Tesla GPU would cost $3.06 per hour[64]. Therefore, processing would add another $193 per month for all assets which breaks down to an added lifetime cost of $211 per asset. Therefore, the total lifetime infrastructure costs for a single asset is $703. The final CBM investment costs for the H-1 helicopter gearbox are shown in Table 9.

Table 9 - H-1 Helicopter Gearbox CBM Investment Costs

Investment Cost Component	***Abbreviation***	***Cost***	***Notes***
Combined recurring and non-recurring costs	$C_{NRE}^{PHM} + C_{REC}^{PHM}$	$455,193	Estimated from IMD Hums Kit costs
Infrastructure costs	C_{INF}^{PHM}	$703	Estimated based on commercial storage and processing costs

IMD-HUMS Estimated ROI

Utilizing the above estimates of cost avoidance and investment costs, the overall ROI of the IMD-HUMS system may be estimated as follows:

$$ROI = \frac{\Delta C_A}{I} \tag{3}$$

$$ROI = \frac{\$1{,}475{,}570}{\$455{,}193 + \$703} = 3.237$$

With a positive ROI, this states that the system provides a positive return on investment across the life of the platform. This application of CBM is beneficial, even if not accounting for all of the other factors aside from maintenance savings. The maintenance savings from the CBM system dominates all other factors in the equation.

2.2.4.4.2 Return on Investment for an FMTV Transmission CBM System

Other applications of vibration monitoring may not provide as beneficial an ROI, so the goal of this analysis is to evaluate the utilization of vibration monitoring in a non-traditional application, ground vehicle

gearboxes. Traditionally, ground vehicles have not included vibration monitoring due to the expense of the capability vs. the benefit on a less expensive platform with lower risks to human life. However, the lower cost MEMS sensors may open the door to this capability. This section will evaluate the ROI of vibration monitoring applied to an Army FMTV transmission. The evaluation will attempt to estimate costs for a more traditional piezo based vibration monitoring system and compare them to a potential MEMS based system.

The FMTV is a family of tactical trucks designed for multiple configurations and uses. As procurement contracts include a variety of configurations, the cost assessment will utilize an average cost per platform. Additionally, all vehicles are assumed to have a similar planned service life of 20 years. Utilizing a few procurement contracts for trucks and trailers, a blended truck acquisition rate was determined to be approximately $179,251[65]. The fleet size of the FMTV vehicles is approximately 114,500 trucks and trailers. Assuming an 80/20 mix of trucks to trailers, there would be approximately 91,600 trucks in the fleet.

From analysis performed under the previous research project[29], it was determined that two transmissions were replaced in the field out of a smaller population of 521 vehicles over 2.35 years. Although this is a much smaller sample size, assuming the data extrapolates to the fleet, this is equivalent to 2,993 transmissions across the fleet in 20 years, representing a 3.27% chance of a transmission failure during a vehicles lifetime. The necessary data for the ROI calculations is gathered in Table 10, with further explanations and calculations following the table.

Table 10 - FMTV Transmission CBM ROI Analysis Costs

Cost Component	***Abbreviation***	***Cost***	***Notes***
Platform Cost	Acq^{p}	*$179,251*	*FMTV Cost, see above*
CBM System Cost	Acq^{CBM}	*~$30,000*	*Estimated based on the cost of the Marine Corps Embedded Platform Logistics System*[66], [67]*)*
CBM+ Maintenance Cost Savings	ΔM_{US}^{CBM}	*$495*	*Calculated below, Savings estimated from previous research*[29]
Cost of Mission objective	ΔC_{MO}	*$438*	*Calculated below*
Cost of Recovery	ΔC_{R}	*$439*	*Calculated below*
Cost of Crew Loss	ΔC_{C}	*$128*	*Calculated below*
Cost of Vehicle Loss	ΔC_{V}	*$15*	*Calculated below*

CBM+ Maintenance Savings

The benefit of the CBM system for the purpose of this analysis are targeted at collection and analysis of vibration signals relative to the FMTV transmission. The cost of transmission replacement in the FMTV, including the transmission components and the cost of labor, is approximately $20,189. Assuming that a

CBM system can prevent 75% of the failures, the average maintenance savings per asset would be calculated as follows:

$$\Delta M_{US}^{CBM} = FR * 0.75 * M_{TR} \quad (30)$$

Where:

$\Delta M_{US}^{CBM} = Delta\ cost\ between\ maintenance\ with\ CBM\ and\ and\ uncheduled\ maintenance\ regime$

$FR = Failure\ Rate\ without\ CBM$

$M_{TR} = Maintenance\ cost\ for\ a\ transmission\ replacement$

Thus:

$$\Delta M_{US}^{CBM} = 0.0327 * .75 * \$20{,}189 = \$495$$

This savings is relatively low due to the already low probability of replacement. However, further analysis is necessary to determine if the additional cost factors will impact the possibility of a positive ROI.

Additional Cost Consideration

The cost of the loss of mission objective relative to an FMTV mission is difficult to estimate. The truck may be hauling critical material in a war zone, or could be out on a simple training mission. Once again, we can assume that the mission would need to be repeated. So, the first assumption is that the mission requires two crew members and ¾ of the fuel capacity to complete the mission. This would equate to 225 miles, at an average of 35 mph, or 6.4 hours * 2 = 12.8 hours.

$$C_{MO} = ((Mission\ duration * Hourly\ crew\ Rate) + (Fuel * Fuel\ Cost)) * FR \quad (31)$$

Where:
C_{MO} = Cost of the loss of the mission objective
$Hourly\ crew\ Rate = Assumed\ to\ be\ \$35/hr$
$Fuel\ Cost = \$400/gal$[68]

Thus:

$$C_{MO} = \big((12.8 * \$35) + (43.5 * \$400)\big) * (0.0327 * 0.75) = \$438$$

With the same 75% reduction in failures, there would be a savings of $438 in loss of mission objectives.

The cost to recover the vehicle is assumed to require two personnel and a wrecker. The time for recovery is assumed to be the same as the original mission time, plus 1 hour for hooking the vehicle up for recovery. This assumes the vehicle on average is halfway to its objective when failure occurs. So, the cost of recovery is very similar to the cost of losing the mission objective, with the exception of two additional man hours.

$$C_R = ((Recovery\ duration * Hourly\ crew\ Rate) + (Fuel * Fuel\ Cost)) * FR \quad (32)$$

$$C_R = \big((14.8 * \$35) + (43.5 * \$400)\big) * (0.0327 * 0.75) = \$439$$

The savings from not needing to perform vehicle recovery would average $439.

The cost of loss of life due to a transmission failure in an FMTV is significantly lower than the previous example for an H-1 helicopter gearbox. The risk to the crew is twofold, either the vehicle becomes disabled in a high risk, combat environment and puts the crew in jeopardy, or the vehicle suffers a catastrophic crash due to the transmission failure. The likelihood of either event can be considered reasonably low. The following assumptions are made to calculate the cost of loss of life: 1) the CBM+ system captures 75% of the potential failures and 2) only 1% of the remaining failures would result in the loss of a vehicle and crew. Based on the earlier equation:

$$HR_{Asset} = failure\ rate * P_C \quad (8)$$

Where:

$$P_C = CBM\ Miss\ Rate * Rate\ of\ loss \quad (25)$$

Therefore:

$$HR_{Asset} = 0.0327 * 0.25 * 0.01 = 0.00008175$$

This is the rate at which the vehicle may be lost, which can be applied to the cost of the vehicle and crew, assumed to be two people. The cost of the loss of crew includes death gratuity, survivor benefits, insurance (service members group life insurance maximum assumed), and the cost of training new personnel[53][54][69]. The survivor benefits are based on 55% of expected retirement salary with an estimated 20 year payout. That is crew pay * 50% retirement income * 55% survivor benefit * 20 years, which is $55,020[55] * 50% * 55% * 20 years = $302,610.

$$C_C = (death\ gratuity + life\ insurance + survivor\ benefit\ plan + Cost\ of\ training) * HR_{Asset} \quad (26)$$

$$C_C = (2 * (\$12{,}410 + \$400{,}000 + \$302{,}610 + \$65{,}000)) * 0.00008175$$

$$C_C = \$128$$

The cost of the replacement FMTV is estimated as follows:

$$C_V = Acq^P * HR_{Asset} \quad (27)$$

$$C_V = \$179{,}251 * 0.00008175 = \$15$$

Based on the previous discussion, the cost of collateral damage is difficult to estimate and will be left out of the calculation of ROI.

Avoided Costs

Bringing the above estimates back to the cost avoidance equation, the total avoided costs may be calculated as:

$$\Delta C_A = \Delta M_{US}^{CBM} + \Delta C_C + \Delta C_V + \Delta C_{MO} + \Delta C_R + \Delta C_D - Acq^{CBM} \quad (28)$$

$$\Delta C_A = \$495 + \$128 + \$15 + \$438 + \$439 + 0 - \$30{,}000$$

$$\Delta C_A = -\$28{,}485$$

Estimated ROI of an FMTV transmission vibration monitoring system

Based on the ROI equation, below, and the negative avoided costs calculated above means that the ROI will be negative.

$$ROI = \frac{\Delta C_A}{I} \quad (3)$$

However, the entire cost of a CBM system is being compared to only one system fault. The same system could probably detect multiple faults across the engine, transmission, brakes and other automotive systems. Instead, in the next analysis, we evaluate the ROI of adding vibration monitoring of the transmission to an existing CBM system.

2.2.4.4.3 Return on Investment when adding capability to an existing CBM system

The above example of vibration monitoring for an FMTV transmission is likely a capability that could be added to an existing CBM system. In this section, we analyze the incremental benefit and cost of the capability to determine if the added capability has a positive ROI. The majority of the information in the previous section is still applicable; however, the cost of the CBM system will be adjusted to only evaluate the cost of the added vibration monitoring equipment, as shown in

Table 11.

Table 11 - FMTV Vibration Monitoring Add-on ROI Costs

Cost Component	***Abbreviation***	***Cost***	***Notes***
Platform Cost	Acq^P	*$179,251*	*FMTV Cost, see previous section*
CBM System Cost	Acq^{CBM}	*~$1,010*	*Calculated below*
CBM+ Maintenance Cost Savings	ΔM_{US}^{CBM}	*$495*	*See previous section*
Cost of Mission objective	ΔC_{MO}	*$438*	*See previous section*
Cost of Recovery	ΔC_R	*$439*	*See previous section*
Cost of Crew Loss	ΔC_C	*$128*	*See previous section*
Cost of Vehicle Loss	ΔC_V	*$15*	*See previous section*

Vibration Capability Cost

It is assumed that the platform has an existing CBM+ system capable of collecting the existing vehicle databus information. For adding vibration monitoring to the platform, it is assumed that the system consists of MEMs vibration sensors, a low cost data acquisition unit, a Jetson Nano for performing machine learning calculations, and mounting hardware and cabling. For a 3-axis vibration monitoring system, three ADXL1002 devices ($84) will be utilized along with a 5-channel USB analog data acquisition unit ($459), and a Jetson Nano ($99). The additional hardware and cabling is estimated to be an additional $200. The total cost to add the vibration monitoring is $1,010.

Avoided Costs

Updating the prior avoided cost calculation to evaluate only the cost of adding the vibration monitoring capability results in a positive avoided cost:

$$\Delta C_A = \Delta M_{US}^{CBM} + \Delta C_C + \Delta C_V + \Delta C_{MO} + \Delta C_R + \Delta C_D - Acq^{CBM} \quad (28)$$

$$\Delta C_A = \$495 + \$128 + \$15 + \$438 + \$439 + 0 - \$1{,}010$$

$$\Delta C_A = \$505$$

Investment Costs

Although the cost of the hardware can be estimated easily, the development of the CBM algorithms that would process the data is much more difficult to estimate. Assuming an upfront engineering effort of $5,000,000 to create the design package and algorithms for the system, across the assumed 91,600 vehicles, this is a cost of $55 per vehicle. Similar to the analysis of the IMD-HUMS investment costs, assume the non-recurring cost and recurring costs can be partially represented by the procurement and replacement costs as:

$$C_{NRE}^{PHM} + C_{REC}^{PHM} = Acq^{CBM} * (1 + FR_{CBM}) + \text{Additional engineering effort} \quad (33)$$

Furthermore, assuming reliability of the vibration monitoring system similar to the IMD-HUMS results in 80% of the system being replaced during the course of the platform service life. This would equate to replacing some sensors, 1 to 2 harnesses, and the data acquisition unit. So the equation above becomes:

$$C_{NRE}^{PHM} + C_{REC}^{PHM} = \$1{,}010 * (1.8) + \$55 = \$1{,}873$$

For the infrastructure costs to maintain the data warehouse, continuously evaluate and update CBM algorithms, etc., the costs are estimated based on commercial rates for data storage and two engineers working halftime to support the CBM program. We are assuming the same numbers as the helicopter example because although there are more platforms, there are fewer sensors and fewer critical failures. In order to estimate costs, the data was assumed to include the entire fleet of FMTV vehicles (approximately 96,100), averaging 30 operating hours per month, and collecting data at a rate of 1/3 GB per hour. Further, it was assumed that data would be kept for no more than 5 years. Therefore, the necessary storage requirement was calculated to be approximately 52 Petabytes (PB) of data. Utilizing published rates for the Amazon S3 storage[63], the average monthly cost for 52 PB of storage is approximately $25,582/month. Therefore, for a single vehicle, across 30 years, the cost equates to $96. Assuming reports are run once daily on the previous days data and it takes roughly 3 hours on a virtual machine with 1 Nvidia Tesla V100 GPU, and SMEs run other reports and analysis for another 3 hours per day, then the total usage is 6 hours per day for 21 work days in the month. An Amazon EC2 P3 instance with the single Nvidia Tesla GPU would cost $3.06 per hour[64]. Therefore, processing would add another $386 per month for all vehicles, which breaks down to an added lifetime cost of $2. Therefore, the total lifetime infrastructure costs for a single platform is $98. The total investment costs for the FMTV transmission CBM system are shown in Table 12.

Table 12 - FMTV Transmission CBM Investment Costs

Investment Cost Component	***Abbreviation***	***Cost***	***Notes***
Combined recurring and non-recurring costs	$C_{NRE}^{PHM} + C_{REC}^{PHM}$	$1,873	Estimated from hardware and engineering costs
Infrastructure costs	C_{INF}^{PHM}	$98	Estimated based on commercial storage and processing costs

Vibration Monitoring Estimated ROI

Utilizing the above estimates of cost avoidance and Investment costs, the overall ROI of the IMD-HUMS system may be estimated as follows:

$$ROI = \frac{\Delta C_A}{I} \quad (3)$$

$$ROI = \frac{\$505}{\$1{,}873 + \$98} = 0.256$$

With a positive ROI, this states that the system provides a positive return on investment across the life of the platform. This application of vibration monitoring has shown that adding vibration data capture and processing capability to an existing vehicle CBM system provides a positive benefit. However, the negative ROI from Section 2.2.4.4.2 shows that the burden of cost of an entire CBM system cannot be justified by evaluating the potential to detect transmission failures only.

2.3 Potential Future Research

The utilization of low cost sensors and GPUs for vibration monitoring in mobile ground assets has been shown to have significant potential to CBM+. The major next step in the technology is the further demonstration of an integrated system on a platform. The integration of the data acquisition system with a GPU for vibration monitoring of multiple vehicular system, such as engine, transmission, alternator, or hydraulic systems would significantly increase the amount of data available for CBM analysis. Of significant interest are rotational systems that currently lack any significant data for analysis (e.g. alternator, hydraulic pumps) on the existing vehicle databus.

2.4 Training Opportunities

RCM is a process for developing maintenance practices to reduce costs and increase uptime. Multiple RIT personnel were involved in the RCM process for the Cummins engine, which was facilitated by a trained RCM professional. Personnel learned how to properly apply RCM principles to a system, specifically targeting condition monitoring outcomes.

Significant progress has been made in understanding the techniques for the application of autoencoders. The proper design and application of autoencoders is sometimes referenced as an art form that requires significant experience to master, which this project has provided.

2.5 Results Dissemination

RIT is presenting two papers at the 14th Annual Conference of the Prognostics and Health Management Society. The papers are titled, "Feasibility of Low-cost Vibration Monitoring for Ground Vehicles" and "Evaluation of NVIDIA Jetson System for Vibration HUMS," and cover the utilization of new technolgoies in vibration montioring for CBM+.

3 Gear Prognostics Research

3.1 Research Goals and Objectives

The Gear Prognostics subproject is focused on the fusion of vibration and oil quality monitoring data to enhance the detection horizon of existing gear prognostics. The subproject seeks to improve anomaly detection by exploiting advances in deep learning, while leveraging emerging, sophisticated, state-of-the art frameworks. This Gear Prognostics subproject has three major objectives:

1) Extend data-driven anomaly detection based on representation learning to more complex gearboxes, such as planetary systems;

2) Further enhance vibration based data-driven approaches with gearbox oil analysis data and pave the way to the subsequent layers of PHM capability, viz. diagnostics and prognostics;

3) Investigate means of adding diagnostic and prognostics capability, including algorithm refinement as more failure data becomes available, equipped with labels associated with the failure modes.

3.1.1 Research team

The research team that worked on this subproject consisted of engineers from Navair, researchers from Navy Research Laboratory (NRL) and Army Research Laboratory (ARL), and researchers, engineers, technicians, and students from RIT.

Navair provided some fleet data, collaborated on developing of automation of some of the human in the loop tasks, actively participated in analyses during the project performance period, and collaborated on publications. Navair has been very effective in using the human-in-the-loop approach to manage the health of their fleets. The health and usage monitoring systems (HUMS) use multiple accelerometers and 60+ condition indicators (CIs). With conservatively set thresholds followed by engineering validation and interpretation, the existing system has been very reliable. Many examples of bearing failures were observed but gear failures are very rare, which reduces the confidence of the engineering interpretation, especially related to breakage, the most harmful of the four gear failure modes (breakage, wear, pitting, and scuffing), as it comes with little to no advanced warning.

NRL performed oil analyses, provided their expertise during the redesign of the lubrication system of the RIT gear test stand, interpreted particles during progression of damage experiments, used some of the vibration data for testing their algorithms, and collaborated on publications. NRL was particularly interested in oil monitoring and oil analyses, especially related to damage progression from scuffing to higher levels of damage.

ARL collaborated during the design of the test process and development of data-driven, representation learning models, and collaborated on publications. ARL has a long tradition in studying CIs for gear fault diagnostics and had multiple prior collaborations with RIT.

3.2 Research Accomplishments

Two main activities associated with gear PHM research can be classified in continued research: 1) anomaly detection and their extensions towards higher PHM capabilities and 2) integration of oil and vibration monitoring. The first activity aligns with the first and third subproject objectives, and the second activity aligns with the second objective. These activities are discussed in turn.

3.2.1 Extending anomaly detection capabilities

The original objective was to apply data driven methods on more complex gearboxes operated by Navair. However, because the test stand at Cherry Point Naval base was not fully operational for the most of the project performance period and because of the general reluctance to run seeded failures on production test stands, the research team decided to expand the capabilities using the existing test stand at RIT. However, the RIT test stand was not equipped for operating complex gearboxes without significant modification, and the modifications planned for this subproject focused on modifying the oil line. To illustrate the limitation of the newly-generated test data, the team applied the modeling approach on a small anonymized set of HUMS data (see Section 3.2.1.3). Extending anomaly detection capabilities was pursued by collecting additional samples of the gears' baselines, followed by crack propagation. The data was collected using the process developed in Section 3.2.1.1. The main approach was purely data-driven, based on deep learning autoencoders, using classical, engineered vibration-based CIs as a reference. The

description of the approach is provided in Section 3.2.1.3 and the work that facilitated comparison with CI computations is described in Section 3.2.1.4. One of the major findings revealed that employing multiple baselines can pave the path to higher level PHM capabilities (beyond anomaly detection), viz. damage assessment and prognostics.

In addition, as part of this activity, RIT also examined subset of fleet data from real assets in collaboration with Navair. The data-driven methods found results consistent with the ground truth.

3.2.1.1 Crack initiation/crack propagation test process and data collection

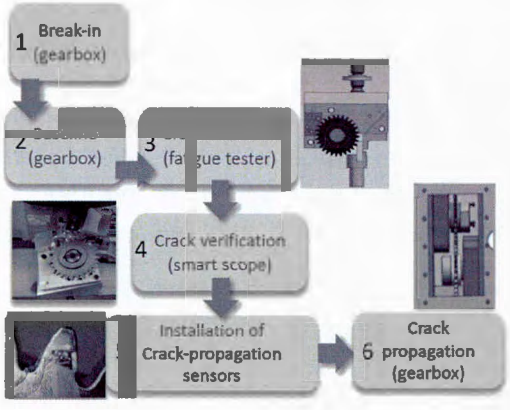

Figure 9: Block diagram of the fatigue tooth breakage process

Figure 9 depicts the test process which consisted of: 1) break-in (low-torque, low-speed) eight hour run, 2) multiple baseline (nominal torque, nominal speed) two hour runs 3) crack initiation [70], 4) crack verification, 5) installation of crack-propagation sensors, and 6) crack propagation until failure. The baseline and propagation runs were executed under the same operating conditions to ensure that that condition indicators were comparable (i.e. do not violate the fundamental axioms of health monitoring [71]). The propagation was carried out only until both cracks propagate to both crack-propagation (CP) sensors, which corresponded to crack propagated to about 50% through a tooth.

Initially, only one baseline test was run for a gear pair, but the last gear crack experiment employed multiple baseline runs, which turned out to be very important for extending capabilities using data-driven methods. This change was made after the observation that anomaly detectors can seem to be almost "too good to be true" because their error was fully separable between data associated with baseline validation data and propagation test data. The first test was a modified tooth breakage test, carefully designed to expand upon previous single-baseline tooth breakage tests. Multiple baselines were introduced to better understand the performance of autoencoders; the models trained on a subset of baselines were then evaluated on the remaining baselines and propagation. To further test if the model can distinguish between damage and small gearbox perturbations, the last two baselines included partial gearbox disassembly.

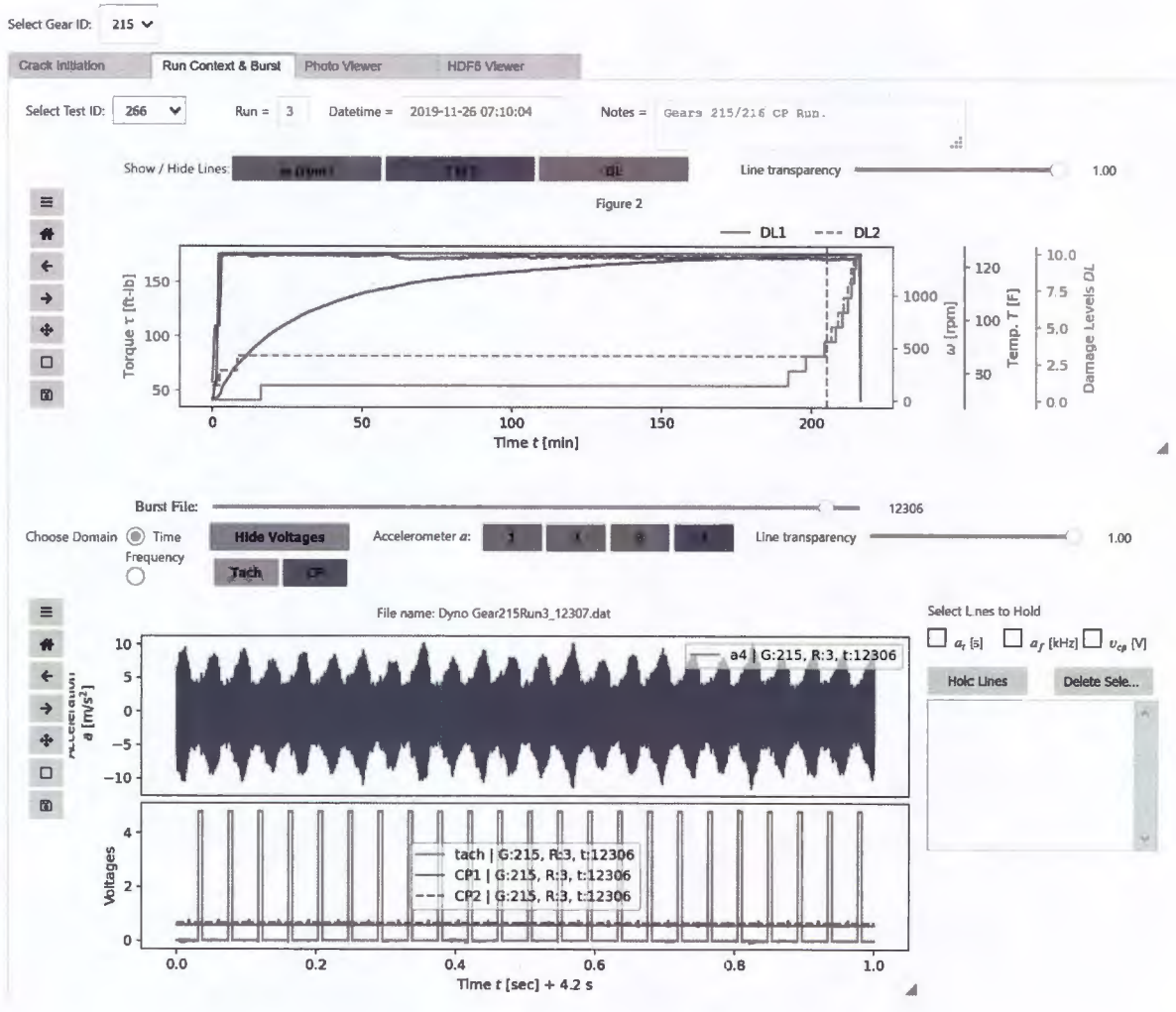

Figure 10: Visualization of the test data

Testing capabilities included development of the software visualization for different test stages: crack initiation, crack propagation, and gear crack surface examination. The tool was developed in Python Scientific Ecosystem (see Figure 10) using standard libraries, e.g. NumPy [72], Matplotlib [73], IPython [74] (in its Jupyter Lab version).

The legacy storage system, comprised of MySQL database (refer to Figure 11 for the schema) and binary files for high-resolution data, was extended with well-organized and documented HDF5 files. These files were created to accelerate model development and facilitate sharing the data among researchers. For example, the data was shared with Navair and ARL to enable reproduction of modeling results. It was also shared with NRL to enable exploring alternative models.

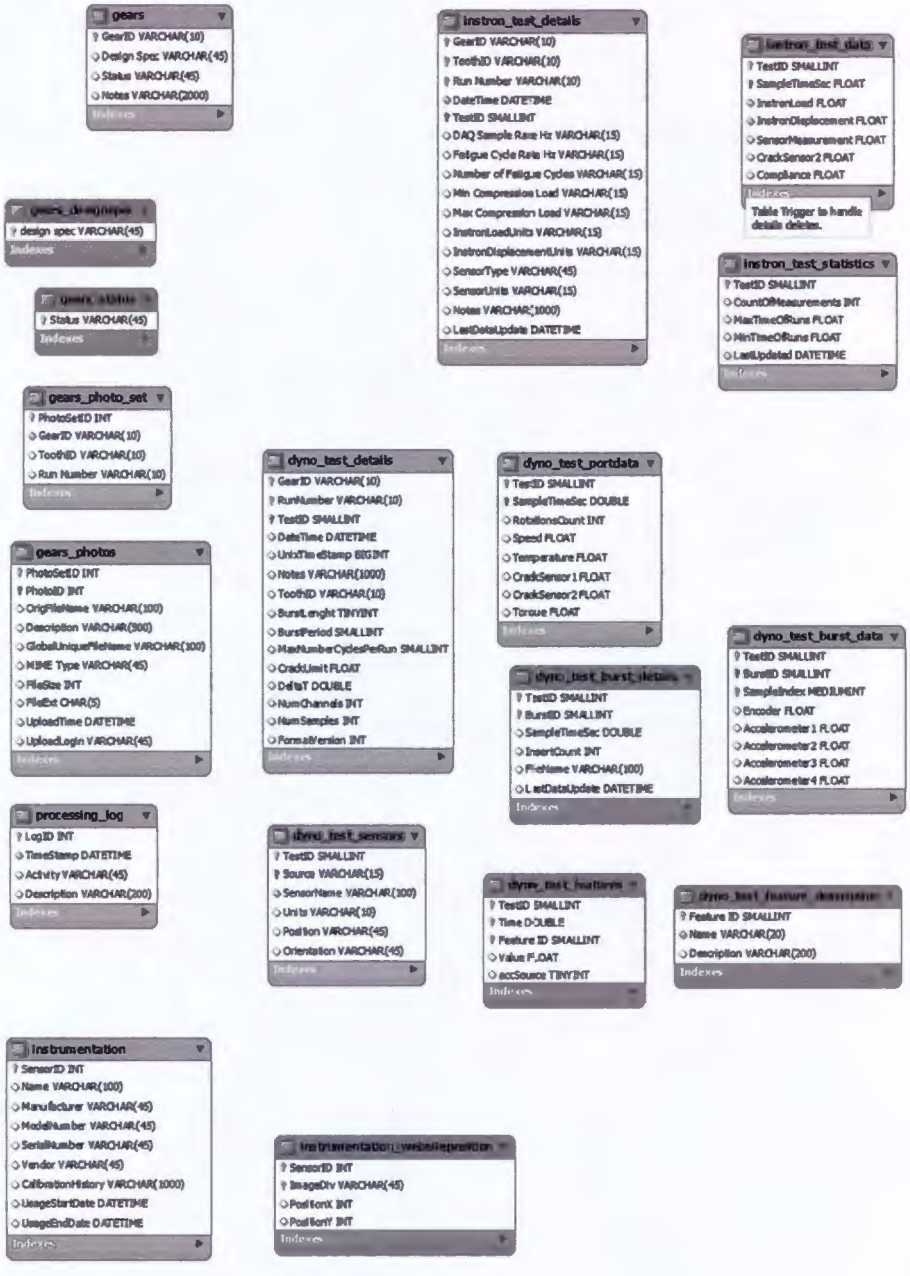

Figure 11 MySQL table organization

The HDF5 data stores consisted of two types: Type 1 and Type 2. Type 1 was lossless and consisted of raw vibration and tachometer data, contextual information (torque τ, speed ω, and temperature T), and state of damage – processed CP data and inferred states of damage, viz. DL_1 and DL_2 (see Section 3.2.1.2 for the definition of damage levels). Type 2 files are compressed files prepared for accelerated machine learning development. Type 2 is very similar, differing only in how vibration information is stored: instead of raw data, Type 2 stores TSA data. TSA was computed using accelerometer data and a tachometer to average over multiple shaft rotations, effectively converting time-domain data into angle domain data in

the range $0 \leq \phi \leq 2\pi$. An accelerometer vector $\boldsymbol{a}(t)$ with length of 100,000 (=10^5), associated with one second of operation, was compressed into the TSA vector $\boldsymbol{x}_{TSA}(\phi)$ with a length of 4,096 (=2^{12}) points. Twenty-four revolutions were used for the average. More details on TSA processing can be found in [75]. Type 1 HDF5 files can be used to produce different TSA processing by changing the length of TSA vectors and number of rotations.

3.2.1.2 Ground truth inference

There are two parts of ground truth: 1) binary information on presence of a crack, and 2) level of damage. The presence of a crack is included in the crack-propagation data capture (see the test process in Figure 9) and required no additional processing. The information of the state of damage is less direct and needed to be inferred.

State of damage inference was estimated from CP sensors. Earlier work on estimation of damage level using CP sensors was reported in [76]. In this project, this process was slightly modified. The first step is to determine the state of crack from the CP sensors. As the crack propagates, it snaps wires of the CP sensor, which result in an increased voltage. Table 13 lists the *nominal* CP voltage levels and the associated state of the CP sensor, denoted as the *damage level DL.*

Table 13: Nominal CP voltage vs. damage levels

CP voltage v_{CP} [V]	Damage level DL
5.000	10
1.667	9
1.000	8
0.714	7
0.556	6
0.455	5
0.385	4
0.333	3
0.294	2
0.263	1
0.238	0

The CP voltage is simply the voltage divider between the pull-up resistor R_o and the resistance of the CP sensor R_{CP}

$$v_{CP} = \frac{R_{CP}}{R_o + R_{CP}} V_s \tag{34}$$

where V_s is the supply voltage set at 5 VDC in this application. R_{CP} is a function of wire resistance of a single wire R_w and the number of unbroken wires m

$$R_{CP} = \frac{R_w}{m} \tag{35}$$

where

$$m = 10 - DL \tag{36}$$

Inserting Eq. (35) into Eq. (34) yields

$$v_{CP} = \frac{1}{1 + mR_o/R_w} V_s \tag{37}$$

which can be solved for m

$$m = \frac{R_w}{R_o}\left(\frac{V_s}{v_{CP}} - 1\right) \tag{38}$$

and expressed directly as DL using Eq. (36)

$$DL = 10 - \frac{R_w}{R_o}\left(\frac{V_s}{v_{CP}} - 1\right) \tag{39}$$

Eq. (39) was used for a regression of the damage levels given measured v_{CP} and V_s. It often produced good results, as illustrated in Figure 12.

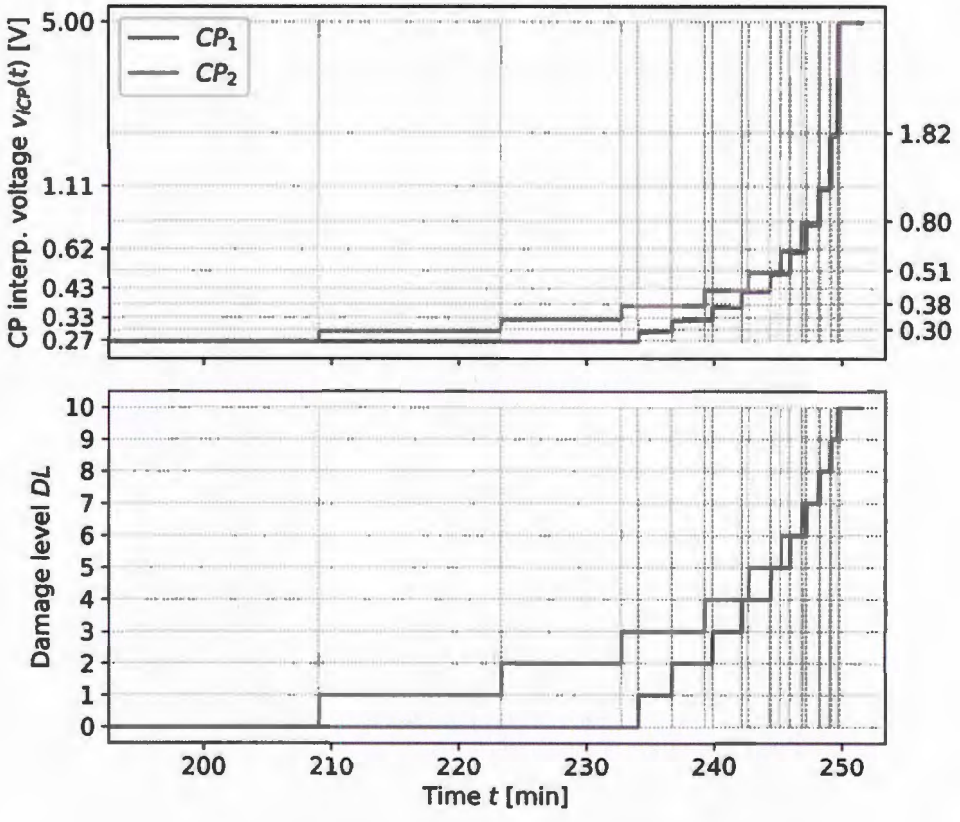

Figure 12 Crack propagation as measured with CP sensors

However, when there was noise in the data, especially for lower levels of damage that differ only in a few tens of millivolts, the above approach was not sufficient and Bayesian inference worked considerably better. Because the noise does not play a significant role for high-levels of damage, the process was developed to proceed backwards, from high to low levels of damage. A sliding window of size N was used to compute probabilities of that window being part of a damage level DL and a state transition ST between damage levels (refer to Figure 13). The output is a vector of labels at each time index for damage level. The prior knowledge consisted of 1) expected voltage at each damage level, with an assumed variance and 2) expected change in voltage from a transition in damage level, with an assumed variance.

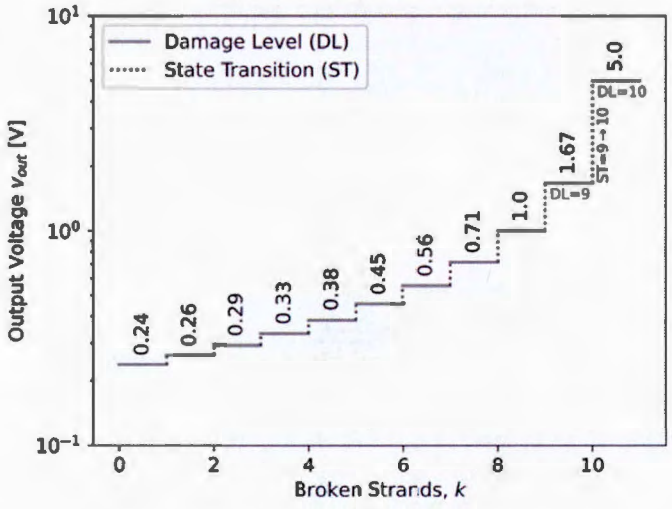

Figure 13 Damage levels and state transitions

Algorithm

1. Reverse order of data of cp voltage: `cp_r = cp[::-1]`
2. Take the first N points: `vs = cp_r[:N]`
3. Compute probability of each damage level based on the observed voltage ($\langle v_{CP} \rangle_N$): `v_obs = np.mean(vs)`
4. Set damage level to level with maximum probability from 3.
5. Compute change in voltage in `vs`: Two options,
   A. Endpoints `Δv_obs = (abs(vs[-2:] - vs[:2])).mean()`
   B. Range `Δv_{obs} = np.ptp(vs)`
6. For each possible transition to a different damage level, compute the probability that that transition occurs given the known damage level, and the observed change in voltage computed in 3:
   A. Compute likelihood of the state transition given the observed change in voltage and known damage level.
   B. Look up prior: Read from a custom made table, containing probabilities of transitioning from a given state to all others.
   C. Compute marginal_likelihood: Probability of the observed change in voltage and the known damage level. This is equal to the sum of the individual probabilities of a change in voltage given a transition from one damage level to another, for all possible transitions from the known damage level.
   D. Compute posterior_j for this DL_j value, using Bayes therom.
   E. Store in list of posterior probabilities for all DL_j.
7. Take DL_j which returns the maximium posterior_j. This is the most probable state transition given the likelihood and prior knowledge.
8. Save the location of the state transition to DL_j (Note: DL_j may be 0, indicating no state transition).
9. Repeat from step 2 by shifting the window of N points once. Continue until all points have been consumed.

Figure 14 Algorithm for Bayesian inference of damage levels from CP voltage

The damage level algorithm is provided in Figure 14. In Step 3, the damage levels were estimated as a function of the observed, average CP voltage

$$\Pr(DL_j|\langle v_{CP}\rangle_N) = \frac{\Pr(\langle v_{CP}\rangle_N|D_j)\Pr(DL_j)}{\Pr(\langle v_{CP}\rangle_N)} \tag{40}$$

In Step 6, the state transition between damage levels DL_i and DL_j was computed using

$$\Pr(ST_{i\to j}|DL_i, DL_j, \langle v_{CP}\rangle_N) = \frac{\Pr(\langle v_{CP}\rangle_N|ST_{i\to j})\Pr((ST_{i\to j}|DL_i, DL_j))\Pr(ST_{i\to j})}{\Pr(DL_i, DL_j, \langle v_{CP}\rangle_N)} \tag{41}$$

Gear crack surface area during the crack propagation was estimated from the estimated CP states, or damage levels DLs. Figure 15 illustrates the process. A cracked tooth instrumented with two CP sensors is shown Figure 15a, with curved cracked surface projection on the plane.

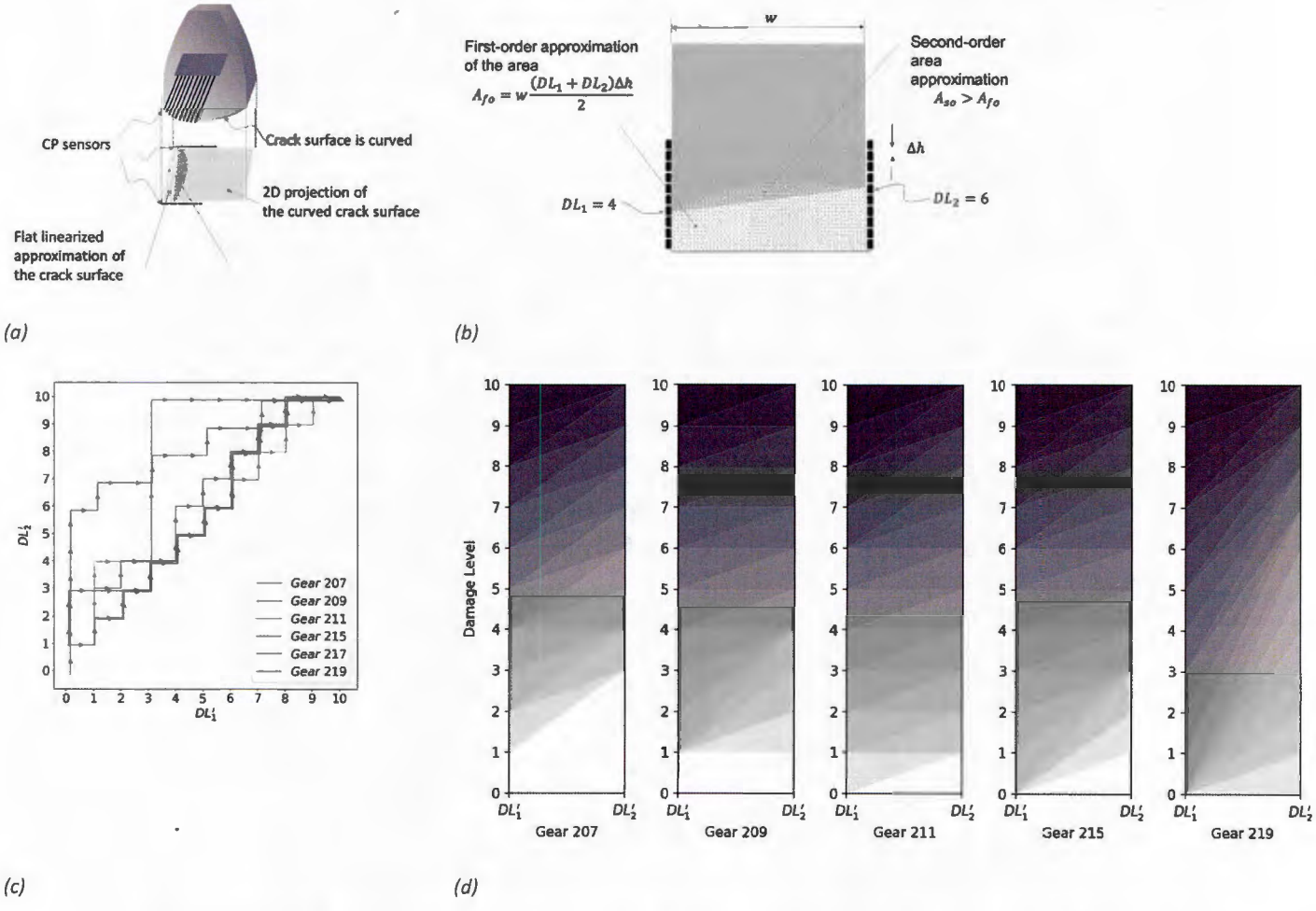

Figure 15 State of damage (a) cracked gear tooth instrumented with CP sensors with surface crack projected on a plane (b) estimation of the area of the crack projection (c) state of damage of gears as measured by cracked surfaces

Figure 15b shows the first-order approximation of the area of the cracked surface projected on the plane

$$A_{fo} \approx \frac{w(DL_1 + DL_2)\Delta h}{2} \tag{42}$$

where w is the depth of the tooth and Δh is the center-to-center distance between adjacent wires of a CP sensor.

Figure 15c and Figure 15d show two different views of the paths of the CP damage advancement during the propagation. Two new symbols were introduced DL' and DL'' defined as

$$DL' = \min(DL_1, DL_2)$$
$$DL'' = \max(DL_1, DL_2) \quad (43)$$

It is interesting to note that some cracks propagate more symmetrically than others. We observed that asymmetric cracks tend to propagate slower than symmetric cracks, which was also observed in prior work [76].

3.2.1.3 Data-driven approach and results

Traditionally, the time and effort associated with extracting effective features is the dominant activity in data-driven PHM. The key distinguishing factor in the success of machine learning approaches is feature engineering [77], which represents ≈90% of industrial machine learning [78]. The promise of modern deep learning approaches is that they can develop better representations directly from data, or with minimum feature engineering. Neural networks applications have a rich history in PHM, with an early successful deployment using autoencoder topology [79], preceding the recent deep learning revolution. In classical machine learning models, datasets have to be balanced and one must distinguish disk-large datasets with statistically large data sets [80]. In contrast, representation models can be learned, in principle, from the abundant and accessible normal data [81]. Autoencoders are currently viewed as the first-class models for anomaly detection [82], the first level of PHM.

A high-level approach to machine learning consists of two main steps: data preprocessing and model training. The diagram in Figure 16 shows the activities associated with the two main steps and their interactions.

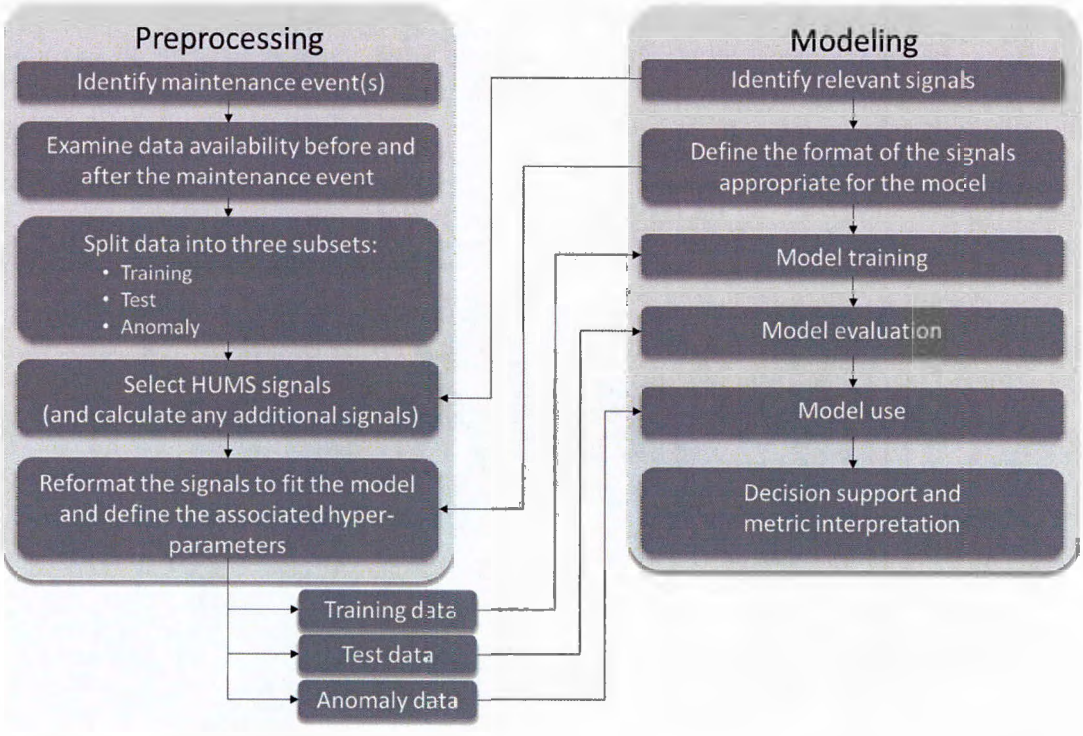

Figure 16: Preprocessing and modeling activities and their interactions.

The interactions between the modeling and preprocessing steps, depicted in Figure 16, suggest that a good way to perform these analyses was to develop an end-to-end workflow and identify hyperparameters – the parameters changed by analysts during the iterative process of model development. The following sections describe these activities in more detail in the context of developing a specific model.

In the present case, the process was greatly simplified, because the only available signal was TSA of vibration signal.

This approach can be illustrated using an anonymized asset Navair dataset, illustrated in Table 14, showing a summary of five TSA captures.

Table 14: A segment from Navair data

			TSA					
Gearboxes	Test run	Torque	0.00	0.04	0.09	...	359.91	359.96
G_o	0	22.62	-14.81	-15.47	-15.78	...	-13.83	-14.15
G_o	1	64.03	-35.25	-27.96	-19.86	...	-44.48	-41.00
G_o	2	19.97	1.68	5.23	8.28	...	-6.02	-2.35
G_o	3	82.56	-28.23	-34.76	-40.11	...	-14.08	-21.04
G_o	4	73.72	9.03	5.78	1.84	...	9.85	10.40

The TSA data is in the '0'-'359.96' columns, totaling 8192 (=2^{13}) data points per single capture. The nomenclature just specifies the degree of the shaft for that vibration value. However, the degrees have

no actual meaning. Zero for one data capture could be 50 for another, and 180 for the next. As such, the values are just a continuous stream that wrap back around to zero, and shifting the datasets to set min/max as the first value is a valid transformation to make learning a representation of a healthy TSA easier (the compressed representation then does not have to learn where to place the min/max value if you are learning via autoencoding).

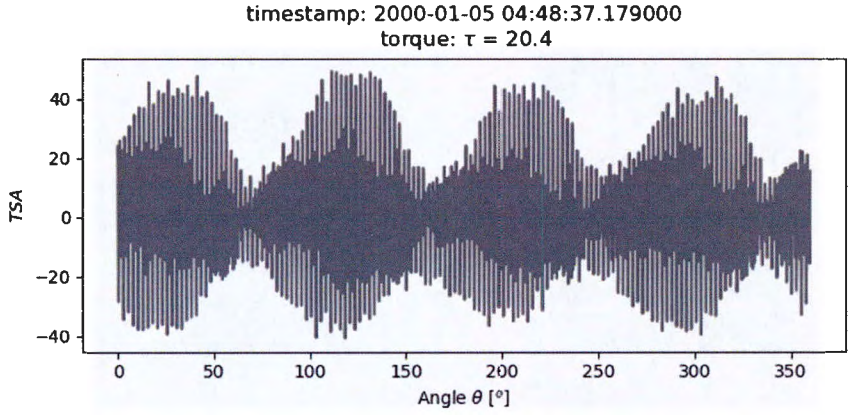

Figure 17: A representative TSA

Figure 17 shows a representative TSA, computed by averaging 200 revolutions (in contrast with the RIT test stand that averaged 24 revolutions), torque is expressed as a percentage. The observed pulsing across the 360 degree revolution is due to interaction between the planet and sub gears in the gearbox.

The goal was to be able to identify which TSA captures correspond to known planetary ring gear faults within the dataset by identifying outliers. All gear/shaft CIs are generated from the TSA, which represents the raw form of the complex gearbox data for modeling gear/shaft health.

Figure 18 summarizes data captures across the gearboxes over a period of time. The numbers indicates the total number of test runs.

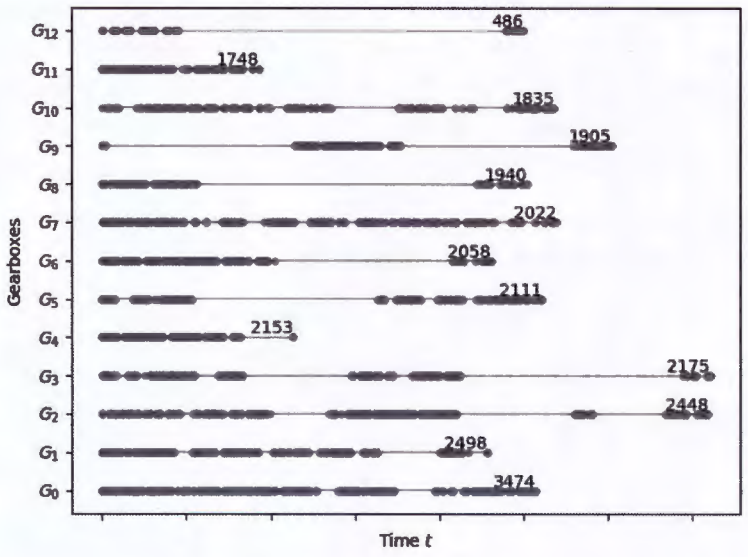

Figure 18: TSA captures across a set of georboxes

A simple CI (variance) identifies that there could be something wrong with G_{12}.

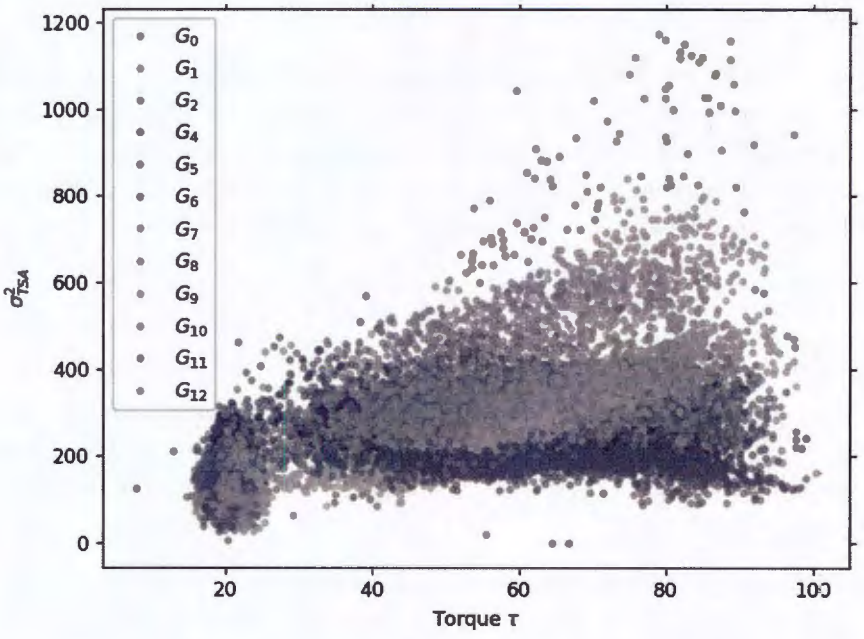

Figure 19: TSA variance vs. torque

The first objective of the analysis was to use this data set to design, train, and evaluate a machine learning model that can detect an onset of anomaly in $gearbox = 12$. Of many possible methods of approaching the problem, the following two were considered:

- Train an autoencoder DNN on a subset of data from a subset of assets (tails) and use the model across the fleet. This model will be referred to as the *fleet model*.
- Develop the model on one asset (e.g., the one with most data) first, then adapt it to any other asset (transfer learning) using *normal data*. This model will be referred to as *digital twin*, because it recognizes the individuality of assets.

We explored both approaches and compared and contrasted their advantages and limitations. At a high level the pros and cons of the two models are listed in Table 15.

Table 15: Fleet model vs. digital twin

Criteria	"Fleet" model	Digital twin model
Model development	+	-
Resolution	-	+
Ease of deployment	+	-
Sensitivity to operation	+	-

The model type and topology is independent of these consideration and the same model was used in both settings. The two methods are described in more details below.

Multi-layered perceptron (MLP) or a *dense* model is typically a starting point for any evaluation. This type of network is based on *fully connected* (FC) layers and are referred to here as *fully connected network* (FCN). A nuance here was to use not the entire TSA, but a vector created by concatenated multiple sub-vectors that had been sub-sampled. The length of the input vector N was a model hyperparameter. In the proposed scheme, the input vector $\overline{s}$ consisted of sub-vectors at different time scales $\overline{s}_{:k}$. For example,

$$\overline{s} = \left[\overline{s}_{:2^0}^T \ \overline{s}_{:2^1}^T \ \dots \ \overline{s}_{:2^M}^T\right]^T \tag{44}$$

where $\overline{s}_{:1}$ denotes a sub-vector of consecutive samples of the input data, $\overline{s}_{:2}$ denotes a sub-vector that takes every other point of the input data, and $\overline{x}_{:2^M}$ is a sub-vector decimated by 2^M. Each sub-vector probed into a specific time scale. The lengths of sub-vectors was another hyperparameter L and the number of time scales was $M = N/L$.

Sub-sampling can give rise to aliasing, so it is usually advisable to pre-filter the data before sub-sampling. Figure 20 illustrates an example of such input vector, showing four levels of sub-sampling: 0, 2, 4, and 8.

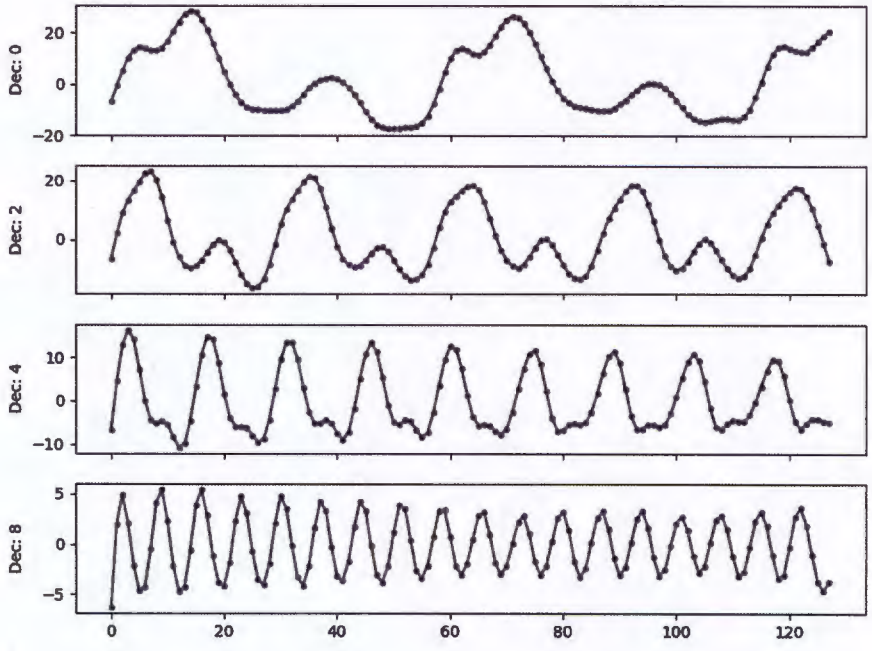

Figure 20: Example of sub-sampling with filtering.

Figure 20 shows the length of sub-vectors in the context of a single TSA capture. Multiple sub-vectors were drawn from a single TSA capture during training.

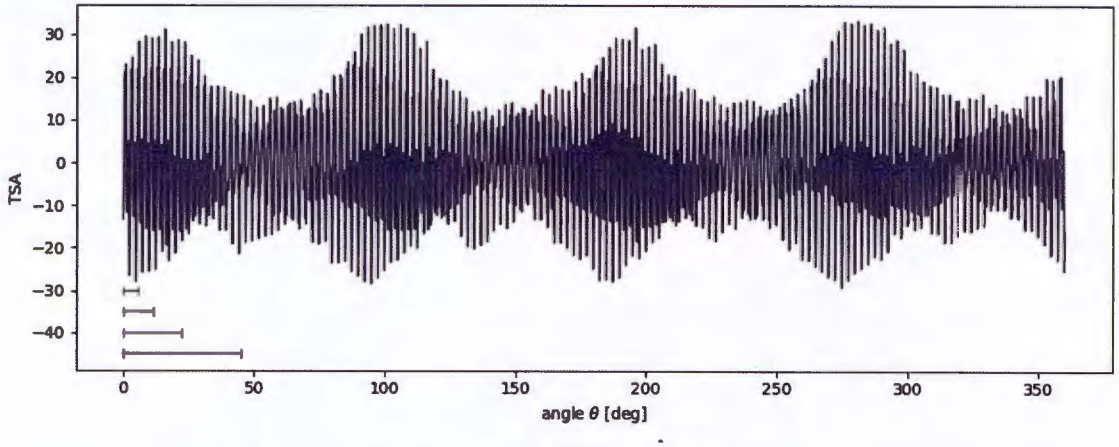

Figure 21: The sub-vectors in the context of a single TSA.

A conceptual view of the FCN topology is depicted in Figure 22. The neurons are full-connected, thus the output vector of the i^{th} layer $\overline{\phi}^{(i)}$ is obtained as a nonlinear transformation of an affine transformation of the output vector of the preceding layer $\overline{\phi}^{(i-1)}$:

$$\underline{\phi}^{(i)} = \mathrm{f}\left(\underline{\underline{W}}^{(i-1)}\,\underline{\phi}^{(i-1)} + \underline{b}^{(i-1)}\right), \tag{45}$$

where $\underline{\underline{W}}^{(i-1)}$ and $\underline{b}^{(i-1)}$ are the associated matrix of weights and the offset vector, respectively and f() is a nonlinear transformation. The most popular choice for f() is rectifier linear unit, or ReLU(), defined as

$$\mathrm{ReLU}(z) = \max(z, 0)\,. \tag{46}$$

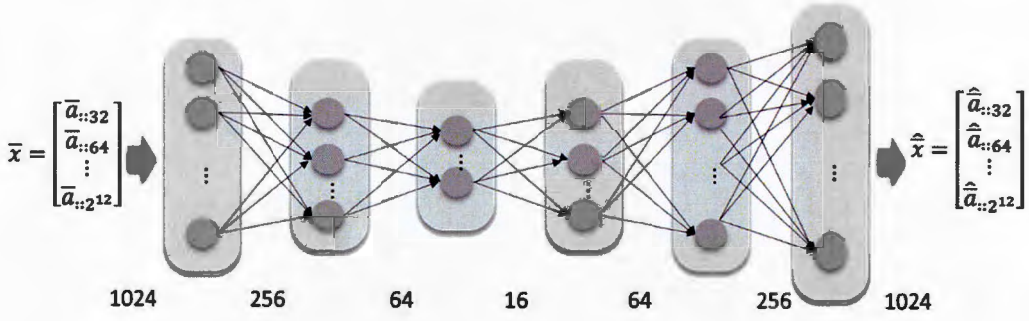

Figure 22: Autoencoder topology with FCN 'ayers applied to test data.

The approach was tested using data from gearbox G_0 and then comparing autoencoder errors associated with evaluation of the model on two other gearboxes, gearbox G_1 and gearbox G_{12}. The results show much larger errors with the fault (G_{12}), as illustrated in Figure 23.

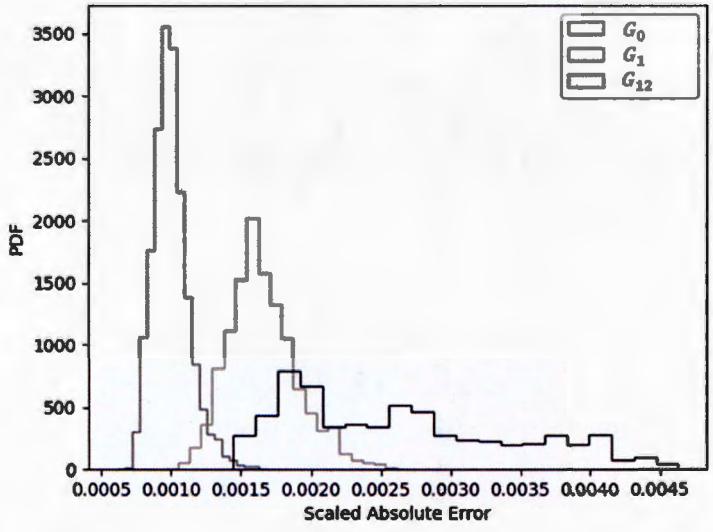

Figure 23: FCN model error for trained asset 0 and two new assets, 1 and 12.

The topology of a 1D *convolutional neural networks* (CNN) is very similar to that of its more popular 2D CNN counterpart. Figure 24 depicts the basic model structure: the model is a series of repeated basic blocks.

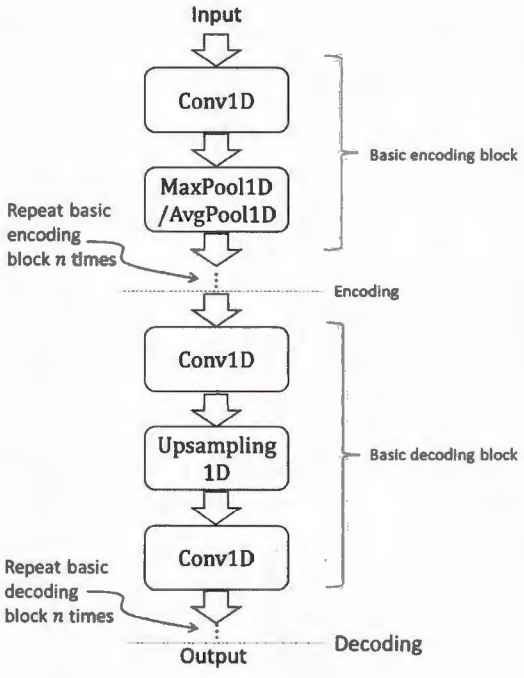

Figure 24: Basic CNN model topology

The basic block for encoding consists of a Conv1D layer and a MaxPool1D/AvgPool1D layer, whereas the basic decoding block consists of a Conv1D layer and an Upsampling1D layer. Conv1D implements a series of functions given by Eq. (48) and depicted in Figure 25. MaxPool1D downsamples the data by taking a maximum and Upsampling1D is its nonlinear inverse (it repeats the same value multiple times).

A 1D CNN model was built as an alternative to the MLP. Here a hidden layer unit ϕ_m, which is a part of a hidden layer

$$\bar{\phi} = [\phi_1 \dots \phi_m \dots \phi_M]^T, \tag{47}$$

is

$$\phi_m = \mathrm{f}_m\left(b_m + \sum_{n=1}^{N} s_n * h_{n,m}\right), \tag{48}$$

where f_m is the activation function (e.g. ReLU), b_m is the bias, $h_{n,m}$ are coefficients of 1D digital filters, and $*$ is 1D convolution operator

$$s_n[k] * h_{n,m}[k] = \sum_{i=-\infty}^{\infty} s[k-i]h_{n,m}[i] \tag{49}$$

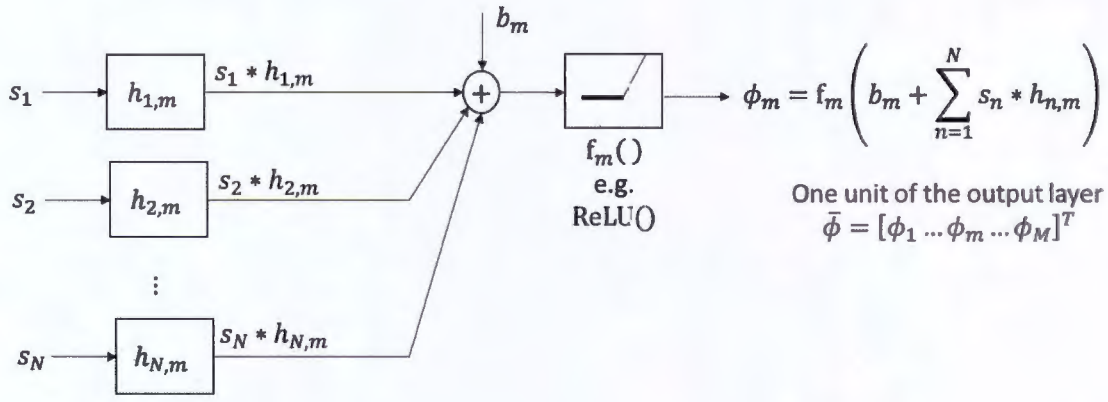

Figure 25: A graphical representation of a hidden unit in 1D CNN.

To investigate advantages and limitations of different autoencoder topologies, the research team first compared three different families of autoencoders – fully-connected networks, 1D CNNs, and *variational autoencoders* (VAEs) – using a synthetic data set that consisted of three different waveforms, viz. sinusoid, square-wave, and triangle, with different frequencies and phases. The fully connected layers trained and tested well on the signals but were not able to generalize - they could perform well only on frequencies and phases that they were trained on, but would predict poorly on frequencies and phases out of the training set. Their lack of generalization can be a feature rather than a defect if the fault manifests itself as a change in frequency. CNNs were very successful in both training and generalization – they performed well on frequencies and phases that were either interpolated or extrapolated from those in the training set. VAEs were more challenging to train, but their ability to generate new samples showed promise.

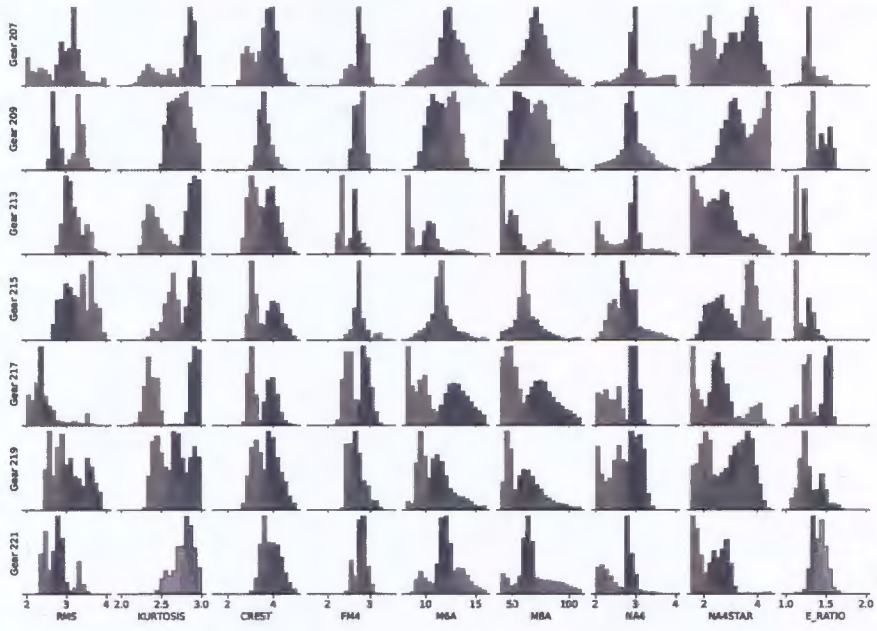

Figure 26 Detecting anomaly using classical condition indicators

After demonstrating that the approach is viable for more complex gearboxes, the focus returned to the newly-generated data. First, we evaluated autoencoders with respect to their ability to detect damage and later to assess the damage. The reference performance was established using classical vibration-based condition indicators (see [83], [84] for the review). To facilitate the comparison, we implemented a new toolbox for their computation in Python scientific ecosystem (see Section 3.2.1.4 for more details). Example performance of 10 selected CIs is shown in Figure 26. Each row signifies a different experiment conducted according to the process depicted in Figure 9. Blue histograms correspond to the baseline data and orange histograms correspond to propagation data. The larger separation between the two represents better ability to distinguish between operation of a healthy gearbox and operation of a gearbox with a cracked tooth.

It is interesting to observe that different CIs outperformed each other on different experiments. For example, NA4 considerably outperformed RMS on Gear 217, but did much worse on Gear 209.

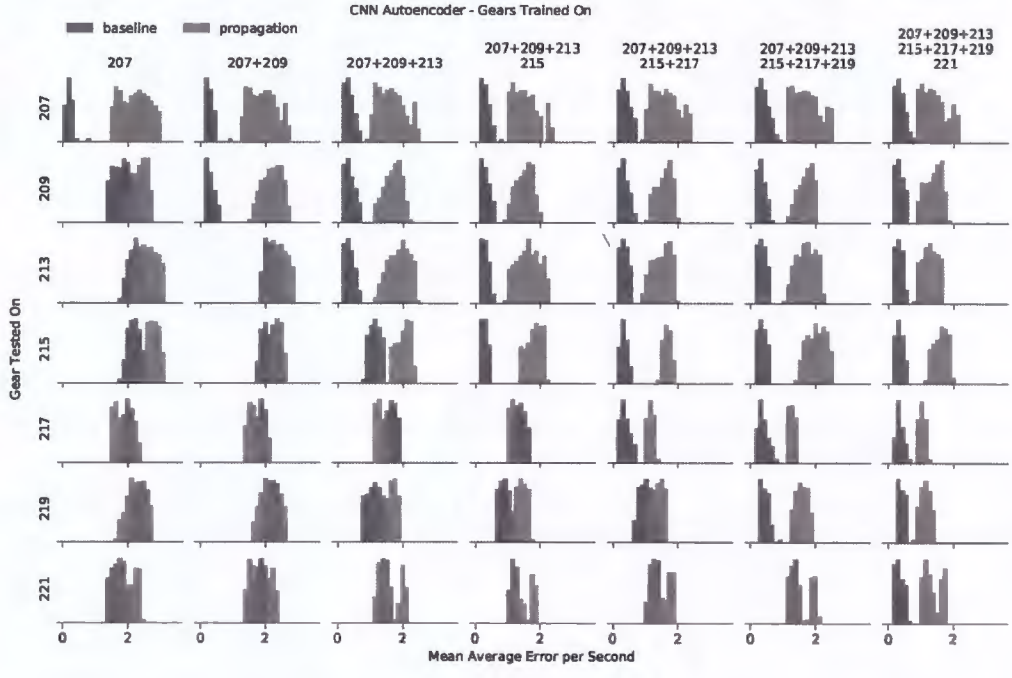

Figure 27 Autoencoders with CNN layers error

To compare data-driven models, we computed autoencoder error for two representative models using CNN and FCN layers (see Figure 28). In both cases, the rows correspond to different experiments. The columns were associated with the data used to train a model. For example, in the first column only data from the baseline of the experiment with cracking Gear 207 was used, in the second column, we used two experiments (207 and 209), etc.

In all cases, we observed perfect performance for gearboxes used in training, which is evidenced with full separations between baselines and propagations on or above the main diagonal of the subplot matrix.

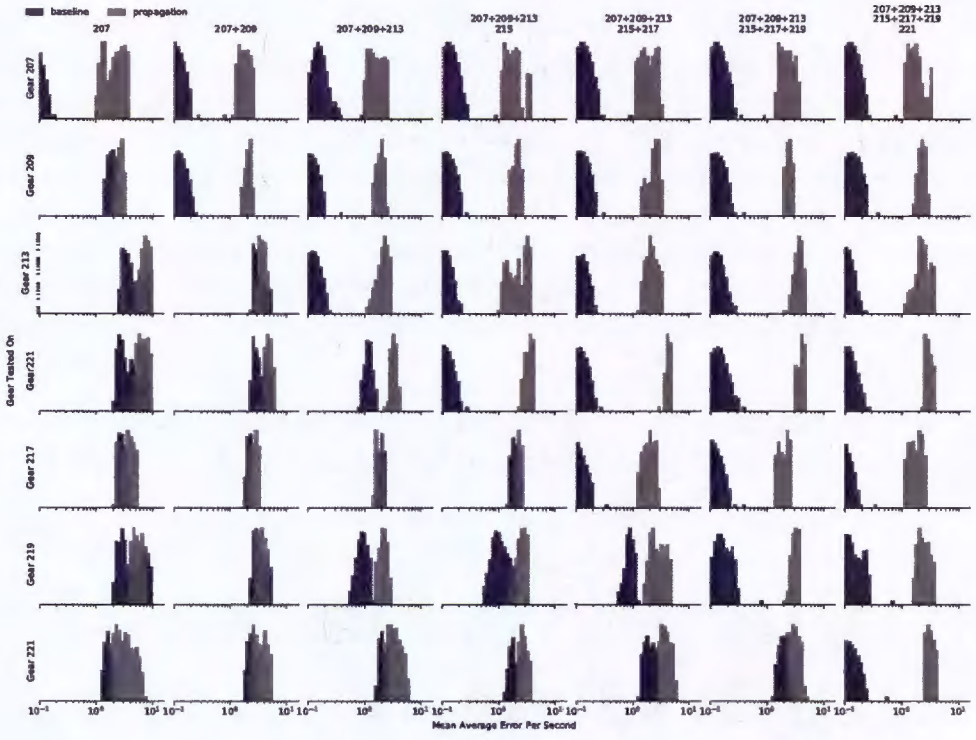

Figure 28 Autoencoders with FCN layers error

Figure 29 summarizes all the data shown in Figure 26, Figure 27, and Figure 28, using *area under the curve* (AUC) of the Receiver Operating Curve (ROC). The data-driven models greatly outperformed classical, engineered, vibration-based CIs.

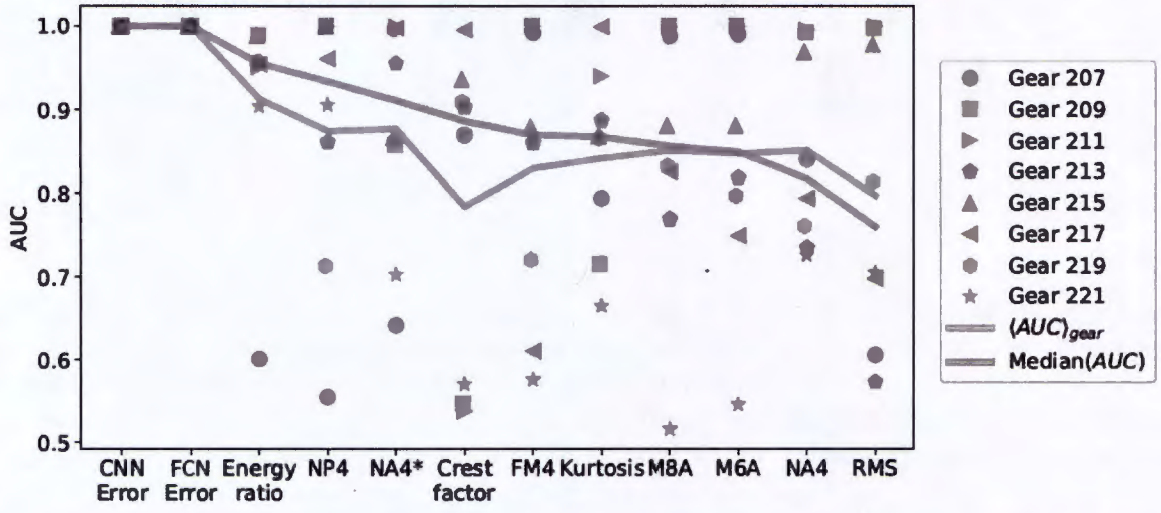

Figure 29: Comparison of two autoencoder errors (one based on CNN layers and the other based on FCN) with several classical CIs.

This excellent performance of data-driven models relative to their ability to distinguish fault from healthy, shown in Figure 29, raised some concerns that the autoencoder models maybe capturing any run-to-run differences. To address this concern, we designed an experiment with multiple baseline and trained autoencoders on subsets of these baselines. The results were very encouraging: the baselines were still distinguishable from the propagation. Moreover, the autoencoder error of some models was highly correlated to the damage level. Note that all models were trained on baseline data only, so the damage assessment came "for free". Ability to track damage level was not observed when the models were trained on a single baseline.

This work was summarized in the manuscript "Autoencoder based anomaly detector for gear tooth bending fatigue cracks", which was presented at the 13th Annual Conference of the Prognostics and Health Management Society and was selected as the best paper of the conference (refer to Section 5.3 for additional details). The abstract is as follows:

This article reports on anomaly detection performance of data-driven models based on a few selected autoencoder topologies and compares them to the performance of a set of popular classical vibration-based condition indicators. The evaluation of these models employed data that consisted of baseline gearbox runs and the associated runs with seeded bending cracks in the root of the gear teeth for eight different gear pairings. The analyses showed that the data-driven models, trained on a subset of baseline data, outperformed classical condition indicators as anomaly detectors and may show promise for damage assessment.

The ability to assess damage was an especially valuable and encouraging feature, because initial attempts to extend PHM capabilities from anomaly detection to damage assessment and prognostics, based on transfer learning, were not successful. The approach was to train an autoencoder using baseline data from multiple gearbox experiments (Illustrated Figure 30a), take the encoding part of the network, freeze the encoding layers, add one or more layers to complete the new network, and train the new network via regression on a part of the data from the propagation experiment (see Figure 30b).

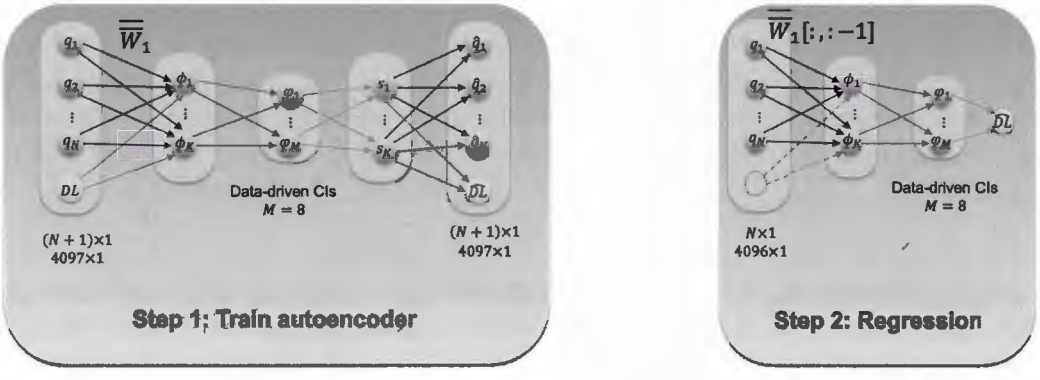

(a) *(b)*

Figure 30 Extending anomoly detection to damage assessment using transfer learning (a) auto-encoder trained on normal data (b) regression model that employs the encoding layers as the feature generator

The training and validation data for the specific experiments were excellent (see Figure 31a), but it generalized very poorly on propagation data from different experiments (see Figure 31b). The first thought was that perhaps it was unfair to expect that the damage progression learning can generalize from one experiment to the next because crack propagation can differ considerably in symmetry and the time that they take to evolve. However, the high correlation between autoencoder errors and damage suggests that creating richer baseline datasets (with multiple baselines) may pave the way to higher-level PHM capabilities at no additional cost.

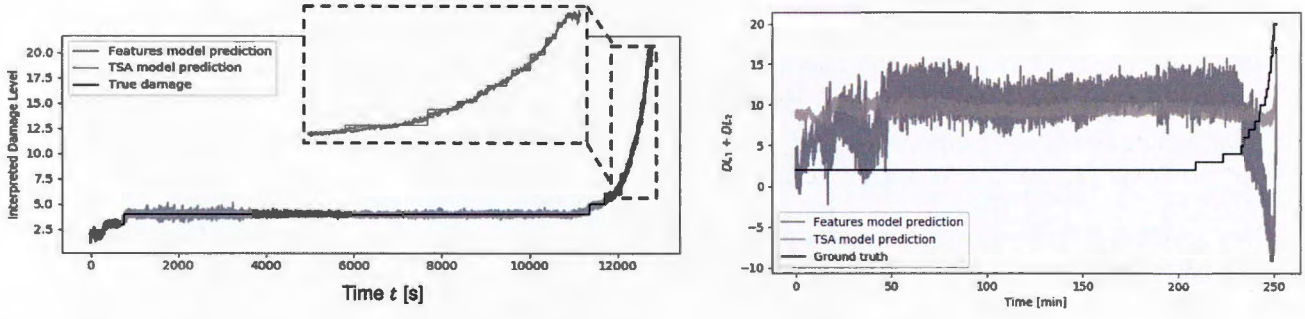

(a) (b)

Figure 31 Results of damage assessment from

3.2.1.4 Computing Classical Condition Indicators

The team refined the toolbox that implements classical vibration-based CIs in the modern Python scientific ecosystem by extending it for analysis of bearings. The toolbox was applied to gear data collected at RIT and to obfuscated, historical data captures from gearboxes captured by NAVAIR. A new visualization and analysis graphical user interface was developed to facilitate the usage of the toolbox in NAVAIR's routine analyses, e.g. for computing and visualizing data transforms (TSA, residual, difference) and CIs (RMS, kurtosis, NA4, FM4, etc.) in the context of operating conditions. In addition, the toolbox was used in bearing analyses, which featured a first-order algorithmic encoding and software implementation of probabilistic reasoning employed by NAVAIR vibration engineers. Finally, the toolbox was applied to data generated at RIT for ranking of the CIs with respect to their capabilities to detect anomalies (using AUC and discriminability) and to track damage. Feature fusion of CIs for damage tracking and short-term (up to 10 min) prognostics also showed promising results.

This toolbox was created for use alongside machine learning algorithms for fault detection, both to compare the performance of classical CIs and to use them for further feature computation. Python was chosen mainly because of commonly used machine learning libraries such as scikit-learn [85], Tensorflow x[86], and Pytorch [87]. Pytorch became our framework of choice for its CUDA support and deep learning functionality. The strength of machine learning lies in the ability to approximate and model statistical patterns in a high dimensional space, which is very similar to the goals of classical condition indicator development. Our primary approach was to create models that sufficiently detected anomalies in fault data, and from there move into assessing damage progression.

The toolbox was created in close collaboration with ARL and Navair. Previously, ARL and RIT have developed a Matlab implementation of the toolbox. The toolbox was tested at RIT, Navair, and ARL.

The organization of the toolbox is depicted in Figure 32. The software takes two main inputs, acceleration signal and indexer (encoder or tachometer), transforms them into several auxiliary signals (e.g. TSA, difference, and residual), and computes metrics, or CIs from various signals.

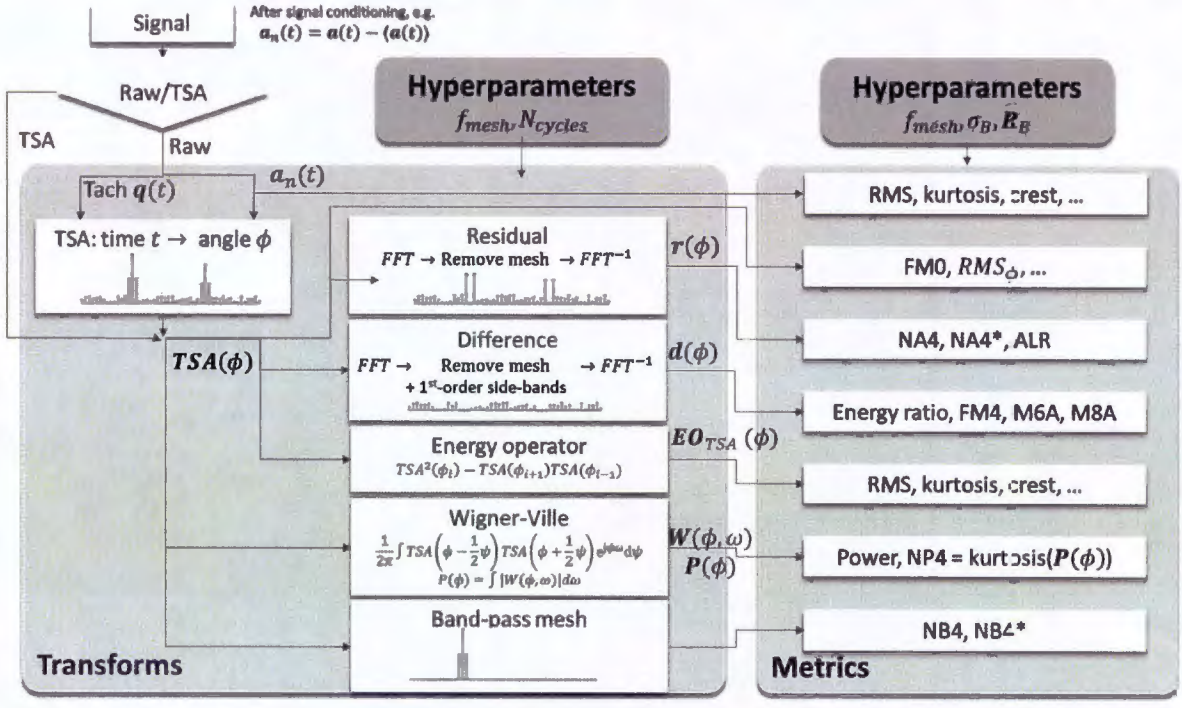

Figure 32: CI toolbox

Several iterations of the toolbox were tested at Navair. To facilitate the use at Navair, a few iterations of a dashboard were developed (see Figure 33). Navair engineers characterized the value of the new tools as "the most significant advancement in several years".

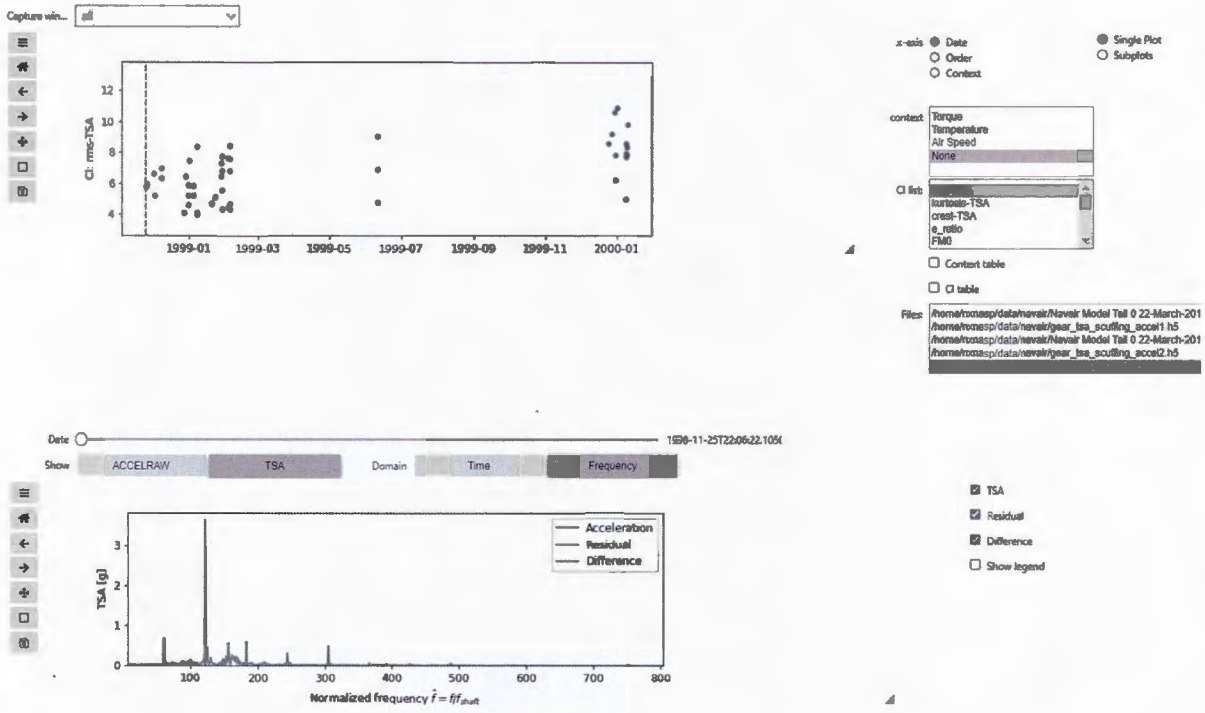

Figure 33 Dashboard developed for Navair testing of the CI toolbox

At the time of this report, ARL was testing the toolbox with their newly-developed Viper test stand, which was designed and intended to perform a variety of seeded tests that were not appropriate for production test stands. The team developed a manuscript (still in final stages) and will publicly share the toolbox on ARL's GitHub page. The abstract is as follows:

This article introduces a new implementation of a toolbox for computing classical, engineered, vibration-based condition indicators *(CI) for assessing gear health in Python Scientific Eco System. The new toolbox is applied on new experimental data on gear crack propagation with seeded cracks. Different CIs were compared relative to their ability to detect cracks and with respect to their ability to assess damage levels and predict future damage levels.*

The toolbox was also employed in comparison of CPU vs. GPU computations (see Section 2.2.3.5 for more details).

3.2.1.5 Bearing analyses

In addition to gearbox analyses, the team extended the tools to bearing analyses application. The extension was on automating some steps in the existing process of bearing diagnostics using *high-frequency enveloping* (HFE).

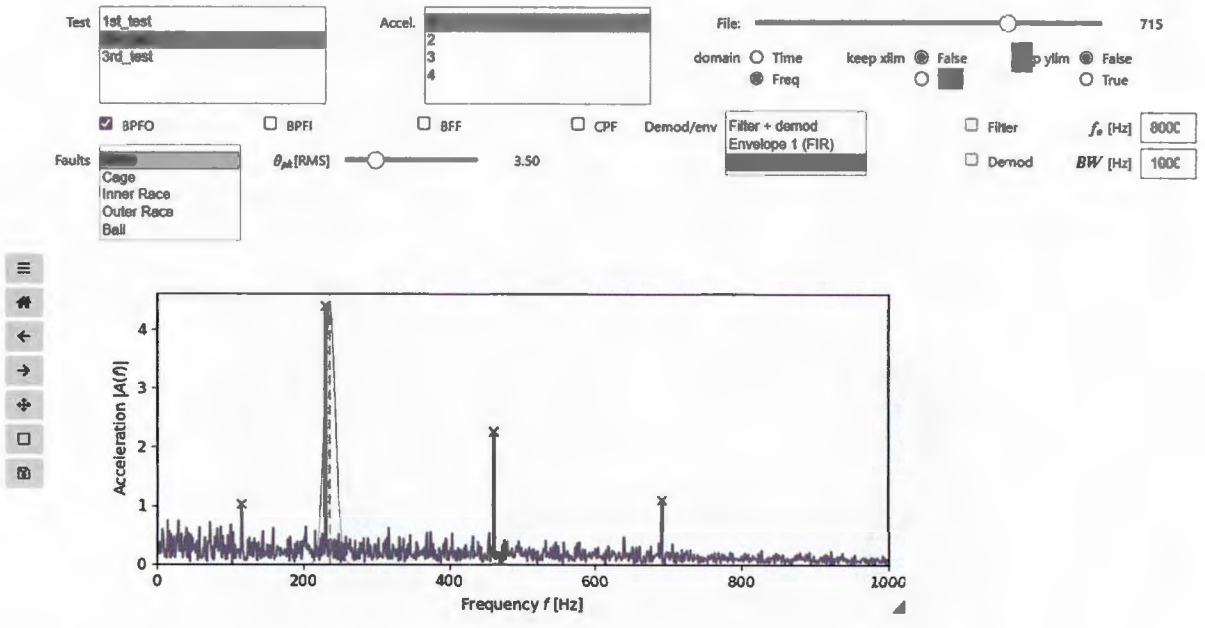

(a)

Symbol	Description
f_s	shaft frequency
n	number of balls
d	ball diameter
D	pitch diameter
θ	contact angle

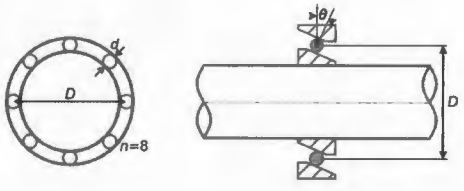

Fault Frequency	Formula
Ball Pass Frequency Outer Race (BPFO):	$BPFO = \frac{nf_s}{2}\left[1 - \frac{d}{D}\cos\theta\right]$
Ball Pass Frequency Inner Race (BPFI):	$BPFI = \frac{nf_s}{2}\left[1 + \frac{d}{D}\cos\theta\right]$
Ball Fault Frequency (BFF):	$BFF = \frac{Df_s}{d}\left[1 - \left(\frac{d}{D}\cos\theta\right)^2\right]$
Cage Pass Frequency (CPF):	$CPF = FTF = \frac{f_s}{2}\left[1 - \frac{d}{D}\cos\theta\right]$

(b)

Figure 34 Toolbox for HFE bearing diagnostics: (a) Toolbox (b) reference geometry

A Python toolbox for HFE is depicted in Figure 34a. The toolbox was developed to operate on the open bearing dataset [88]. The example above operated specifically on the second test, wh ch had a seeded failure on the outer race. The plot shows the result of the frequency analyses, with red "x" markers signifying BPFO failure (see Figure 34b for the reference and the notation).

3.2.2 Integrating Oil and Vibration Testing

This part of the investigation was motivated by the need to better understand progression of damage from scuffing to micro-pitting, pitting, and eventual cracking.

Two main experiments were performed: one served as a pilot to set up the operating conditions and the other operated for 500 hours to capture gradual progression of damage.

3.2.2.1 Test process and magnetic filter

The test stand was built around a Mustang transmission dynamometer that used an electric motor to apply load to the gearbox and an eddy current brake to produce the reaction torque. Spray lubrication of the gears was provided through oil impingement on the outlet of the gear mesh with a total flow rate of

0.8 L/min. The lubricant was Super Brand synthetic gear oil having a viscosity of 500 SSU at 38 °C and was actively cooled by a heat exchanger that maintained the oil temperature near 35 °C throughout the test. The oil outlet from the gearbox was plumbed at a constant downward slope to a reservoir having a conical bottom geometry that terminated at a drain valve port. This geometry feature was implemented to reduce locations where particles could settle out of the oil before reaching either the drain port or the downstream filter elements where oil samples were collected. The oil line was redesigned, with expert inputs from NRL, to facilitate oil sampling suitable for their test needs. The key new features included a new, smaller oil tank and a magnetic filter. Figure 35 shows the design for the new oil line.

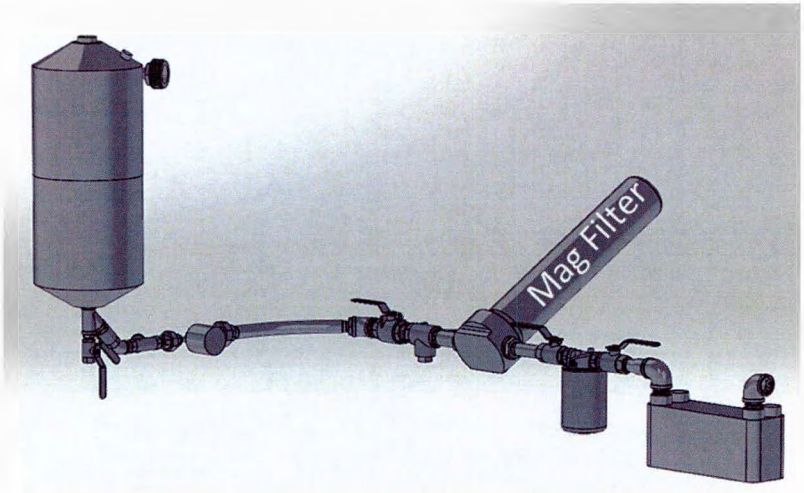

Figure 35 Redesigned oil line featuring smaller tank and magnetic filter

The outlet port from the oil reservoir was connected to a 20-inch long modified magnetic filter element from Eclipse Magnetics. Further downstream of the magnetic filter was a helical gear pump that subsequently led to a 3-micron rated hydraulic paper filter and the liquid-liquid heat exchanger before returning to the gearbox. Periodic oil sampling intervals were implemented and a portable USB digital microscope with 2MP resolution and 40 to 1000× zoom was also setup to capture ground truth images of the spur gear tooth faces as damage progressed over the course of testing. The microscope was setup for approximately 88×, giving a resolution of 3.2 micron/pixel. Lighting was provided by a USB powered LED strip light with custom diffuser to flatten the light. Before imaging, the room was first darkened to prevent reflections, then the light and microscope were positioned using custom fixtures on the gearbox. Images were captured via USB interface to a laptop using MS Camera, as shown in Figure 36.

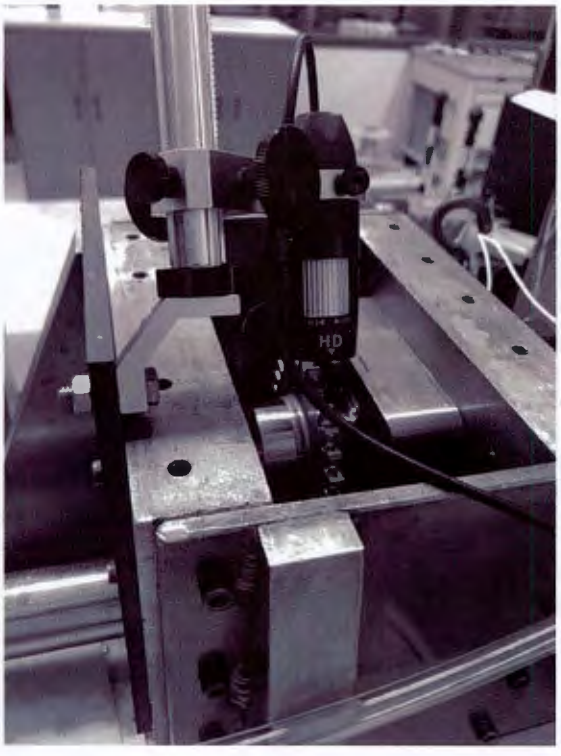

Figure 36 Capturing surface damage ground truth using optical camera

To obtain additional information related to scuffing damage and to test the effectiveness of the periodic oil sample method, we captured the particles using the magnetic filter and developed a new process for collecting the particles from the magnet and to suspend them in oil for analysis: Figure 37a shows the magnetic filter that continually collects particles as the oil circulates; Figure 37b shows the magnetic core removed from the filter, with particles forming lines at the magnetic field maxima; and Figure 37c shows an example particle transferred from the magnetic core.

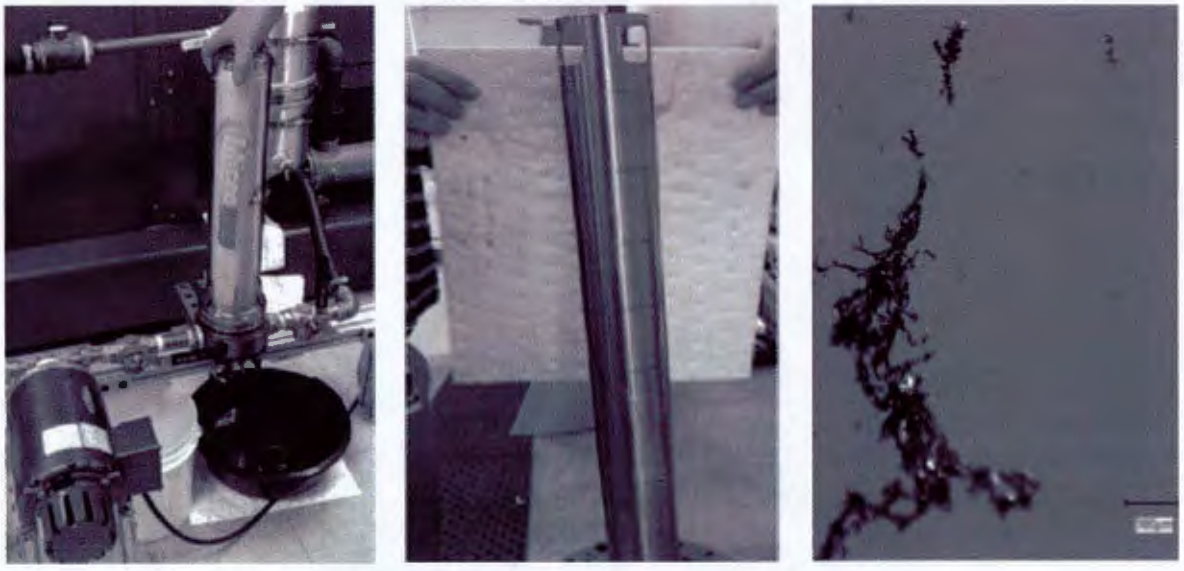

(a) (b) (c)

Figure 37: Magnetic filter and process: (a) in-line magnetic filter (b) magnetic element removed with captured particles (the lines form at maxima of magnetic field) (c) example of particles removed from the magnetic element

The magnetic filter can be considered a sensor that effectively integrates the particles for a period of time between collection intervals. The magnetic filter system was modified from the oversized commercially available product by machining a plastic insert between the outer housing and magnetic filter, which decreased the volume of oil in the filter. This modification also changed the spacing between the magnet and particles, thus increasing magnetic force relative to viscous drag. Benchtop experiments were conducted to empirically determine the desired spacing and oil space velocity by using high speed photography and metal 3D printing powder having a known powder size distribution at the lower end of the gear particles of interest. The final addition to the system was a 127 micron thick fluorinated ethylene propylene (FEP) sleeve placed around the magnetic element that allowed the particles to be attracted to the magnets then removed for post-test collection and analysis. Periodically, oil samples were extracted from the reservoir drain and the particles collected on the magnetic filter element were then suspended in oil for analysis. NRL used a LaserNet Fines wear debris analyzer to determine size distribution and wear type of the particles collected from the gearbox scuffing test. Particle concentration, size distribution, and image maps were determined for particles between 5 µm to 200 µm in size.

The study empirically examined progression of surface damage in spur gears and included three modes of monitoring: 1) optical imaging of damaged gear surfaces; 2) characterization of particles suspended in oil; and 3) vibration monitoring of the gearbox. Each experiment ran for more than 500 hours.

3.2.2.2 Outcomes of the experiment

A simple, deterministic image-based feature showed strong correlation with test time and with vibration-based features. Ten engineered vibration CIs and three data-driven vibration CIs were computed, with seven showing about 70% or better absolute correlation with the image-based condition indicator.

Particle captured by periodic oil samples (after each test interval) did not contain meaningful representation of damage, but particles captured by the magnetic filter included large particles that served as evidence of significant surface damage.

Potential future research will include inline optical and inline magnetic oil monitoring, refining of the image-based ground truth indicators, and (Bayesian) integration of the two statistically-independent health indicators (oil-analysis-based and vibration-based).

The summary of this work was presented in a manuscript, "Progression of surface damage in spur gears," to be submitted to the Journal of Mechanical Systems and Signal processing. The abstract is as follows:

We present an empirical investigation of gradual progression of damage in spur gears, starting from scuffing, via micro-pits, to macroscopic pits, using two statistically-independent data sources: oil monitoring and vibration measurements. The test stand was equipped with a commercial magnetic filter and a novel test process was developed to remove particles from the magnetic filter and suspend it in oil. In addition, oil samples were drawn periodically. Oil analyses did not find significant particles in the oil samples drawn from the oil tank, but found relatively large particles in the particles collected from the magnetic filter. Both data-driven and classical vibration-based condition indicators were computed and compared to simple, image-based estimation of the ground truth of the surface damage. with some of the indicators showing more than 80% correlation to the estimated ground truth.

3.3 Potential Future Research

To extend the results on oil and vibration monitoring and health assessment, we outlined the following concept that consists of four components: 1) characterization and model development, using vibration and oil data, of progression of failure of spur gears, starting from scuffing and gradually progressing through micro-pitting, pitting, and cracking; 2) detection of failure; 3) diagnostic methods for differentiation between failures; and 4) damage assessment of individual failure modes.

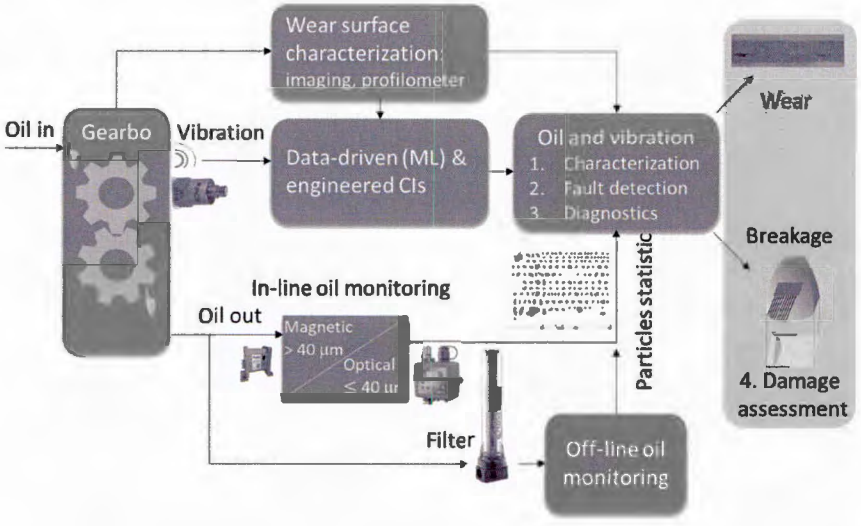

Figure 38 Study at a glance

The key challenges and the lack of satisfactory screening criteria associated with predicting scuffing phenomena were identified in a manuscript more than 40 years ago [89], but know edge gaps remain

open and the problems are still of considerable interest and relevance for practical operation of gearboxes. Furthermore, all stages of damage progression continue to draw interest of both practitioners and researchers. For example, a recent empirical study of initiation and micropitting identified the key factors in micro-pits formation: excessive loading, gear tooth micro-geometry, surface roughness and lubricant film thickness [90]; interesting new work on image-based analysis of micro-pitting has started to emerge [91].

Vibration-based machine learning models were shown to be able to outperform their classical engineered counterparts for the ability to detect damage [92]. More broadly, machine learning modeling approaches based on autoencoders have establish themselves as a very powerful methodology for predictive maintenance [79], [82], [93], especially for the first level of capability, anomaly detection. While purely data-driven models have shown considerable success recently, modeling and simulation of gear damage level [94], [95] can inform and reduce the complexity of data-driven models.

3.4 Training Opportunities

One mechanical engineering and three computer science students were trained on the fundamentals on machine learning and deep learning in particular. The students were able to help with the design of different autoencoders for anomaly detection. Two students actively participated in coding of the CI toolbox. One student participated in development of the dashboard for demonstrating the toolbox at Navair. Three students also participated in manuscript development as coauthors. Both Pytorch and TensorFlow frameworks were used.

3.5 Results Dissemination

RIT conducted weekly meetings with NRL and NAVAIR for sharing the knowledge on oil analyses, and additional weekly meeting with ARL and NAVAIR focused on development of vibration-based PHM models, both classical and deep learning.

4 Additive Manufacturing Research

Maintenance and sustainment of high value assets often relies on replacing damaged components, rather than repairing them. In the case of components that no longer have an option for replacement by original equipment components, 3D printing technologies are being considered to print these components from scratch. For some parts, this may be feasible, but for many parts using current printing technologies is not feasible for a variety of reasons including timing and material properties. Additionally, repair is usually more cost effective than replacing with new original equipment manufacturers' or 3D printed components, and is often functionally preferable over printing replacements. The strong interest in additive manufacturing (AM) for the heavy equipment and aerospace industries has revitalized development of AM technologies that have direct applicability to component repair.

Before repairing parts, however, it is necessary that the performance and durability level of repaired parts be known, and ensure that this level of performance meets the requirements of the end application. Currently, there is a knowledge gap in terms of how to evaluate particular component repair approaches against the original part performance. Furthermore, an AM technology is often evaluated as a general option to component repair, but in practice, each particular component (e.g. S/N 123) must be evaluated as to its condition and suitability for repair. Therefore, an interaction between component repair and

condition based maintenance, in which knowledge of the condition of a particular component, including its usage history, facilitates the repair decision. Conversely, CBM decision making can also be affected by the expected performance and durability characteristics of a repaired component, such as effects on lead time and increased fatigue life.

4.1 Research Goals and Objectives

The Additive Manufacturing Repair Technology subproject focused on closing the knowledge gaps relating to additive repair material properties and advancing the state of technology to facilitate the adoption of additive manufacturing repair processes. The research project had two major objectives; the first was to close the AM knowledge gap, and the second was to develop an AM repair analysis framework. Additional details on each objective are provided below.

1) Close the Knowledge Gap: RIT identified existing materials properties knowledge, such as fatigue, wear, adhesion, corrosion, of AM repair processes and highlighted the critical gaps in the availability of property data. Based on these gaps, RIT empirically developed detailed material data sets for selected material/AM process pairs.

2) Develop an AM Repair Analysis Framework: RIT developed a detailed framework to evaluate the feasibility and performance of specific repair options for components using additive manufacturing technologies. The framework uses a function and failure mode based approach to provide an assessment of capability for potential AM repair approaches relative to the existing material of the original component.

4.2 Research Accomplishments

RIT developed an analysis framework that evaluates an existing damaged component for functional requirements and known failure modes then identifies potential materials and technologies for repair. Should the component be a candidate for repair with an additive process, the framework presents the user with a ranked order of potentially viable AM processes, including material properties. A multi-criteria decision analysis, based on a custom implementation of the Grey Decision Making method, was integrated into the analysis and tested for accuracy by using a suspension torsion bar as an example component. Additionally, the framework was enhanced to factor in the material properties resulting from post-processing of components, such as heat treatment, carburizing, and nitriding. For each additive process technology, a full list of material properties to be captured into a material database to aid the decision making process was identified, including: hardness, tensile strength, fatigue strength, abrasive and reciprocating wear, corrosion resistance, and fatigue. RIT extracted property information from standards, handbooks, journal articles, and other published works to capture properties of traditional wrought and cast materials as well as additive processes. The test data from the RIT experiments was added to this database during the course of the work.

RIT identified a series of technologies consisting of directed energy deposition (DED), cold spray, thermal spray, additive friction stir welding, and cold metal transfer (CMT) to be assessed under this project. A set of substrates and additive materials were selected for optimization with each technology through experiments and collection of test results. Specifically, RIT created additive stir welding specimens through a contract with MELD by fusing different additive materials onto a variety of substrates. Ultrasonic non-destructive examination was performed on the samples to identify potential voids before they are machined and cut into test specimens. Similarly, a contract with a High Pressure Cold Spray (HPCS) vendor allowed RIT to access the spray system operating parameter data used when creating specimens – this enabled dissemination of informative data to the repair community that is not usually published in its

entirety. For DED, work performed included integration of an updated lens and nozzle system that was used to produce weld beads that were analyzed through microscopy and mechanical property testing. Furthermore, RIT investigated properties of M2 and H13 tool steels on hardened steel substrate through a detailed design of experiments. Though there was a lack of literature on this topic, RIT hypothesized these hard materials could restore high strength shaft and bearing surface components without cracking. A CMT welding system was installed, debugged, and used to create tensile and fatigue specimens of aluminum 5052 sheet material. Additionally, fatigue specimens of cast aluminum A356 coupons were investigated.

RIT developed an analysis framework that evaluates a damaged component for functional requirements and failure modes, then identifies potential materials and technologies for repair. Should the component be a candidate for an AM repair process, the framework presents the user with a ranked order of processes, including material properties and process settings. A custom multi-criteria decision analysis, based on a Grey Decision Making method, was tested by using a vehicle suspension torsion bar as an example component. Test outcomes identified several algorithm changes that were required and enhancements for presenting the results to the user. Further optimization is necessary by repeating this process with other component trials. As part of the component trials, RIT continued to work with the Amphibious Assault Vehicle (AAV) community through virtual review meetings to provide updates on the capability of AM repair processes and framework. Components identified by the AAV community that are difficult to repair through conventional repair processes, such as cast aluminum housings, high-strength steel shafts, wrought aluminum gearboxes and hard plating, were used as framework test cases. Characteristics of these components allow demonstration of the operation and robustness of the framework for a diverse set of inputs. Similarly, RIT reached out to commercial remanufacturers of land and air vehicles and identified additional example components to evaluate in the framework that include cast iron and grade 8xxx steel.

Summaries of the detailed work performed under this project are provided in Appendices B & C.

4.3 Potential Future Research

Areas for potential future research on Additive Manufacturing Repair Technologies for CBM include imbedding the framework into a fully functional software tool to assist maintainers with quick, accurate decisions on pathways for component repair. First, additional components and use cases should be investigated to understand the capabilities and limitations of the framework across industries, material sets, applications, and component failure modes. In conjunction with this research, further study of the impact that coatings and post-processing techniques have on material properties, and subsequent failure mode avoidance, should be ascertained relative to the framework computations. To support the future framework software functionality, there is also a need for an open-source database on additive repair and traditionally manufactured material properties such that a consistent format can be used when making comparisons. Since additive repair properties are strongly related to the baseline material and processing environment, these factors must be captured within the dataset. A standard guide for evaluating and reporting material properties, similar to the ASTM standards for additive manufacturing, that captures the unique aspects of additive repair would benefit the community.

4.4 Training Opportunities

On the additive manufacturing subproject, the team has gained significant knowledge on each additive process through review of existing literature related to operation and results from previous experiments.

Through vendor training, the team learned how to proficiently operate new CMT and DED hardware systems for repair applications. Additionally, co-op students were engaged on setup and testing of each additive manufacturing process, which enhanced their knowledge base beyond the typical classroom education. For the cold spray process, RIT worked to enhance the performance of an existing system, which required engineers to learn the physics behind the process and implement that knowledge in practice. This understanding was then turned into a new design for the cold spray gun that should increase particle velocities at the point of surface impact. For the cold spray process, junior engineers worked through enhancements on the performance of the novel adhesion pull fixture that afforded them the opportunity to learn finite element methods and gain knowledge from senior eng neers. Lastly, an engineer was able to virtually attend a conference on the latest research in thermal spray technologies and share that knowledge with the remainder of the team.

4.5 Results Dissemination

For the additive manufacturing subproject, RIT conducted multiple conference calls with the AAV program office and visited the Albany, GA depot to discuss aspects of the framework and potential applications of additive manufacturing repair. RIT also provided an overview of the AM repair program to engineers at the Army Depot at Anniston. Furthermore, three presentations were delivered over the course of the project. The first presentation topic was on repair of cast ductile iron materials using twin wire arc coatings. The second presentation was on the structure of the additive repair framework at the TechConnect World Innovation conference in Austin, TX 2021. The third presentation was on the High Pressure Cold Spray data that was captured using a novel adhesion test methodology in comparison to traditional test methods. Several publications, listed in the Products section of this report, were reviewed by ONR and disseminated to the additive repair community through academic journals. Refer to the Appendix B for abstracts of the papers.

5 Other Reporting Elements of Interest

5.1 Technology Transfer

RIT delivered the software toolbox and dashboard for comparison of machine learning and vibration CI development on gears, listed in the products section, to NAVAIR and ARL. Delivery allowed for user testing and multiple iterations of the tools. ARL is currently utilizing the software on their newly-developed Viper test stand, which is intended for performing seeded fault tests.

5.2 Honors and Awards

RIT presented a conference paper at the 13th Annual Conference of the Prognostics and Health Management Society titled, "Autoencoder based anomaly detector for gear tooth bending fatigue cracks," which was subsequently selected as the best paper of the conference.

5.3 Products

A list of publications, conference papers, and conference presentations that were disseminated to the public over the course of this project are listed below. Additional information, such as abstracts, are provided in the Appendices.

1. Publication
    a. Article Title: *Repair of Aluminum 6061 Plate by Additive Friction Stir Deposition*
    b. Journal: The International Journal of Advanced Manufacturing Technology
    c. Authors: L. Peter Martin, Allen Luccitti, and Mark Walluk
    d. Keywords: Additive Friction Stir Deposition, AFSD, 6061-T6, Repair
    e. Distribution Statement: Open for public distribution
    f. Publication Status: Published
    g. Publication Identifier Type: DOI
    h. Publication Identifier: https://doi.org/10.1007/s00170-021-07953-z
    i. Publication Date: September 8, 2021
    j. Volume: 118
    k. Issue: 3
    l. First Page Number: 759
    m. Publication Location: Online
    n. Acknowledgement of Federal Support? Yes
    o. Peer Reviewed? (Yes/No) Yes
2. Publication
    a. Article Title: *Evaluation of Additive Friction Stir Deposition for the Repair of Cast Al-1.4Si-1.1Cu-1.5Mg-2.1Zn*
    b. Journal: Journal of Manufacturing Science and Engineering
    c. Authors: Peter Martin, Allen Luccitti, and Mark Walluk
    d. Keywords: Additive manufacturing, advanced materials and processing, nontraditional manufacturing processes
    e. Distribution Statement: Open for public distribution
    f. Publication Status: Published
    g. Publication Identifier Type: DOI
    h. Publication Identifier: https://doi.org/10.1115/1.4052759
    i. Publication Date: December 3, 2021
    j. Volume: 144
    k. Issue: 6
    l. First Page Number: 061006-1
    m. Publication Location: New York, USA
    n. Acknowledgement of Federal Support? Yes
    o. Peer Reviewed? (Yes/No) Yes
3. Publication
    a. Article Title: *Investigation of Mechanical Properties of Twin wire Arc Repair of Cast Iron Components*
    b. Journal: Journal of Thermal Spray Technology
    c. Authors: K. DePalma, M. Walluk, L. Martin, and K. Sisak
    d. Keywords: feedstock, adhesion testing processing, stainless steel properties, elastic modulus properties, testing, abrasive wear testing, three point bending wire arc spray
    e. Distribution Statement: Open for public distribution

f. Publication Status: Published
g. Publication Identifier Type: DOI
h. Publication Identifier: https://doi.org/10.1007/s11666-021-01304-w
i. Publication Date: January 3, 2022
j. Volume: 31
k. Issue: 1
l. First Page Number: 315
m. Publication Location: Online
n. Acknowledgement of Federal Support? Yes
o. Peer Reviewed? (Yes/No) Yes

4. Publication
   a. Article Title: *Evaluation of additive friction stir deposition of AISI 316L for repairing surface material loss in AISI 4340*
   b. Journal: The International Journal of Advanced Manufacturing Technology
   c. Authors: L. Martin, A. Luccitti, and M. Walluk
   d. Keywords:
   e. Distribution Statement: Open for public distribution
   f. Publication Status: Published
   g. Publication Identifier Type: DOI
   h. Publication Identifier: https://doi.org/10.1007/s00170-022-09507-3
   i. Publication Date: June 10, 2022
   j. Volume: 121
   k. Issue: 3
   l. First Page Number: 2365
   m. Publication Location: Online
   n. Acknowledgement of Federal Support? Yes
   o. Peer Reviewed? (Yes/No) Yes
5. Publication
   a. Article Title: *Mechanical Properties of High Carbon Steel Coatings on Gray Cast Iron Formed by Twin Wire Arc*
   b. Journal: Journal of Thermal Spray Technology
   c. Authors: K. DePalma, M. Walluk, L.P. Martin
   d. Keywords: feedstock, adhesion testing processing, stainless steel properties, elastic modulus properties, testing, abrasive wear testing, three point bending wire arc spray
   e. Distribution Statement: Open for public distribution
   f. Publication Status: Submitted
   g. Publication Identifier Type: TBD
   h. Publication Identifier: TBD
   i. Publication Date: TBD
   j. Volume: TBD
   k. Issue: TBD
   l. First Page Number: TBD

m. Publication Location: TBD
n. Acknowledgement of Federal Support? Yes
o. Peer Reviewed? (Yes/No) Yes

6. Publication
    a. Article Title: Exhaust-gas Temperature Model and Condition Indicator for Diesel Engines
    b. Journal: Applied Thermal Engineering
    c. Authors: Matthew Sullivan, Michael Thurston, Sean McConky
    d. Keywords: Condition monitoring, Prognostics, Fault Detection, Exhaust Gas Temperature, Diesel Engine
    e. Distribution Statement: Open for public distribution
    f. Publication Status: submitted
    g. Publication Identifier Type: TBD
    h. Publication Identifier: TBD
    i. Publication Date: TBD
    j. Volume: TBD
    k. Issue: TBD
    l. First Page Number: TBD
    m. Publication Location: TBD
    n. Acknowledgement of Federal Support? Yes
    o. Peer Reviewed? Yes
7. Publication
    a. Article Title: Prognostics Health Monitoring of Diesel Fuel Injectors
    b. Journal: *Mechanical Systems and Signal Processing*
    c. Authors: Michael Thurston, Nenad Nenadic, Abu Islam, Mathieu Sullivan, Sean McConky, Adam Agosti
    d. Keywords: Prognostics Health Monitoring, Condition monitoring, Prognostics, Fault Detection, Diesel Fuel injectors, Diesel Engine
    e. Distribution Statement: Open for public distribution
    f. Publication Status: In preparation
    g. Publication Identifier Type: TBD
    h. Publication Identifier: TBD
    i. Publication Date: TBD
    j. Volume: TBD
    k. Issue: TBD
    l. First Page Number: TBD
    m. Publication Location: TBD
    n. Acknowledgement of Federal Support? Yes
    o. Peer Reviewed? Yes
8. Publication
    a. Article Title: A Python Toolbox for Classical Vibration Condition Indicators with Application to Gear Tooth Breakage
    b. Journal: Mechanical Systems and Signal Processing

c. Authors: Adrian Hood, Josiah Martuscello, Nicholas Gardner, Allen Jones, Patrick Horney, Christopher Valant, Nenad Nenadic
d. Keywords: crack detection, crack assessment, crack forecasting, HUMS, Transmission Diagnostics, Python Toolbox
e. Distribution Statement: Open for public distribution
f. Publication Status: In preparation
g. Publication Identifier Type: TBD
h. Publication Identifier: TBD
i. Publication Date: TBD
j. Volume: TBD
k. Issue: TBD
l. First Page Number: TBD
m. Publication Location: TBD
n. Acknowledgement of Federal Support? Yes
o. Peer Reviewed? Yes

9. Publications
    a. Article Title: Progression of surface damage in spur gears
    b. Journal:
    c. Authors: Mark Walluk, John Tucker, Allen Jones, Patrick Horney, Wiley Matthews, Adrian Hood, Nenad Nenadic
    d. Keywords: Scuffing, scoring, micropitting , pitting, gears, vibration monitoring, oil monitoring, magnetic filtering
    e. Distribution Statement: Open for public distribution
    f. Publication Status: In preparation
    g. Publication Identifier Type: TBD
    h. Publication Identifier: TBD
    i. Publication Date: TBD
    j. Volume: TBD
    k. Issue: TBD
    l. First Page Number: TBD
    m. Publication Location: TBD
    n. Acknowledgement of Federal Support? Yes
    o. Peer Reviewed? Yes
10. Conference Paper
    a. Title: Evaluation of 1D CNN Autoencoders for Lithium-ion Battery Condition Assessment Using Synthetic Data
    b. Authors: Christopher Valant, Jay Wheaton, Michael Thurston, Sean McConky, Nenad Nenadic
    c. Conference Name: 11th Annual Conference of the Prognostics and Health Management Society
    d. Conference Date: September 23-24, 2019
    e. Conference Location: Scottsdale, AZ

f. Publication Status: Published
g. Publication Date: September 2019
h. Publication Identifier Type: DOI
i. Publication Identifier: 10.36001/phmconf.2019.v11i1.876
j. Acknowledgement of Federal Support? Yes

11. Conference Paper
    a. Title: *Investigation of Mechanical Properties of Twin Wire Arc Repair of Cast Iron Components*
    b. Authors: Kyle DePalma, Mark Walluk, Peter Marin, and Kristin Sisak
    c. Conference Name: International Thermal Spray Conference
    d. Conference Date: May 2021
    e. Conference Location: Virtual
    f. Publication Status: Published Journal of Thermal Spray Technology
    g. Publication Date: NA
    h. Publication Identifier Type: NA
    i. Publication Identifier: NA
    j. Acknowledgement of Federal Support? Yes
12. Conference Paper
    a. Title: Autoencoder Based Anomaly Detector for Gear Tooth Bending Fatigue Cracks
    b. Authors: Adrian Hood, Christopher Valant, Patrick Horney, Allen Jones, Jared Lantner, Josiah Martuscello, Nenad Nenadic
    c. Conference Name: 13th Annual Conference of the Prognostics and Health Management Society
    d. Conference Date: Nov 15-16 and Nov. 18-19, 2021
    e. Conference Location: Virtual conference (due to Covid-19)
    f. Publication Status : Published
    g. Publication Date: November 19, 2021
    h. Publication Identifier Type: DOI
    i. Publication Identifier: https://doi.org/10.36001/phmconf.2021.v13i1.3003
    j. Acknowledgement of Federal Support? Yes
13. Conference Paper
    a. Title: Feasibility of Low-cost Vibration Monitoring for Ground Vehicles
    b. Authors: Abu Islam, Matthew Sullivan, Sean McConky, Michael Thurston, Adam Agosti, and Nenad Nenadic
    c. Conference Name: 14th Annual Conference of the Prognostics and Health Management Society
    d. Conference Date: November 1-4, 2022
    e. Conference Location: Nashville, TN
    f. Publication Status: Published
    g. Publication Date: October 28, 2022
    h. Publication Identifier Type: DOI
    i. Publication Identifier: https://doi.org/10.36001/phmconf.2022.v14i1.3207

j. Acknowledgement of Federal Support? Yes

14. Conference Paper
    a. Title: Evaluation of NVIDIA Jetson System for Vibration HUMS
    b. Authors: Christopher Valant, Sean McConky, Michael Thurston, Patrick Horney, Allen Jones, and Nenad Nenadic
    c. Conference Name: 14th Annual Conference of the Prognostics and Health Management Society
    d. Conference Date: November 1-4, 2022
    e. Conference Location: Nashville, TN
    f. Publication Status: Published
    g. Publication Date: October 28, 2022
    h. Publication Identifier Type: DOI
    i. Publication Identifier: https://doi.org/10.36001/phmconf.2022.v14i1.3232
    j. Acknowledgement of Federal Support? Yes
15. Conference Presentation
    a. Title: *Investigation of Mechanical Properties of Twin Wire Arc Repair of Cast Iron Components*
    b. Authors: K. DePalma, M. Walluk, L.P. Martin, and K. Sisak
    c. Conference Name: International Thermal Spray Conference
    d. Conference Date: May 2021
    e. Conference Location: Virtual
    f. Publication Status: NA
    g. Publication Date: NA
    h. Publication Identifier Type: NA
    i. Publication Identifier: NA
    j. Acknowledgement of Federal Support? Yes
16. Conference Presentation
    a. Title: *Development of a Framework for Component Repair Using Additive Manufacturing*
    b. Authors: A. Luccitti, M. Walluk, B. Hilton, B. Baker, K. DePalma, K. Sisak, P. Martin, and M. Thurston
    c. Conference Name: TechConnect World Innovation Conference 2021
    d. Conference Date: October 20, 2021
    e. Conference Location: Maryland, USA
    f. Publication Status: Published
    g. Publication Date: NA
    h. Publication Identifier Type: NA
    i. Publication Identifier: NA
    j. Acknowledgement of Federal Support? Yes
17. Conference Presentation
    a. Title: *Adhesion Test Method and Material Properties for High-strength High-pressure Cold Spray Coatings on Hardened 4340 Steel*
    b. Authors: G. Hurley, K. DePalma, M. Walluk, J. Siegfried, D. Maiola, and R. Holding

c. Conference Name: Cold Spray Action Team Conference
d. Conference Date: June 2022
e. Conference Location: Massachusetts, USA
f. Publication Status: NA
g. Publication Date: NA
h. Publication Identifier Type: NA
i. Publication Identifier: NA
j. Acknowledgement of Federal Support? Yes

18. Other Product
    a. Toolbox for computing classical condition indicators in Python. Tested at Navair and ARL, to be released publicly via GitHub
    b. Product Type (drop-down: audio or video, databases, data and research material, educational aids or curricula, evaluation instruments, instruments or equipment, models, physical collections, protocols, software or netware, survey instruments, other).
    c. Other Product Type: Software
19. Other Product
    a. Dashboard for applying CI toolbox and data visualization of gear vibration data
    b. Product Type (drop-down: audio or video, databases, data and research material, educational aids or curricula, evaluation instruments, instruments or equipment, models, physical collections, protocols, software or netware, survey instruments, other).
    c. Other Product Type: Software

5.4 Participants

The following RIT personnel worked one person month or more for the project (number of person months over the course of the project are indicated). There were no participants who are National Academy Members; there were no foreign collaborators; there was no international travel.

- Mike Thurston, Ph.D. - Co-PI (4)
- Mark Walluk - Co-PI (10)
- Nenad Nenadic, Ph.D. - Co-PI (18)
- Sean McConky - Co-PI (27)
- Peter Martin, Ph.D. - Faculty (Staff Scientist) (6)
- Matthew Sullivan - Other Professional (26)
- Kyle DePalma - Other Professional (18)
- Chris Valant - Other Professional (15)
- Adam Agosti - Other Professional (14)
- Allen Luccitti - Other Professional (13)
- Gerald Hurley - Other Professional (8)
- Kristin Sisak - Other Professional (5)
- Abu Islam. Ph.D. - Other Professional (5)
- Brian Hilton - Other Professional (4)
- Timothy Murtaugh - Other Professional (4)

- Jay Wheaton - Other Professional (3)
- Brandon Baker - Other Professional (2)
- Chuck Faisst - Other Professional (2)
- Scott Nichols - Other Professional (1)
- James Larrabee - Other Professional (1)
- Martin Schooping - Other Professional (1)
- John Dettmer - Other Professional (1)
- Chris Piggott - Other Professional (1)
- Michael Leaty – Technician (12)
- Domenic Maiola – Technician (17)

5.5 Students

Fourteen undergraduate and four graduate STEM students participated on the project. Fifteen students (marked with *) received a STEM degree as of the date of this final report submission.

- Josiah Martuscello* - Undergraduate Student
- Bram Valure* - Undergraduate Student
- Jared Lantner - Undergraduate Student
- Nicholas Gardner - Graduate Student
- Caleb Hilton* - Undergraduate Student
- Jason Purvee* - Graduate Student
- William Evan Amerine* - Undergraduate Student
- Carson McNatt* - Undergraduate Student
- Matthew Fuller* - Undergraduate Student
- Georgiy Rozenshteyn* - Undergraduate Student
- Tyler Walsh* - Undergraduate Student
- Nicole Gover - Undergraduate Student
- Henry Gagliardi* - Undergraduate Student
- Kaylie Glynn* - Graduate Student
- Kathryn Backman* - Undergraduate Student
- Matthew Lindstedt* - Undergraduate Student
- Owen Straub* - Graduate Student
- Craig Pettingill* - Undergraduate Student

6 References

[1] D. A. S. of D. fro Maintenance, "Condition based Maintenance Plus (CBM+): 2013 CBM+ Plan." Sep. 2013, [Online]. Available: https://www.acq.osd.mil/log/mpp/.cbm+.html/CBM+_Plan2013v2.pdf.

[2] U. S. D. of Defense, "Condition Based Maintenance Plus (CBM+) DoD Guidebook." 2012, [Online]. Available: https://acc.dau.mil/CommunityBrowser.aspx?id=498822.

[3] "Airbus A220-300 - Aircraft Details, History, Specifications and Price - Hangar.Flights." https://hangar.flights/aircraft/airbus-a220-300/ (accessed Sep. 12, 2022).

[4] "2023 KENWORTH T680 For Sale In Lubbock, Texas | TruckPaper.com." https://www.truckpaper.com/listings/trucks/for-sale/216688593/2023-kenworth-t680 (accessed Sep. 12, 2022).

[5] NVIDIA, "Embedded systems developer kits & modules from NVIDIA Jetson," *NVIDIA Developer*, 2020. https://www.nvidia.com/en-us/autonomous-machines/embedded-systems/ (accessed Feb. 04, 2022).

[6] "Autonomous Car Development Platform | NVIDIA DRIVE AGX." https://www.nvidia.com/en-us/self-driving-cars/drive-platform/ (accessed Apr. 29, 2020).

[7] "The future of advanced-edge computing is actually in autonomous cars," 2017, [Online]. Available: https://www.recode.net/2017/3/14/14924892/autonomous-car-self-driving-cloud-fog-advanced-edge-computing.

[8] C. Peeters, T. Verstraeten, A. Nowé, P. J. Daems, and J. Helsen, "Advanced vibration signal processing using edge computing to monitor wind turbine drivetrains," Dec. 2019, doi: 10.1115/IOWTC2019-7622.

[9] T. Verstraeten, F. Gomez Marulanda, C. Peeters, P.-J. Daems, A. Nowé, and J. Helsen, "Edge computing for advanced vibration signal processing," Jul. 2019. Accessed: Apr. 16, 2020. [Online]. Available: https://hal.archives-ouvertes.fr/hal-02188766.

[10] A. Albarbar, F. Gu, A. D. Ball, and A. Starr, "Acoustic monitoring of engine fuel injection based on adaptive filtering techniques," *Appl. Acoust.*, vol. 71, no. 12, pp. 1132–1141, Dec. 2010, doi: 10.1016/j.apacoust.2010.07.001.

[11] A. Albarbar, F. Gu, and A. D. Ball, "Diesel engine fuel injection monitoring using acoustic measurements and independent component analysis," *Meas. J. Int. Meas. Confed.*, vol. 43, no. 10, pp. 1376–1386, Dec. 2010, doi: 10.1016/j.measurement.2010.08.003.

[12] S. K. Mathew and Y. Zhang, "Acoustic-based engine fault diagnosis using WPT, PCA and bayesian optimization," *Appl. Sci.*, vol. 10, no. 19, pp. 1–18, Oct. 2020, doi: 10.3390/APP10196890.

[13] "Nvidia Xavier sampling in Q1 18." https://www.fudzilla.com/news/45328-nvidia-xavier-sampling-in-q1-18 (accessed Apr. 22, 2020).

[14] M. Lebold, K. McClintic, R. Campbell, C. Byington, and K. Maynard, "Review of vibration analysis methods for gearbox diagnostics and prognostics," pp. 623–634.

[15] K. Mcclintic, M. Lebold, K. Maynard, C. Byington, and R. Campbell, "Residual and Difference Feature Analysis with Transitional Gearbox Data."

[16] G. Jiang, H. He, P. Xie, and Y. Tang, "Stacked multilevel-denoising autoencoders: A new representation learning approach for wind turbine gearbox fault diagnosis," *IEEE Trans. Instrum. Meas.*, vol. 66, no. 9, pp. 2391–2402, Sep. 2017, doi: 10.1109/TIM.2017.2698738.

[17] H. Shao, H. Jiang, H. Zhao, and F. Wang, "A novel deep autoencoder feature learning method for rotating machinery fault diagnosis," *Mech. Syst. Signal Process.*, vol. 95, pp. 187–204, Oct. 2017, doi: 10.1016/j.ymssp.2017.03.034.

[18] J. Tan, W. Lu, J. An, and X. Wan, "Fault diagnosis method study in roller bearing based on wavelet transform and stacked auto-encoder," in *Proceedings of the 2015 27th Chinese Control and Decision Conference, CCDC 2015*, Jul. 2015, pp. 4608–4613, doi: 10.1109/CCDC.2015.7162738.

[19] Z. Chen and W. Li, "Multisensor feature fusion for bearing fault diagnosis using sparse autoencoder and deep belief network," *IEEE Trans. Instrum. Meas.*, vol. 66, no. 7, pp. 1693–1702, Jul. 2017, doi: 10.1109/TIM.2017.2669947.

[20] H. Zhu, R. Ting, X. Wang, Y. Zhou, and H. Fang, "Fault diagnosis of hydraulic pump based on stacked autoencoders," in *2015 IEEE 12th International Conference on Electronic Measurement and Instruments, ICEMI 2015*, Jun. 2016, vol. 1, pp. 58–62, doi: 10.1109/ICEMI.2015.7494195.

[21] Y. Qu, M. He, J. Deutsch, and D. He, "Detection of Pitting in Gears Using a Deep Sparse Autoencoder," *Appl. Sci.*, vol. 7, no. 5, p. 515, May 2017, doi: 10.3390/app7050515.

[22] M. Sohaib and J.-M. Kim, "Reliable Fault Diagnosis of Rotary Machine Bearings Using a Stacked Sparse Autoencoder-Based Deep Neural Network," 2018, doi: 10.1155/2018/2919637.

[23] H. Liu, J. Zhou, Y. Zheng, W. Jiang, and Y. Zhang, "Fault diagnosis of rolling bearings with recurrent neural network-based autoencoders," *ISA Trans.*, vol. 77, pp. 167–178, Jun. 2018, doi: 10.1016/j.isatra.2018.04.005.

[24] W. Sun, S. Shao, R. Zhao, R. Yan, X. Zhang, and X. Chen, "A sparse auto-encoder-based deep neural network approach for induction motor faults classification," *Meas. J. Int. Meas. Confed.*, vol. 89, pp. 171–178, Jul. 2016, doi: 10.1016/j.measurement.2016.04.007.

[25] S. Mittal, "A Survey on optimized implementation of deep learning models on the NVIDIA Jetson platform," *Journal of Systems Architecture*, vol. 97. Elsevier B.V., pp. 428–442, Aug. 01, 2019, doi: 10.1016/j.sysarc.2019.01.011.

[26] C. Y. Lin, C. P. Weng, L. C. Wang, H. H. Shuai, and W. P. Tseng, "Edge-Based RNN Anomaly Detection Platform in Machine Tools," *Smart Sci.*, vol. 7, no. 2, pp. 139–146, Apr. 2019, doi: 10.1080/23080477.2019.1578921.

[27] P. Lipnicki, D. Lewandowski, M. Syfert, A. Sztyber, and P. Wnuk, "Inteligent IoTSP - Implementation of embedded ML AI tensorflow algorithms on the NVIDIA jetson Tx Chip," in *Proceedings - 2019 International Conference on Future Internet of Things and Cloud, FiCloud 2019*, Aug. 2019, pp. 296–302, doi: 10.1109/FiCloud.2019.00049.

[28] "Introduction to Reliability Centered Maintenance (RCM) Part 1." http://www.plant-maintenance.com/RCM-intro.shtml (accessed Feb. 11, 2021).

[29] G. Thurston, Michael, G; McConky, Sean, P; Valant, Chris, J; Nenadic, Nenad, "Feasibility of Diagnostics, Prognostics and Hybrid Prognostics across Multiple Platforms," Rochester, NY, 2019. [Online]. Available: https://apps.dtic.mil/sti/pdfs/AD1076028.pdf.

[30] A. Taghizadeh-Alisaraei and A. Mahdavian, "Fault detection of injectors in diesel engines using vibration time-frequency analysis," *Appl. Acoust.*, vol. 143, pp. 48–58, Jan. 2019, doi: 10.1016/j.apacoust.2018.09.002.

[31] A. P. Carlucci, F. F. Chiara, and D. Laforgia, "Analys s of the relation between injection parameter variation and block vibration of an internal combustion diesel engine," *J. Sound Vib.*, vol. 295, no. 1–2, pp. 141–164, Aug. 2006, doi: 10.1016/j.jsv.2005.12.054.

[32] J. A. Pagán Rubio, F. Vera-García, J. Hernandez Grau, J. Muñoz Cámara, and D. Albaladejo Hernandez, "Marine diesel engine failure simulator based on thermodynamic model," *Appl. Therm. Eng.*, vol. 144, pp. 982–995, Nov. 2018, doi: 10.1016/j.applthermaleng.2018.08.096.

[33] J. Porteiro, J. Collazo, D. Patiño, and J. L. Míguez, "Diesel engine condition monitoring using a multi-net neural network system with nonintrusive sensors," 2011, doi: 10.1016/j.applthermaleng.2011.08.020.

[34] T. Figlus, Š. Liščák, A. Wilk, and B. Łazarz, "Condition monitoring of engine timing system by using wavelet packet decomposition of a acoustic signal," *J. Mech. Sci. Technol.*, vol. 28, no. 5, pp. 1663–1671, May 2014, doi: 10.1007/s12206-014-0311-3.

[35] J. Flett and G. M. Bone, "Fault detection and diagnosis of diesel engine valve trains," *Mech. Syst. Signal Process.*, vol. 72–73, pp. 316–327, May 2016, doi: 10.1016/j.ymssp.2015.10.024.

[36] "D&W Diesel." https://www.dwdiesel.com/home (accessed Sep. 21, 2022).

[37] A. Prajapati, J. Bechtel, and S. Ganesan, "Condition based maintenance: a survey," doi: 10.1108/13552511211281552.

[38] N. M. Vichare and M. G. Pecht, "Prognostics and health management of electronics," *IEEE Trans. Components Packag. Technol.*, vol. 29, no. 1, pp. 222–229, 2006, doi: 10.1109/TCAPT.2006.870387.

[39] M. J. Ashby and R. J. Byer, "An approach for conducting a cost benefit analysis of aircraft engine prognostics and health management functions," in *IEEE Aerospace Conference Proceedings*, 2002, vol. 6, pp. 2847–2856, doi: 10.1109/AERO.2002.1036124.

[40] T. Zaman and A. Bayoumi, "Estimation of Econcmic Effectiveness of HUMS equipped AH-64 Aircraft: An ROI Approach," 2016.

[41] V. & B. Blechertas Abdel & Goodman, Nicholas & Shah, Ronak & Shin, Yong-June, "CBM Fundamental Research at the University of South Carolina: A Systematic Approach to U.S. Army Rotorcraft CBM and the Resulting Tangible Benefits," 2009.

[42] A. Bayoumi, N. Goodman, R. Shah, L. Eisner, L. Grant, and J. Keller, "Conditioned-based maintenance at USC - Part IV: Examination and cost-benefit analysis of the CBM process," *Am. Helicopter Soc. Int. - AHS Int. Cond. Based Maint. Spec. Meet. 2008*, no. October, pp. 32–41, 2008.

[43] N. B. Hölzel, T. Schilling, and V. Gollnick, "An aircraft lifecycle approach for the cost-benefit analysis of Prognostics and condition-based maintenance based on discrete-event simulation," *PHM 2014 - Proc. Annu. Conf. Progn. Heal. Manag. Soc. 2014*, pp. 435–450, 2014.

[44] J. C. Banks, E. Crow, K. Reichard, and R. Ruark, "A cost-renefits analysis of the effect of condition-based maintenance strategies for military ground vehicles," *IEEE Aerosp. Conf. Proc.*, vol. 7, no. February 2017, pp. 3227–3237, 2003, doi: 10.1109/AERO.2003.1234166.

[45] M.-H. Chang, P. Sandborn, M. Pecht, W. K. C. Yung, and W. Wang, "A return on investment analysis of applying health monitoring to LED lighting systems," in *Microelectronics Reliability*, 2015, pp. 527–537.

[46] P. S. and T. J. K. Feldman, "The analysis of Return on Investment for PHM applied to electronic systems," in *International Conference on Prognostics and Health Management*, 2008, pp. 1–9.

[47] P. Sandborn, *Cost Analysis of Electronic Systems*, vol. 1. WORLD SCIENTIFIC, 2013.

[48] K. Feldman, P. Sandborn, and T. Jazouli, "The analysis of return on Investment For PHM applied to electronic systems," *2008 Int. Conf. Progn. Heal. Manag. PHM 2008*, 2008, doi: 10.1109/PHM.2008.4711415.

[49] S. M. Wood and D. L. Goodman, "Return-on-investment (ROI) for electronic prognostics in high reliability telecom applications," 2006, doi: 10.1109/INTLEC.2006.251619.

[50] R. Bakhshi, P. Sandborn, X. Lei, and A. Kashani-Pour, "Return on Investment Modeling to Support Cost Avoidance Business Cases for Wind Farm O&M," *EWEA Offshore 2015*, no. 1, 2015, [Online]. Available: http://s3.amazonaws.com/academia.edu.documents/44486305/Return_on_Investment_Modeling_to_Support20160406-4352-12pugzp.pdf?AWSAccessKeyId=AKIAIWOWYYGZ2Y53UL3A&Expires=1495580289&Signature=3x0tqAPeNEBK5zukGWn5VSLK97Y%253D&response-content-disposition=inline.

[51] R. M. Kent and D. A. Murphy, "Health Monitoring System Technology Assessments Ð Cost Benefits Analysis," 2000. Accessed: Feb. 11, 2021. [Online]. Available: http://www.sti.nasa.gov.

[52] M. H. Chang, P. Sandborn, M. Pecht, W. K. C. Yung, and W. Wang, "A return on investment analysis of applying health monitoring to LED lighting systems," *Microelectron. Reliab.*, vol. 55, no. 3–4, pp. 527–537, 2015, doi: 10.1016/j.microrel.2015.01.009.

[53] "Federal Benefits | The Official Army Benefits Website." https://myarmybenefits.us.army.mil/Benefit-Library/Federal-Benefits (accessed Oct. 28, 2022).

[54] "US Military Active Duty Death Benefits & Entitlements." https://www.liveabout.com/active-duty-death-entitlements-3356940 (accessed Sep. 19, 2022).

[55] "Infantryman Salaries in the United States for U.S. Army | Indeed.com." https://www.indeed.com/cmp/U.S.-Army/salaries/Infantryman (accessed Oct. 24, 2022).

[56] "AH-1Z Viper and UH-1Y Venom Helicopters > United States Navy > Displayy-FactFiles." https://www.navy.mil/Resources/Fact-Files/Display-FactFiles/Article/2160217/ah-1z-viper-and-uh-1y-venom-helicopters/ (accessed Sep. 18, 2022).

[57] A. Jones, "NAVAIR CBM+ Initiative and H-1 Case Study." National Center for Manufacturing Sciences, 2020, Accessed: Jan. 27, 2022. [Online]. Available: https://jteg.ncms.org/wp-content/uploads/2019/09/06-NAVAIR-JTEG-CBM.pdf.

[58] "Fiscal Year (FY) 2011 Budget Estimates Defense Contract Audit Agency (DCAA)," 2010, Accessed: Jan. 27, 2022. [Online]. Available: www.dcaa.mil.

[59] "HeliHub.com : Simmonds Precision Products awarded $8M contract for H-1 HUMS systems - HeliHub.com." https://helihub.com/2015/03/23/simmonds-precision-products-awarded-8m-

contract-for-h-1-hums-systems/ (accessed Feb. 16, 2022).

[60] G. Frawley, *The International Directory of Military Aircraft*. Aerospace Publications, 2002.

[61] M. G. Mattock, B. J. Asch, J. Hosek, and M. Boito, "The Relative Cost-Effectiveness of Retaining Versus Accessing Air Force Pilots," 2019, Accessed: Sep. 19, 2022. [Online]. Available: www.rand.org/t/RR2415.

[62] "Military Times 2019 Pay Raise," 2019. [Online]. Available: https://partner-mco-archive.s3.amazonaws.com/client_files/1546544795.pdf.

[63] "Amazon S3 Simple Storage Service Pricing - Amazon Web Services." https://aws.amazon.com/s3/pricing/ (accessed Sep. 20, 2022).

[64] "Amazon EC2 P3 – Ideal for Machine Learning and HPC - AWS." https://aws.amazon.com/ec2/instance-types/p3/ (accessed Sep. 20, 2022).

[65] "Oshkosh Family of Medium Tactical Vehicles (FMTV) - Army Technology." https://www.army-technology.com/projects/oshkosh-family-of-medium-tactical-vehicles-fmtv/ (accessed Sep. 22, 2022).

[66] "Marine Corps Embedded Platform Logistic System on Track for July Delivery, Nine Months After Contract Award - Mar 20, 2008." https://news.lockheedmartin.com/2008-03-20-Marine-Corps-Embedded-Platform-Logistic-System-on-Track-for-July-Delivery-Nine-Months-After-Contract-Award (accessed Oct. 24, 2022).

[67] M. Eugene and L. Morin, "2008 DoD Maintenance Symposium Marine Corps Autonomic Logistics."

[68] "Real cost of gas at Afghan bases: $400/gal. - CBS News." https://www.cbsnews.com/news/real-cost-of-gas-at-afghan-bases-400-gal/ (accessed Sep 22, 2022).

[69] "OPAT reducing trainee attrition, avoiding millions in wasted training dollars, officials say | Article | The United States Army." https://www.army.mil/article/207956/opat_reducing_trainee_attrition_avoiding_millions_in_wasted_training_dollars_officials_say (accessed Oct. 24, 2022).

[70] N. G. Nenadic, J. A. Wodenscheck, M. G. Thurston, and D. G. Lewicki, "Seeding Cracks Using a Fatigue Tester for Accelerated Gear Tooth Breaking Rotating Machinery, Structural Health Monitoring, Shock and Vibration, Volume 5," vol. 8, Springer New York, 2011, pp. 349–357.

[71] K. Worden, C. R. Farrar, G. Manson, and G. Park, "The fundamental axioms of structural health monitoring," *Proc. R. Soc. A Math. Phys. Eng. Sci.*, vol. 463, no. 2082, p. 1639, 2007.

[72] T. E. Oliphant, *A Guide to NumPy*, vol. 1. Trelgol Publishing USA, 2006.

[73] J. D. Hunter, "Matplotlib: A 2D graphics environment," *Comput. Sci. Eng.*, vol. 9, pp. 90–95, 2007.

[74] F. Perez and B. E. Granger, "IPython: a system for interactive scientific computing," *Comput. Sci. Eng.*, vol. 9, no. 3, pp. 21–29, 2007.

[75] E. Bechhoefer and M. Kingsley, "A review of time synchronous average algorithms," in *Annual Conference of the PHM society*, 2009, vol. 1, no. 1.

[76] N. G. Nenadic, P. A. Ardis, A. Hood, M. G. Thurston, and D. G. Lewicki, "Processing and interpretation of crack-propagation sensors," 2015.

[77] P. Domingos, "A few useful things to know about machine learning," *Commun. ACM*, vol. 55, no. 10, pp. 78–87, 2012.

[78] Y. Bengio, I. J. Goodfellow, and A. Courville, "Deep Learning," 2015.

[79] N. Japkowicz, C. Myers, and M. Gluck, "A novelty detection approach to classif cation," in *IJCAI*, 1995, vol. 1, pp. 518–523.

[80] C. M. Bishop, "Model-based machine learning," *Philos. Trans. R. Soc. London A Math. Phys. Eng. Sci.*, vol. 371, no. 1984, p. 20120222, 2013.

[81] W. Yang, S. Sheng, and R. Court, "Operational-Condition-Independent Criteria Dedicated to Monitoring Wind Turbine Generators," *IJPHM Spec. Issue Wind Turbine PHM*, p. 3, 2012.

[82] N. Eklund, "Anomaly Detection Tutorial." Annual Conference of the Prognostics and Health Management Society, Philadelphia, PA, 2018.

[83] M. Lebold, K. McClintic, R. Cambell, C. Byington, and K. Maynard, "Review of Vibration Analysis Methods for Gearbox Diagnostics and Prognostics," in *Proceedings of the 54th Meeting of the Society for Machinery Failure Prevention Technology*, 2000, pp. 623–634.

[84] P. D. Samuel and D. J. Pines, "A review of vibration-based techniques for helicopter transmission diagnostics," vol. 282, no. 1–2, pp. 475–508, 2005, doi: 10.1016/j.jsv.2004.02.058.

[85] F. Pedregosa *et al.*, "Scikit-learn: Machine learning in Python," *J. Mach. Learn. Res.*, vol. 12, pp. 2825–2830, 2011.

[86] M. Abadi *et al.*, "TensorFlow: Large-Scale Machine Learning on Heterogeneous Distributed Systems," *arXiv Prepr. arXiv1603.04467*, 2016.

[87] N. Ketkar, "Introduction to PyTorch," in *Deep Learning with Python*, Springer, 2017, pp. 195–208.

[88] H. Qiu, J. Lee, J. Lin, and G. Yu, "Wavelet filter-based weak signature detection method and its application on rolling element bearing prognostics," *J. Sound Vib.*, vol. 289, no. 4–5, pp. 1066–1090, 2006.

[89] A. Dyson, "Scuffing - a review," *Tribol. Int.*, vol. 8, no. 2, pp. 77–87, Apr. 1975, doi: 10.1016/0301-679X(75)90056-0.

[90] I. S. Al-Tubi, H. Long, J. Zhang, and B. Shaw, "Experimental and analytical study of gear micropitting initiation and propagation under varying loading conditions," *Wear*, vol. 328–329, pp. 8–16, Apr. 2015, doi: 10.1016/J.WEAR.2014.12.050.

[91] J. W. Key and J. Kacher, "Establishing first order correlations between pitting corrosion initiation and local microstructure in AA5083 using automated image analysis," *Mater. Charact.*, vol. 178, p. 111237, Aug. 2021, doi: 10.1016/J.MATCHAR.2021.111237.

[92] A. Hood *et al.*, "Autoencoder Based Anomaly Detector for Gear Tooth Bending Fatigue Cracks," *Annu. Conf. PHM Soc.*, vol. 13, no. 1, Nov. 2021, doi: 10.36001/PHMCONF.2021.V13I1.3003.

[93] R. Zhao, R. Yan, Z. Chen, K. Mao, P. Wang, and R. X. Gao, "Deep learning and its applications to machine health monitoring," *Mech. Syst. Signal Process.*, vol. 115, pp. 213–237, Jan. 2019, doi: 10.1016/J.YMSSP.2018.05.050.

[94] F. Chaari, W. Baccar, M. S. Abbes, and M. Haddar, "Effect of spalling or tooth breakage on gearmesh

stiffness and dynamic response of a one-stage spur gear transmission," *Eur. J. Mech. - A/Solids*, vol. 27, no. 4, pp. 691–705, Jul. 2008, doi: 10.1016/J.EUROMECHSOL.2007.11.005.

[95] B. Zhang, H. Liu, C. Zhu, and Y. Ge, "Simulation of the fatigue-wear coupling mechanism of an aviation gear," *Frict. 2020 96*, vol. 9, no. 6, pp. 1616–1634, Dec. 2020, doi: 10.1007/S40544-020-0447-3.

7 Appendix A: Reliability Centered Maintenance Analysis of a Cummins Diesel Engine

A reliability centered maintenance (RCM) analysis was performed on the Cummins diesel engine. For the purpose of the analysis, the engine and the directly attached subsystems were considered. The attached subsystems consist of: the turbocharger, engine lubrication system, engine fuel metering system, water pump and thermostat, engine block (including all internal components), and the exhaust manifold. The failure modes and effects analysis for the systems is included in Appendix A, Section 7.1. Each failure mode is further analyzed to identify the consequences of the failure and to identify the type of maintenance task necessary. The resulting outcomes of the analysis are Run-to-Failure (RTF), On-Condition (OC) maintenance, Scheduled Repair (SR), or redesign. For this analysis, the focus was on maintenance tasks and not whether redesign was warranted. The outcome of the RCM analysis is included in Appendix A, Section 7.2.

7.1 Failure Modes and Effects Analysis

The failure modes and effects analysis (FMEA) provided below is the result of a group analysis of the engine and attached subsystems. The output of the FMEA is utilized when evaluating the failures in the RCM process.

System	Function	Functional Failure	Failure Mode	Failure Evidence	Effect Description	Occurrence	Severity	Detection	RPN	Operator Compensation
1: Turbocharger	A: Maintain lubrication of bearing surfaces	1: Insufficient or reduced lubrication	1.1, Normal wear							
1: Turbocharger	A: Maintain lubrication of bearing surfaces	1: Insufficient or reduced lubrication	1, Bearing wear	Sluggish response from turbo, noise. Lower boost.	Lack of lubrication increase wear of bearings.	3	7	5	105	More throttle
1: Turbocharger	A: Maintain lubrication of bearing surfaces	1: Insufficient or reduced lubrication	2.1, Premature shutdown of engine preventing proper cool down of turbo							
1: Turbocharger	A: Maintain lubrication of bearing surfaces	1: Insufficient or reduced lubrication	2, Coke bearing surface	Reduced power. Low boost gauge pressure	Reduced power, vibration, bearing failure.	3	7	7	147	More throttle
1: Turbocharger	A: Maintain lubrication of bearing surfaces	1: Insufficient or reduced lubrication	1.2, Premature shutdown of engine preventing proper cool down of turbo							
1: Turbocharger	B: Contains Oil	1: Does not contain oil	1, Seal leaks	None	Oil coating intercooler, reducing efficiency.	5	1	10	50	More Throttle
1: Turbocharger	B: Contains Oil	1: Does not contain oil	2, Fitting leaks	Smoke under hood, low oil light, low oil pressure warning light	Supply side - starvation of oil to turbo. Return side - visible oil	3	7	3	63	Shutdown engine
1: Turbocharger	C: Compress intake air	1: Insufficient compression of intake air	2.1, Stuck linage	Sluggish performance, reduced boost	Delayed response from turbo, low engine power output	1	4	3	12	More throttle
1: Turbocharger	C: Compress intake air	1: Insufficient compression of intake air	1, Worn bearings	Sluggish response from turbo, noise. Lower boost.	Lack of lubrication increase wear of bearings.	3	7	5	105	More throttle
1: Turbocharger	C: Compress intake air	1: Insufficient compression of intake air	2.2, Diaphragm spring failure	Sluggish performance, reduced boost	Delayed response from turbo, low engine power output	3	4	3	36	More throttle
1: Turbocharger	C: Compress intake air	1: Insufficient compression of intake air	2, Waste Gate Stuck Open	Sluggish performance, reduced boost	Delayed response from turbo, low engine power output	1	4	3	12	More throttle

System	Function	Functional Failure	Failure Mode	Failure Evidence	Effect Description	Occurrence	Severity	Detection	RPN	Operator Compensation
1: Turbocharger	C: Compress intake air	2: Over compression of intake air	1.1, Diaphragm failure	Over boost, air leak hiss, turbo whine	Over boost	3	4	1	12	Less throttle
1: Turbocharger	C: Compress intake air	2: Over compression of intake air	1, Waste Gate stuck closed							
1: Turbocharger	C: Compress intake air	2: Over compression of intake air	1.2, linkage stuck	Over boost, turbo whine	Over boost	3	4	3	36	Less throttle
1: Turbocharger	C: Compress intake air	2: Over compression of intake air	1.3, Air hose failure/disconnection	Over boost?, air leak hiss, turbo whine	Over boost?	3	4	1	12	Less throttle
1: Turbocharger	C: Compress intake air	3: Fails to compress air	1, Sheared or damaged turbine blades	Low power, noise,	No compressed air going to engine. Engine damaged via ingresses metal. Clog exhaust pathway.	1	7	5	35	Stop engine.
1: Turbocharger	C: Compress intake air	3: Fails to compress air	2, Shaft broken	Low power, very noisy, engine shutdown	No compressed air going to engine. Engine damaged via ingresses metal. Clog exhaust pathway. Exhaust turbine going to seize. Internal oil leak.	1	7	1	7	Stop engine.
1: Turbocharger	C: Compress intake air	3: Fails to compress air	3, Bearing seized	Low power, noise	No compressed air going to engine. Metal filings in oil.	3	7	5	105	Stop engine.
1: Filter Bypass Valve	A: Maintain oil flow under restricted filter conditions	1: Does not close at proper pressure	1, Debris caught in sealing face	None	Dirty oil cause clogs or accelerated wear	3	1	10	30	None
1: Filter Bypass Valve	A: Maintain oil flow under restricted filter conditions	1: Does not close at proper pressure	2, failed spring	None	Spring does not apply pressure to close plate	3	1	10	30	None
1: Filter Bypass Valve	A: Maintain oil flow under restricted filter conditions	2: Does not open at set pressure	1, Jammed by debris	Oil pressure too high - under certain conditions	High differential pressure being too high	3	1	10	30	None
1: Filter Bypass Valve	A: Maintain oil flow under restricted filter conditions	3: Opens at too low of a pressure	1, Weakened spring	None	Oil not going through filter, premature engine wear	1	1	10	10	none
2: Oil Thermostat	A: Maintain oil temperature	1: Allowing oil to overheat	1, Return spring failure	Temp gauge on dash, idiot light, force engine shutdown	Spring failure will not force oil through heat exchanger	3	7	3	63	None, shut down

System	Function	Functional Failure	Failure Mode	Failure Evidence	Effect Description	Occurrence	Severity	Detection	RPN	Operator Compensation
2: Oil Thermostat	A: Maintain oil temperature	1: Allowing oil to overheat	2, Debris not allowing to seat	Elevated oil temp under high load	minor chance	1	1	7	7	none
2: Oil Thermostat	A: Maintain oil temperature	2: Premature cooling of the oil	1, Thermostat stuck sealing bypass	Takes longer for oil to heat up	Oil does not comes up to temp	1	1	7	7	none
3: Oil Pump	A: Create pressurized oil flow	1: Reduced oil flow	1, Wear of side plates	reduced oil pressure, elevated oil temp	Reduced oil pressure and flow through system. Reduced level of lubrication to critical components	3	4	7	84	drive slower, minimize load on engine
3: Oil Pump	A: Create pressurized oil flow	1: Reduced oil flow	2, Wear of pump lobes	reduced oil pressure, elevated oil temp	Reduced oil pressure and flow through system. Reduced level of lubrication to critical components	3	4	7	84	drive slower, minimize load on engine
3: Oil Pump	A: Create pressurized oil flow	2: Fail to create oil flow	1, Failure of pump gerotor	No oil pressure, noise under hood, engine stop, temp increase	Oil not flowing through engine. Excessive wear of engine.	1	7	1	7	Stop engine
4: Oil Pressure Regulator	A: Contain oil in pressurized section of system below X PSI	1: Allows premature flow of oil to sump	1, Valve stuck due to debris	Low oil pressure, engine temp raise, noise	lack of lubrication to critical bearings, turbo, piston squirters; increase of temp on wear surfaces, increase wear, possible seized engine	1	7	3	21	engine shutdown
4: Oil Pressure Regulator	A: Contain oil in pressurized section of system below X PSI	1: Allows premature flow of oil to sump	2, Broken/weak spring	Low oil pressure, engine temp raise, noise	lack of lubrication to critical bearings, turbo, piston squirters; increase of temp on wear surfaces, increase wear, possible seized engine	3	7	3	63	engine shutdown
4: Oil Pressure Regulator	B: Prevent excess oil pressure	1: Fails to relieve over pressure	1, Valve seized	High oil pressure, set off warning light?	increase pressure through journal bearings, excessive wear on pump, unlikely to cause catastrophic consequences	1	4	3	12	limit engine RPM
5: Oil Filter Assembly	A: Contain Oil	1: Rupture of canister	1, Road debris strike	Sudden drop of oil pressure, low oil light, noise	Oil drained, lack of lubrication on all critical surfaces, increase engine temp, engine failure	1	7	3	21	Shut down engine

System	Function	Functional Failure	Failure Mode	Failure Evidence	Effect Description	Occurrence	Severity	Detection	RPN	Operator Compensation
5: Oil Filter Assembly	A: Contain Oil	2: Leaking O-ring	1, Knick in O-ring	Oil on ground and engine. Smoke from exhaust/hood.	Lose lubrication to critical surfaces.	3	7	3	63	shutdown engine
5: Oil Filter Assembly	A: Contain Oil	2: Leaking O-ring	2, Install problem	Oil on ground and engine. Smoke from exhaust/hood.	Lose lubrication to critical surfaces.	3	7	3	63	shutdown engine
5: Oil Filter Assembly	B: Collect and contain dirt and debris	1: Internal relief is actuated	1, Filter is clogged	none	Excessive wear, larger debris passing through filter.	3	1	10	30	none
6: Cooler Assembly	A: Prevent mixture of oil and coolant	1: Cross contamination of coolant and oil	1, Fatigue failure of the plates	White smoke in exhaust, slow oil consumption. Raising coolant temp	Oil is higher pressure, so would see oil in coolant.	3	1	10	30	reduce throttle, top off fluids
6: Cooler Assembly	B: Contain oil	1: Leaks Oil to engine compartment	1, Gasket failure of outside edge of casting	Smoke from oil hitting exhaust, smell burning oil, low oil on dipstick	No performance issues	3	1	3	9	None
6: Cooler Assembly	C: Transfer Heat from oil to cooling system	1: Inefficient removal of heat	1, Debris\sludge inside of fins	none	Insulating layer of sludge, reduced heat transfer. Breakdown of oil properties, engine wear	3	1	10	30	none
6: Cooler Assembly	C: Transfer Heat from oil to cooling system	1: Inefficient removal of heat	2, Corrosion of fins on coolant side	if oil temp gauge, would see elevated temp	oil less viscous	1	1	10	10	none
1: Fuel Injector Assembly	A: Contain fuel	1: Leaking fuel	1, Cracked injector body	Poor fuel economy, high oil on dip stick	Poor lubrication, poor fuel economy.	1	4	10	40	No compensation.
1: Fuel Injector Assembly	A: Contain fuel	1: Leaking fuel	3.1, Damaged O-ring	Rough operation, blow black smoke.	Rough operation, low power output	1	4	3	12	More throttle
1: Fuel Injector Assembly	A: Contain fuel	1: Leaking fuel	2.1, Damaged fitting	Leaking fuel, fuel odor	Poor fuel economy, misfire, no start, fuel in oil	1	4	3	12	Stop engine
1: Fuel Injector Assembly	A: Contain fuel	1: Leaking fuel	2, Fitting failure							
1: Fuel Injector Assembly	A: Contain fuel	1: Leaking fuel	3, O-ring failure							
1: Fuel Injector Assembly	B: Measured amount and timing of fuel into the cylinders	1: No fuel	1, Solenoid coil short	Misfire, reduction of power	Lack of fuel into cylinder, engine stumbling	3	7	3	63	More throttle

System	Function	Functional Failure	Failure Mode	Failure Evidence	Effect Description	Occurrence	Severity	Detection	RPN	Operator Compensation
1: Fuel Injector Assembly	B: Measured amount and timing of fuel into the cylinders	1: No fuel	2, Clog of injector orifice	misfire, lack of power, erratic engine RPM, trouble starting	low power output, rough engine, none or poor spray of fuel into cylinder	3	7	3	63	more throttle
1: Fuel Injector Assembly	B: Measured amount and timing of fuel into the cylinders	2: Excessive fuel	1, Solenoid Stuck Open	Bad idle, diesel smell in exhaust, misfire	Poor fuel mileage, turbo overheating	3	4	5	60	More throttle
1: Fuel Injector Assembly	B: Measured amount and timing of fuel into the cylinders	2: Excessive fuel	2, Solenoid ball erosion	Not starting, hard to start, poor fuel economy, engine knock	diesel leaks into cylinder, elevated return flow	3	1	5	15	crank engine longer when starting during operation - nothing
1: Fuel Injector Assembly	B: Measured amount and timing of fuel into the cylinders	2: Excessive fuel	3, Erosion of orifice	Poor fuel economy, blueish white smoke, poor idle, rough start	Excess fuel leaking into cylinder. Cylinder knocking.	3	4	1	12	Nothing
1: Fuel Injector Assembly	B: Measured amount and timing of fuel into the cylinders	2: Excessive fuel	4, Return spring weakens	Run rough	Opens early, closes later, poor combustion	5	1	7	35	more throttle
1: Fuel Injector Assembly	B: Measured amount and timing of fuel into the cylinders	3: Insufficient Fuel	1, Solenoid coil short	Misfire, reduction of power	Lack of fuel into cylinder, engine stumbling	3	7	3	63	More throttle
1: Fuel Injector Assembly	B: Measured amount and timing of fuel into the cylinders	3: Insufficient Fuel	2, Clog of injector orifice	misfire, lack of power, erratic engine RPM, trouble starting	low power output, rough engine, none or poor spray of fuel into cylinder	3	7	3	63	more throttle
2: Mechanical Fuel Pump	A: Contains fuel	1: Fuel leakage	1, Failure of the pump head seal	slight potential of decreased power	Fuel leakage may decrease the ability to compress he fuel efficiently. Thereby causing a decrease in fuel rail pressure. This may be slightly mitigated by the fact it is a two piston pump.	1	4	7	28	More throttle

System	Function	Functional Failure	Failure Mode	Failure Evidence	Effect Description	Occurrence	Severity	Detection	RPN	Operator Compensation
2: Mechanical Fuel Pump	B: Transmit fuel at a specified pressure and flow rate	1: Excessive pressure	1, Flow control valve/solenoid failure	Potential decrease in power.	The flow control valve is stuck open, allowing full flow to the piston pump. The pressure will increase until the fuel rail pressure relief opens at 1800 bar. This will be followed by a potential decrease in pressure to 1000 bar.	3	4	7	84	More throttle if a decrease in power is sensed.
2: Mechanical Fuel Pump	B: Transmit fuel at a specified pressure and flow rate	2: No fuel flow	1, Piston failure/stuck	Vehicle shutdown or vehicle won't start	Piston breaks and sticks in a position to prevent the cam from rotating. Cam is unable to rotate to produce pressure. This failure could also lead to tearing up the drive gear which will lead to no fuel flow.	1	7	1	7	Do not attempt to restart.
2: Mechanical Fuel Pump	B: Transmit fuel at a specified pressure and flow rate	2: No fuel flow	2, Support Bearing Failure	Noise from bearings, vehicle shutdown, vehicle won't start	The support bearing will begin whining and making noise as failure occurs. If the bearing completely fails, it may seize or produce enough friction to prevent the starter from starting the engine.	1	7	5	35	None.
2: Mechanical Fuel Pump	B: Transmit fuel at a specified pressure and flow rate	3: Insufficient pressure	1, Inlet Check Valve Sticking	Decrease in power	The piston will be continuously open to the low pressure side of the pump, thereby limiting the ability of the piston to build pressure. The lower pressure will prevent the output check valve from opening and no a fuel will flow from that piston into the	3	7	7	147	More throttle

System	Function	Functional Failure	Failure Mode	Failure Evidence	Effect Description	Occurrence	Severity	Detection	RPN	Operator Compensation
2: Mechanical Fuel Pump	B: Transmit fuel at a specified pressure and flow rate	3: Insufficient pressure	2, Outlet Check Valve Sticking	Decrease in power	An outlet check that is stuck open will allow pressurized fuel to flow back into the piston chamber during the piston downstroke. Thereby preventing new fuel from entering the chamber. Over time the fuel rail pressure will decrease, potentially limiting	3	4	7	84	More throttle
2: Mechanical Fuel Pump	B: Transmit fuel at a specified pressure and flow rate	3: Insufficient pressure	3, Piston Wear	Decrease in power	Piston wear may lead to leakage around the piston, thereby reducing the pressure the piston may generate. This will reduce fuel pressure and possible engine power. Additionally, he piston could become stuck, preventing the fuel pump from generating any f	3	7	5	105	More throttle
2: Mechanical Fuel Pump	B: Transmit fuel at a specified pressure and flow rate	3: Insufficient pressure	4, Camshaft or tappet wear	Potential decrease in power	Camshaft or tappet wear will decrease the stroke of the piston. This will lead to a decrease in efficiency and maximum attainable pressure. Overall this has the potential to decrease the overall fuel rail pressure, and thus engine power.	3	4	7	84	More throttle

System	Function	Functional Failure	Failure Mode	Failure Evidence	Effect Description	Occurrence	Severity	Detection	RPN	Operator Compensation
2: Mechanical Fuel Pump	B: Transmit fuel at a specified pressure and flow rate	3: Insufficient pressure	5, Flow Control Valve/Solenoid Failure	Potential decrease in power.	The flow control valve is stuck open, allowing full flow to the piston pump. The pressure will increase until the fuel rail pressure relief opens at 1800 bar. This will be followed by a potential decrease in pressure to 1000 bar.	3	4	7	84	More throttle if a decrease in power is sensed.
3: Low pressure supply lines	A: Transport low pressure fuel - Supply connector to HP Pump	1: Insufficient fuel flow	1, Major crack in hose	Rough operation, possible shutdown	Engine starved of fuel.	3	7	3	63	More Throttle, should turn off vehicle
4: High pressure supply line	A: Transport pressurized fuel (High Pressure fuel pump to injectors)	1: Insufficient flow of fuel	1, Fitting Leak	Drop of fuel pressure gauge. Engine stumble. Loss of engine power.	Reduction in fuel economy, loss of power.	1	4	5	20	More throttle. Shutdown
4: High pressure supply line	A: Transport pressurized fuel (High Pressure fuel pump to injectors)	1: Insufficient flow of fuel	2, Rupture in line	Drop of fuel pressure gauge. Engine stumble. Loss of engine power.	Reduction in fuel economy, loss of power.	1	4	5	20	More throttle. Shutdown
4: High pressure supply line	A: Transport pressurized fuel (High Pressure fuel pump to injectors)	1: Insufficient flow of fuel	3, Blockage in line	Rough running engine, loss of power. Possible engine stall/no start.	Insufficient fuel to one or more injectors.	1	7	7	49	More throttle
4: High pressure supply line	A: Transport pressurized fuel (High Pressure fuel pump to injectors)	2: Fuel pressure too low	1, Crack in HP line or Fuel Rail	Rough operation, check engine light/trouble code, fuel odor. Engine shutdown. No start.	Engine starved of fuel. Loss of power.	3	7	5	105	Shut down vehicle.
4: High pressure supply line	A: Transport pressurized fuel (High Pressure fuel pump to injectors)	2: Fuel pressure too low	2, Fitting Failure	Rough operation, check engine light/trouble code, fuel odor. Engine shutdown. No start.	Engine starved of fuel. Loss of power.	1	7	5	35	Shut down vehicle.
4: High pressure supply line	A: Transport pressurized fuel (High Pressure fuel pump to injectors)	2: Fuel pressure too low	3, Pressure relief valve failure	Rough operation, check engine light/trouble code, fuel odor. Engine shutdown. No start.	Engine starved of fuel. Loss of power.	1	7	10	70	Shut down vehicle.

System	Function	Functional Failure	Failure Mode	Failure Evidence	Effect Description	Occurrence	Severity	Detection	RPN	Operator Compensation
6: Fuel Filter	A: Contain Fuel	1: Rupture of canister	1, Road debris strike	Fuel pressure warning. Smell of fuel. Rough engine/engine shutdown.	Starve fuel to high pressure pump and engine.	1	7	3	21	More throttle. Shutdown engine.
6: Fuel Filter	A: Contain Fuel	2: Leaking O-ring	1, Knick in O-ring	Fuel on ground. Smell of fuel.	Minimal loss of fuel	1	1	7	7	none
6: Fuel Filter	A: Contain Fuel	2: Leaking O-ring	2, Install Problem	Fuel on ground and engine.	(none)	1	1	7	7	(none)
6: Fuel Filter	B: Collect and contain dirt and debris	1: Inability to supply enough fuel through filter	1, Filter is clogged	Loss of performance during high need.	Engine starved of fuel when under high load.	3	4	10	120	Less throttle
1: Water Pump Assembly	A: Contain coolant	1: Coolant leaks from the water pump to housing mounting surface at the O-ring	1, Thermal fatigue of O ring	Elevated engine/coolant temp, coolant odor, steam	Engine overheating, loss of engine power, degradation of engine oil	3	4	3	36	Add coolant/water to overflow reservoir, reduce engine loading and operation
1: Water Pump Assembly	A: Contain coolant	2: Coolant leaks from the water pump shaft seal	1, Seal wear	Coolant leaking on front of engine. Steam from coolant on hot engine. Belt squealing.	Coolant loss, coolant on belt causing slippage	5	1	5	25	Add coolant to coolant reservoir
1: Water Pump Assembly	B: Create coolant flow	1: No flow of coolant from water pump	1, Pump drive pulley shears from pump drive shaft	Overheat, loss serpentine belt and power steering(?), alternator.	Loss of coolant flow, loss of alternator power	1	7	3	21	pull over
1: Water Pump Assembly	B: Create coolant flow	1: No flow of coolant from water pump	2, Seized pump shaft/bearing	Overheat, serpentine belt noise; belt loss after significant time	Loss of coolant flow; belt heating and wear	1	7	3	21	pull over
1: Water Pump Assembly	B: Create coolant flow	2: Reduced coolant flow from water pump	1, Slippage of press fit	Intermittent overheating, particularly at high RPMs	Low coolant flow, increased coolant temps	3	4	7	84	Keep RPMs low
1: Water Pump Assembly	B: Create coolant flow	2: Reduced coolant flow from water pump	2, Corrosion and cavitation on impellers	Increased coolant temps.	Low coolant flow, increased coolant temps	5	4	7	140	Keep RPMs low, keep load down
2: Thermostat	A: Direct coolant to radiator to maintain temperature	1: Low fluid flow to the radiator	1, Thermostat stuck partially open	Take too long to get coolant to temp. Cabin heater stays cool. At normal temps, potential overheating situation.	Coolant temp not well regulated. Coolant taking longer to reach operating temp. Coolant temp overshoots and is too hot.	5	4	5	100	More throttle when too cool, less throttle when too hot.

System	Function	Functional Failure	Failure Mode	Failure Evidence	Effect Description	Occurrence	Severity	Detection	RPN	Operator Compensation
2: Thermostat	A: Direct coolant to radiator to maintain temperature	2: Too much fluid flow to radiator	1, Thermostat stuck open	Take too long to get coolant to temp. Cabin heater stays cool.	Coolant temp not well regulated. Coolant taking longer to reach operating temp. Engine may not reach operating temp.	5	1	3	15	More throttle when too cool.
2: Thermostat	A: Direct coolant to radiator to maintain temperature	3: No fluid flow to radiator	1, Thermostat stuck closed	Overheating situation.	Coolant temp overshoots and is too hot.	5	7	3	105	Stop and let vehicle cool down.
7: Engine Block Assembly	A: Provide pathways for lubrication	1: Restricted or blocked lubrication pathway	1, Clogged oil passageways	Pressure gauge higher or lower than normal. Rough operation. Possible heat buildup. Possible vibration.	Clog will starve one or more bearings or piston squirters of oil. Cause to excess heat and wear.	1	7	5	35	Stop
7: Engine Block Assembly	A: Provide pathways for lubrication	1: Restricted or blocked lubrication pathway	2, Clogged oil pickup	No oil pressure. Rough operation. High operating temp	All bearing surfaces starved of oil. High wear and scaring of bearing surfaces.	1	7	3	21	Stop engine
7: Engine Block Assembly	B: Contain oil for lubrication	1: Major loss of oil (> quart/ 12 hours or 475 miles of operation)	1, Head gasket failure	Engine temp increase. Blue smoke in exhaust.	Cross contamination of fluids. Decrease in cooling efficiency. Coking inside cylinders.	3	4	5	60	Reduce engine load or shutdown.
7: Engine Block Assembly	B: Contain oil for lubrication	1: Major loss of oil (> quart/ 12 hours or 475 miles of operation)	2, Front crank seal failure	Leak on ground. Possible belt slippage and squeak. Possible overheating.	If on belt, potential for slippage of alternator and water pump.	3	4	5	60	Potential shutdown of vehicle.
7: Engine Block Assembly	B: Contain oil for lubrication	1: Major loss of oil (> quart/ 12 hours or 475 miles of operation)	3, Front timing cover seal failure	Leak on ground. Potential for overheating.	If on belt, potential for slippage of alternator and water pump.	3	4	5	60	Potential shutdown.
7: Engine Block Assembly	B: Contain oil for lubrication	1: Major loss of oil (> quart/ 12 hours or 475 miles of operation)	4, Rear main seal failure	Bad shifting/clutch due to oil on clutch surface.	Clutch slippage and	3	7	3	63	Stop.
7: Engine Block Assembly	B: Contain oil for lubrication	1: Major loss of oil (> quart/ 12 hours or 475 miles of operation)	5, Turbo oil supply line leak	Oil on side of engine. Smoke from oil burning off. Drop in oil pressure.	Lack of oil to turbo, bearing overheating.	3	7	3	63	Stop engine
7: Engine Block Assembly	B: Contain oil for lubrication	1: Major loss of oil (> quart/ 12 hours or 475 miles of operation)	6, Turbo oil return line leak	Leak on the ground. Possible smoke from oil on exhaust. Low oil light.	No impact if vehicle has low oil light.	3	4	3	36	Stop engine when low oil light goes on.

System	Function	Functional Failure	Failure Mode	Failure Evidence	Effect Description	Occurrence	Severity	Detection	RPN	Operator Compensation
7: Engine Block Assembly	B: Contain oil for lubrication	1: Major loss of oil (> quart/ 12 hours or 475 miles of operation)	7, Damaged oil pan	Low oil light. Thunk.	Lack of lubrication if not shut down quickly.	1	7	1	7	Shut down engine
7: Engine Block Assembly	C: Maintain adequate compression within engine cylinders	1: Loss of Cylinder Pressure	1.1, Gear tooth failure	Loss of power, noise, misfiring, no start.	bending valves, piston damage, sleeve damage, FUBAR, Contaminated oil	1	7	10	70	Nothing
7: Engine Block Assembly	C: Maintain adequate compression within engine cylinders	1: Loss of Cylinder Pressure	2.1, Crack in piston	White Smoke. Loud noise.	Loss of power	1	7	3	21	Stop engine.
7: Engine Block Assembly	C: Maintain adequate compression within engine cylinders	1: Loss of Cylinder Pressure	1, Improper Timing	Loss of power, noise, misfiring, no start.	bending valves, piston damage, sleeve damage, FUBAR	1	7	10	70	Nothing
7: Engine Block Assembly	C: Maintain adequate compression within engine cylinders	1: Loss of Cylinder Pressure	3.1, Bent valve	Noise, run poorly - rough idle, back fire. Black smoke.	Loss of power. Back firing. Injector damage. Turbo damage?	1	7	10	70	More throttle
7: Engine Block Assembly	C: Maintain adequate compression within engine cylinders	1: Loss of Cylinder Pressure	3.2, Bad return spring	Rough Idle, loss of power	Loss of ability to maintain speed and torque	3	1	7	21	More throttle
7: Engine Block Assembly	C: Maintain adequate compression within engine cylinders	1: Loss of Cylinder Pressure	2.2, Rod Failure	Loud noise. Engine slow down/stop.	Oil leak. No power.	1	7	1	7	Shutdown
7: Engine Block Assembly	C: Maintain adequate compression within engine cylinders	1: Loss of Cylinder Pressure	2, Piston Damage							
7: Engine Block Assembly	C: Maintain adequate compression within engine cylinders	1: Loss of Cylinder Pressure	1.2, Gear retaining bolt back out	Loss of power, noise, misfiring, no start.	bending valves, piston damage, sleeve damage, gear damage, timing cover damage	1	7	10	70	Nothing
7: Engine Block Assembly	C: Maintain adequate compression within engine cylinders	1: Loss of Cylinder Pressure	3, Valve not sealing							
7: Engine Block Assembly	C: Maintain adequate compression within engine cylinders	1: Loss of Cylinder Pressure	1.3, Gear keyway breakage	Loss of power, noise, misfiring, no start.	bending valves, piston damage, sleeve damage, gear damage, timing cover damage	1	7	10	70	Nothing

System	Function	Functional Failure	Failure Mode	Failure Evidence	Effect Description	Occurrence	Severity	Detection	RPN	Operator Compensation
7: Engine Block Assembly	C: Maintain adequate compression within engine cylinders	1: Loss of Cylinder Pressure	3.3, Damaged Valve Seat	Noise, run poorly - rough idle, back fire. Black smoke.	Loss of power. Back firing. Injector damage.	1	7	10	70	More throttle
7: Engine Block Assembly	C: Maintain adequate compression within engine cylinders	1: Loss of Cylinder Pressure	4, Worn Cylinder Wall	Reduced engine power. Audio piston slap.	Loss of power, rough idle	3	4	5	60	increase throttle
7: Engine Block Assembly	C: Maintain adequate compression within engine cylinders	1: Loss of Cylinder Pressure	5, Worn Piston Ring	Reduced engine power. Audio piston slap.	Loss of power, rough idle	3	4	5	60	increase throttle
7: Engine Block Assembly	D: Contain exhaust	1: Does not provide adequate path to turbo	1, Blockage of pathway	Reduced power. Engine knock due to premature detonation.	Carbon buildup restricting flow of exhaust pathway. Possible hotter cylinders causing combustion issues.	3	4	7	84	More throttle.
7: Engine Block Assembly	D: Contain exhaust	2: Exhaust gasses not contained	1, Crack in head	Loss of power.	Crack could impact oil and coolant pathways.	1	7	1	7	Shutdown engine
7: Engine Block Assembly	D: Contain exhaust	2: Exhaust gasses not contained	2, Manifold gasket leaks	Loss of power.	Loss of power due to lower exhaust pressure for turbo.	1	4	3	12	Shutdown engine
7: Engine Block Assembly	E: Translate linear piston motion to rotational motion of crankshaft	1: Fails to rotate	1, Head gasket failure	Blowing smoke, rough engine, engine stall.	Excess fluid prevents piston going all the way up to top of travel.	3	7	7	147	Stop engine
7: Engine Block Assembly	E: Translate linear piston motion to rotational motion of crankshaft	1: Fails to rotate	2, Crack Piston	Engine noise, sudden engine seize. Excess smoke.	Excess loading will cause crack. Damage bore. Engine suddenly stopping.	1	7	7	49	Call tow truck.
7: Engine Block Assembly	E: Translate linear piston motion to rotational motion of crankshaft	1: Fails to rotate	3, Melt hole in top of piston	Rough engine operation.	Excess fuel injected on top of piston and burns hole into piston. No compression in cylinder. High pressure in crankcase.	1	7	7	49	Stop engine
7: Engine Block Assembly	E: Translate linear piston motion to rotational motion of crankshaft	2: Fails to rotate at certain efficiency level relative to performance curve	1, Bent Rod	Lose power, engine vibration	Lose compression. Engine balance off.	1	7	7	49	More throttle!

System	Function	Functional Failure	Failure Mode	Failure Evidence	Effect Description	Occurrence	Severity	Detection	RPN	Operator Compensation
7: Engine Block Assembly	E: Translate linear piston motion to rotational motion of crankshaft	2: Fails to rotate at certain efficiency level relative to performance curve	2, Wrist pin bearing failure	Bearing noise/knock.	Loose fit - cause piston to rock.	1	1	10	10	Nothing - he would likely not know it occurred.
7: Engine Block Assembly	E: Translate linear piston motion to rotational motion of crankshaft	2: Fails to rotate at certain efficiency level relative to performance curve	3, Rod journal bearing failure	Bearing noise/knock.	Loose fit - rod-piston to crank.	3	1	7	21	Nothing - they would likely not know it occurred.
7: Engine Block Assembly	E: Translate linear piston motion to rotational motion of crankshaft	2: Fails to rotate at certain efficiency level relative to performance curve	4, Crank Journal Bearing failure	Bearing noise/knock. Lower oil pressure.	Loose crank.	3	1	7	21	Nothing - they would likely not know it occurred.
7: Engine Block Assembly	E: Translate linear piston motion to rotational motion of crankshaft	2: Fails to rotate at certain efficiency level relative to performance curve	5, Fuel wash on cylinder liner	Knock from pre-detonation. Lack of power.	Leaky injector, fuel washes off lubricating from sidewall of cylinder and allow metal to metal contact. Excess wear on piston rings/bore causes lack of compression and lack of power.	3	7	7	147	More throttle!
7: Engine Block Assembly	F: Contain coolant	1: Coolant Leaks	1, Inlet/outlet flange gaskets	Coolant on the ground. Engine running hot. Steam.	Air injection causing inefficient heat transfer. Water pump cavitate.	1	4	3	12	Slow and/or stop engine.
7: Engine Block Assembly	F: Contain coolant	1: Coolant Leaks	2, Soft plugs	Increased engine temp, white smoke.	Engine overheats, warps head.	3	4	3	36	Stop engine, add coolant
7: Engine Block Assembly	F: Contain coolant	1: Coolant Leaks	3, Head gasket failure	Low coolant, external leaks, oil contamination, over heating	overheating, engine seizes, warped cylinder head	3	4	5	60	top off coolant
7: Engine Block Assembly	G: Provide cooling pathways	1: Blocked Pathway	1, Debris							
7: Engine Block Assembly	H: Maintain injector fuel return flow	1: Blocked pathway	1, Varnish/debris build up	None						
1: Manifold	A: Pathway for exhaust exiting head to turbo	1: Leaks exhaust	1, Creak in manifold	Excess engine noise. Loss of power, no turbo boost.	Reduced boost, reduced power.	3	4	3	36	None

7.2 RCM Analysis Consequences and Tasks

The RCM consequences and tasks is the output of the RCM process. The process evaluates the failures as to whether they are hidden failures and what type of consequences the failure has (safety, environmental, operational or non-operational). Furthermore, the analysis determines the type of maintenance task (run-to-failure, scheduled restoration or discard (SD), or on-condition (OC) replacement.

System	Function	Functional Failure	Failure Mode	Hidden	Safety Consequences	Environmental	Operational	Non-Operational	Maintenance Category	Occurrence	Severity	Detection	RPN	Task Type	Task Description	Frequency	Level of Maintenance	Proposed Change	Study Required	Comment	CBM Sensor Notes
1: Filter Bypass Valve	A: Maintain oil flow under restricted filter conditions	1: Does not close at proper pressure	1, Debris caught in sealing face	Y						3	1	10	30	RTF	Replace oil filter mount	As needed	3	N	N		Diff pressure across filter
1: Filter Bypass Valve	A: Maintain oil flow under restricted filter conditions	1: Does not close at proper pressure	2, failed spring	Y						3	1	10	30	RTF	Replace oil filter mount	As needed	3	N	N		Diff pressure sensor across filter
1: Filter Bypass Valve	A: Maintain oil flow under restricted filter conditions	2: Does not open at set pressure	1, Jammed by debris	Y						3	1	10	30	RTF	Replace oil filter mount	as needed	3	N	N		Diff pressure across filter
1: Filter Bypass Valve	A: Maintain oil flow under restricted filter conditions	3: Opens at too low of a pressure	1, Weakened spring	Y						1	1	10	10	RTF	Replace oil filter mount	as needed	3	N	N		Filter diff pressure sensor
1: Fuel Injector Assembly	A: Contain fuel	1: Leaking fuel	1, Cracked injector body	Y			Y	?		1	4	10	40	RTF	Replace injector	as needed	3	N	N		oil quality
1: Fuel Injector Assembly	A: Contain fuel	1: Leaking fuel	2, Fitting failure	?	?	?	?	?										N	N		

System	Function	Functional Failure	Failure Mode	Hidden	Safety Consequences	Environmental	Operational	Non-Operational	Maintenance Category	Occurrence	Severity	Detection	RPN	Task Type	Task Description	Frequency	Level of Maintenance	Proposed Change	Study Required	Comment	CBM Sensor Notes
1: Fuel Injector Assembly	A: Contain fuel	1: Leaking fuel	2.1, Damaged fitting			Y	Y	?		1	4	3	12	RTF	Replace injector and tube	On condition	3	N	N	This is most likely a failure caused by the maintainer and will be detected prior to the asset returning to service	
1: Fuel Injector Assembly	A: Contain fuel	1: Leaking fuel	3, O-ring failure	?	?	?	?	?										N	N		
1: Fuel Injector Assembly	A: Contain fuel	1: Leaking fuel	3.1, Damaged O-ring				Y	?		1	4	3	12	RTF	replace o-ring and reseat injector	on occurrence	3	N	N		
1: Fuel Injector Assembly	B: Measured amount and timing of fuel into the cylinders	1: No fuel	1, Solenoid coil short	Y			Y	?		3	7	3	63	RTF	Replace injector assembly	as needed	3	N	N		
1: Fuel Injector Assembly	B: Measured amount and timing of fuel into the cylinders	1: No fuel	2, Clog of injector orifice				Y	?		3	7	3	63	RTF	test and replace injector(s)	as needed	3	N	N		acoustic, vibration, cylinder or exhaust temp

System	Function	Functional Failure	Failure Mode	Hidden	Safety Consequences	Environmental	Operational	Non-Operational	Maintenance Category	Occurrence	Severity	Detection	RPN	Task Type	Task Description	Frequency	Level of Maintenance	Proposed Change	Study Required	Comment	CBM Sensor Notes
1: Fuel Injector Assembly	B: Measured amount and timing of fuel into the cylinders	2: Excessive fuel	1, Solenoid Stuck Open				Y	?		3	4	5	60	RTF	Test and replace injector(s)	as needed	3	N	N	Fuel debris, filter failure	acoustic, cylinder temp, exhaust temp
1: Fuel Injector Assembly	B: Measured amount and timing of fuel into the cylinders	2: Excessive fuel	2, Solenoid ball erosion	Y			Y	?		3	1	5	15	RTF	Test and replace injector(s)	as needed	3	N	N	Failure mode caused by age or fuel quality. May require inspection of other fuel system components.	accelerometer, audio sensor
1: Fuel Injector Assembly	B: Measured amount and timing of fuel into the cylinders	2: Excessive fuel	3, Erosion of orifice				Y	?		3	4	1	12	RTF	Replace injectors	as needed	3	N	N	fuel erosion root cause	accelerometer & acoustic sensors
1: Fuel Injector Assembly	B: Measured amount and timing of fuel into the cylinders	2: Excessive fuel	4, Return spring weakens	Y			Y	?		5	1	7	35	RTF	Test and replace injectors	as needed	3	N	N		audio or accelerometer sensor
1: Fuel Injector Assembly	B: Measured amount and timing of fuel into the cylinders	3: Insufficient Fuel	1, Solenoid coil short	Y			Y	?		3	7	3	63					N	N		

System	Function	Functional Failure	Failure Mode	Hidden	Safety Consequences	Environmental	Operational	Non-Operational	Maintenance Category	Occurrence	Severity	Detection	RPN	Task Type	Task Description	Frequency	Level of Maintenance	Proposed Change	Study Required	Comment	CBM Sensor Notes
1: Fuel Injector Assembly	B: Measured amount and timing of fuel into the cylinders	3: Insufficient Fuel	2, Clog of injector orifice				Y	?		3	7	3	63					N	N		
1: Manifold	A: Pathway for exhaust exiting head to turbo	1: Leaks exhaust	1, Creak in manifold				Y	?		3	4	3	36	RTF	Replace manifold	as needed	3	N	N		
1: Turbocharger	A: Maintain lubrication of bearing surfaces	1: Insufficient or reduced lubrication	1, Bearing wear				Y	?		3	7	5	105	RTF	Replace turbo	As needed.	3	N	N		Vibration, RPM, temp
1: Turbocharger	A: Maintain lubrication of bearing surfaces	1: Insufficient or reduced lubrication	1.1, Normal wear	?	?	?	?	?										N	N		
1: Turbocharger	A: Maintain lubrication of bearing surfaces	1: Insufficient or reduced lubrication	1.2, Premature shutdown of engine preventing proper cool down of turbo	?	?	?	?	?										N	N		
1: Turbocharger	A: Maintain lubrication of bearing surfaces	1: Insufficient or reduced lubrication	2, Coke bearing surface	Y			Y	?		3	7	7	147	RTF	Replace turbo	as needed	3	N	N		
1: Turbocharger	A: Maintain lubrication of bearing surfaces	1: Insufficient or reduced lubrication	2, Coke bearing surface	Y			Y	?		3	7	7	147	OC	Measure turbo efficiency, replace when efficiency drops below limits	Continuous	3	Y	Y		RPM, temp, vibration

System	Function	Functional Failure	Failure Mode	Hidden	Safety Consequences	Environmental	Operational	Non-Operational	Maintenance Category	Occurrence	Severity	Detection	RPN	Task Type	Task Description	Frequency	Level of Maintenance	Proposed Change	Study Required	Comment	CBM Sensor Notes
1: Turbocharger	A: Maintain lubrication of bearing surfaces	1: Insufficient or reduced lubrication	2.1, Premature shutdown of engine preventing proper cool down of turbo	?	?	?	?	?										N	N		
1: Turbocharger	B: Contains Oil	1: Does not contain oil	1, Seal leaks	Y						5	1	10	50	RTF	Replace/Rebuild turbo	as needed	3	N	N		
1: Turbocharger	B: Contains Oil	1: Does not contain oil	2, Fitting leaks				Y	?		3	7	3	63	RTF	Replace hoses and fittings	as needed	3	N	N		
1: Turbocharger	C: Compress intake air	1: Insufficient compression of intake air	1, Worn bearings				Y	?		3	7	5	105	RTF	Replace turbo	As needed.	3	N	N		Vibration, RPM, temp
1: Turbocharger	C: Compress intake air	1: Insufficient compression of intake air	2, Waste Gate Stuck Open				Y	?		1	4	3	12	OC	Diagnose a pneumatic problem or mechanical waste gate problem	as need	3	N	Y		Boost pressure, RPM, turbo exhaust pressure
1: Turbocharger	C: Compress intake air	1: Insufficient compression of intake air	2.1, Stuck linage				Y	?		1	4	3	12	OC	replace turbo	as need	3	N	Y		RPM, boost, shaft speed,
1: Turbocharger	C: Compress intake air	1: Insufficient compression of intake air	2.2, Diaphragm spring failure				Y	?		3	4	3	36	RTF	Replace waste gate actuator	as needed	3	N	N		
1: Turbocharger	C: Compress intake air	2: Over compression of intake air	1, Waste Gate stuck closed	?	?	?	?	?										N	N		
1: Turbocharger	C: Compress intake air	2: Over compression of intake air	1.1, Diaphragm failure				Y	?		3	4	1	12	RTF	Replace waste gate actuator	as needed	3	Y	N		

System	Function	Functional Failure	Failure Mode	Hidden	Safety Consequences	Environmental	Operational	Non-Operational	Maintenance Category	Occurrence	Severity	Detection	RPN	Task Type	Task Description	Frequency	Level of Maintenance	Proposed Change	Study Required	Comment	CBM Sensor Notes
1: Turbocharger	C: Compress intake air	2: Over compression of intake air	1.2, linkage stuck				Y	?		3	4	3	36	OC	Replace turbo	as needed	3	Y	Y		boost pres. Exhaust inlet pres. RPM, engine load
1: Turbocharger	C: Compress intake air	2: Over compression of intake air	1.3, Air hose failure/disconnection				Y	?		3	4	1	12	RTF	Replace hose	as needed	3	N	N		
1: Turbocharger	C: Compress intake air	3: Fails to compress air	1, Sheared or damaged turbine blades				Y	?		1	7	5	35	RTF	Replace turbo and oil change	as needed	3	N	N		
1: Turbocharger	C: Compress intake air	3: Fails to compress air	2, Shaft broken				Y	?		1	7	1	7	RTF	Replace turbo and oil change	as needed	3	N	N		
1: Turbocharger	C: Compress intake air	3: Fails to compress air	3, Bearing seized				Y	?		3	7	5	105	OC	Replace as inefficiencies dictate	As needed	3	Y	Y	Model air inlet and outlet pressures and shaft speed. vs. Engine RPM & Load and accelerator position	Air inlet pressure, exhaust manifold pressure exhaust outlet pressure, shaft speed...
1: Water Pump Assembly	A: Contain coolant	1: Coolant leaks from the water pump to housing mounting surface at the O-ring	1, Thermal fatigue of O ring				Y	?		3	4	3	36	RTF	Remove water pump, inspect, replace seal, flush coolant	On occurrence	3	N	N		
1: Water Pump Assembly	A: Contain coolant	2: Coolant leaks from the water pump shaft seal	1, Seal wear							5	1	5	25	RTF	Replace water pump and gasket, drain fluids, flush and fill	as needed	3	N	N		

System	Function	Functional Failure	Failure Mode	Hidden	Safety Consequences	Environmental	Operational	Non-Operational	Maintenance Category	Occurrence	Severity	Detection	RPN	Task Type	Task Description	Frequency	Level of Maintenance	Proposed Change	Study Required	Comment	CBM Sensor Notes
1: Water Pump Assembly	B: Create coolant flow	1: No flow of coolant from water pump	1, Pump drive pulley shears from pump drive shaft				Y	?		1	7	3	21	RTF	Replace pump, belt and fluids	as needed	3	N	N		
1: Water Pump Assembly	B: Create coolant flow	1: No flow of coolant from water pump	2, Seized pump shaft/bearing				Y	?		1	7	3	21	OC	Replace pump, belt and fluids	as needed	3	Y	Y		Vibration of acoustic admission
1: Water Pump Assembly	B: Create coolant flow	2: Reduced coolant flow from water pump	1, Slippage of press fit	Y			Y	?		3	4	7	84	OC	Replace water pump and fluids	as needed	3	Y	Y		Acoustic and flow
1: Water Pump Assembly	B: Create coolant flow	2: Reduced coolant flow from water pump	2, Corrosion and cavitation on impellers	Y			Y	?		5	4	7	140	OC	Replace water pump and fluids	as needed	3	Y	Y		Coolant and ambient temp, flow, RPM
2: Mechanical Fuel Pump	A: Contains fuel	1: Fuel leakage	1, Failure of the pump head seal				Y	?		1	4	7	28	RTF	Replace pump and send pump to depot for maintenance	as necessary	3	N	N		
2: Mechanical Fuel Pump	B: Transmit fuel at a specified pressure and flow rate	1: Excessive pressure	1, Flow control valve/solenoid failure	Y			Y	?		3	4	7	84	OC	Monitor fuel rail pressure. Replace pump when over pressure followed by under pressure is detected.	as necessary	3	Y	Y		Fuel rail pressure
2: Mechanical Fuel Pump	B: Transmit fuel at a specified pressure and flow rate	2: No fuel flow	1, Piston failure/stuck	Y			Y	?		1	7	1	7	OC	Measure vibration of the pump and monitor for piston slap. Monitoring fuel pressure may identify a precursor, but at the point of failure/sticking,	as needed	3	Y	Y		accelerometer

System	Function	Functional Failure	Failure Mode	Hidden	Safety Consequences	Environmental	Operational	Non-Operational	Maintenance Category	Occurrence	Severity	Detection	RPN	Task Type	Task Description	Frequency	Level of Maintenance	Proposed Change	Study Required	Comment	CBM Sensor Notes
															measuring pressure will not help keep the vehicle operating.						
2: Mechanical Fuel Pump	B: Transmit fuel at a specified pressure and flow rate	2: No fuel flow	2, Support Bearing Failure	Y			Y	?		1	7	5	35	OC	Measure vibration for changes in frequencies caused by the bearing wear. Replace pump as necessary	as needed	2	Y	Y		Accelerometer
2: Mechanical Fuel Pump	B: Transmit fuel at a specified pressure and flow rate	3: Insufficient pressure	1, Inlet Check Valve Sticking	Y			Y	?		3	7	7	147	OC	Monitor fuel rail pressure. Monitor pump vibration as fuel flows are modified. Replace pump as necessary.	as necessary	3	Y	Y		fuel rail pressure, accelerometer
2: Mechanical Fuel Pump	B: Transmit fuel at a specified pressure and flow rate	3: Insufficient pressure	2, Outlet Check Valve Sticking	Y			Y	?		3	4	7	84	OC	Monitor for a decrease in fuel rail pressure; Monitor pump vibration to identify vibration patterns associated with flow of fuel back into the piston chamber from the fuel rail (limited potential). Replace pump as necessary	as needed	3	Y	Y		Fuel Rail Pressure, accelerometer

System	Function	Functional Failure	Failure Mode	Hidden	Safety Consequences	Environmental	Operational	Non-Operational	Maintenance Category	Occurrence	Severity	Detection	RPN	Task Type	Task Description	Frequency	Level of Maintenance	Proposed Change	Study Required	Comment	CBM Sensor Notes
2: Mechanical Fuel Pump	B: Transmit fuel at a specified pressure and flow rate	3: Insufficient pressure	3, Piston Wear	Y			Y	?		3	7	5	105	OC	Monitor fuel rail pressure for a reduction in pressure (flow). Monitor vibration to identify additional frequencies generated by wear. Replace pump as necessary	As necessary	3	Y	Y		Fuel Rail pressure, accelerometer
2: Mechanical Fuel Pump	B: Transmit fuel at a specified pressure and flow rate	3: Insufficient pressure	4, Camshaft or tappet wear	Y			Y	?		3	4	7	84	OC	Monitor fuel rail pressure for drop in overall pressure. Monitor vibration of the pump for additional frequencies induced by wear. Replace pump as necessary	as needed	3	Y	Y		Fuel Rail pressure, accelerometer
2: Mechanical Fuel Pump	B: Transmit fuel at a specified pressure and flow rate	3: Insufficient pressure	5, Flow Control Valve/Solenoid Failure	Y			Y	?		3	4	7	84	OC	Monitor fuel rail pressure. Replace pump when over pressure followed by under pressure is detected.	as necessary	3	Y	Y		
2: Oil Thermostat	A: Maintain oil temperature	1: Allowing oil to overheat	1, Return spring failure				Y	?		3	7	3	63	RTF	Replace thermostat	as needed	3	N	N		

System	Function	Functional Failure	Failure Mode	Hidden	Safety Consequences	Environmental	Operational	Non-Operational	Maintenance Category	Occurrence	Severity	Detection	RPN	Task Type	Task Description	Frequency	Level of Maintenance	Proposed Change	Study Required	Comment	CBM Sensor Notes
2: Oil Thermostat	A: Maintain oil temperature	1: Allowing oil to overheat	2, Debris not allowing to seat							1	1	7	7	RTF	rebuild oil cooler and replace thermostat	as need	3	N	N		
2: Oil Thermostat	A: Maintain oil temperature	2: Premature cooling of the oil	1, Thermostat stuck sealing bypass							1	1	7	7	OC	Replace thermostat	as need	3	Y	N	Compare heat transfer of oil cooler	oil temp, coolant temp ambient temp
2: Thermostat	A: Direct coolant to radiator to maintain temperature	1: Low fluid flow to the radiator	1, Thermostat stuck partially open	Y			Y	?		5	4	5	100	RTF	Replace thermostat, flush and fill coolant	as needed	3	N	N		
2: Thermostat	A: Direct coolant to radiator to maintain temperature	2: Too much fluid flow to radiator	1, Thermostat stuck open	Y			Y	?		5	1	3	15	RTF	Replace thermostat, flush and fill coolant	as needed	3	N	N	Most likely due to a broken return spring.	
2: Thermostat	A: Direct coolant to radiator to maintain temperature	3: No fluid flow to radiator	1, Thermostat stuck closed	Y			Y	?		5	7	3	105	RTF	Replace thermostat, flush and fill coolant	as needed	3	N	N	Wax piston failed	
3: Low pressure supply lines	A: Transport low pressure fuel - Supply connector to HP Pump	1: Insufficient fuel flow	1, Major crack in hose				Y	?		3	7	3	63	RTF	Replace hose and end fittings	As needed	3	N	N		
3: Oil Pump	A: Create pressurized oil flow	1: Reduced oil flow	1, Wear of side plates							3	4	7	84	RTF	Replace oil pump	as needed	3	N	N		Oil pressure, sump & outlet temp of oil

System	Function	Functional Failure	Failure Mode	Hidden	Safety Consequences	Environmental	Operational	Non-Operational	Maintenance Category	Occurrence	Severity	Detection	RPN	Task Type	Task Description	Frequency	Level of Maintenance	Proposed Change	Study Required	Comment	CBM Sensor Notes
3: Oil Pump	A: Create pressurized oil flow	1: Reduced oil flow	2, Wear of pump lobes							3	4	7	84	RTF	Replace oil pump	as needed	3	N	N		Oil pressure, oil temp at pump and outlet
3: Oil Pump	A: Create pressurized oil flow	2: Fail to create oil flow	1, Failure of pump gerotor				Y			1	7	1	7	OC	replace oil pump, filter, oil and cooler	as needed	3	Y	N		Oil temp & pressure
4: High pressure supply line	A: Transport pressurized fuel (High Pressure fuel pump to injectors)	1: Insufficient flow of fuel	1, Fitting Leak				Y	?		1	4	5	20	RTF	Replace pipe or fittings as needed	as needed	3	N	N		
4: High pressure supply line	A: Transport pressurized fuel (High Pressure fuel pump to injectors)	1: Insufficient flow of fuel	2, Rupture in line				Y	?		1	4	5	20	RTF	Replace pipe as needed	as needed	3	N	N		
4: High pressure supply line	A: Transport pressurized fuel (High Pressure fuel pump to injectors)	1: Insufficient flow of fuel	3, Blockage in line	Y			Y			1	7	7	49	RTF	Diagnose and rebuild high pressure fuel lines	as needed	3	N	N		Solenoid current for fuel pump
4: High pressure supply line	A: Transport pressurized fuel (High Pressure fuel pump to injectors)	2: Fuel pressure too low	1, Crack in HP line or Fuel Rail				Y	?		3	7	5	105	RTF	Replace rail or tube as needed	as needed	3	N	N		

System	Function	Functional Failure	Failure Mode	Hidden	Safety Consequences	Environmental	Operational	Non-Operational	Maintenance Category	Occurrence	Severity	Detection	RPN	Task Type	Task Description	Frequency	Level of Maintenance	Proposed Change	Study Required	Comment	CBM Sensor Notes
4: High pressure supply line	A: Transport pressurized fuel (High Pressure fuel pump to injectors)	2: Fuel pressure too low	2, Fitting Failure				Y	?		1	7	5	35	RTF	Replace fitting/rail or tube as needed	as needed	3	N	N		
4: High pressure supply line	A: Transport pressurized fuel (High Pressure fuel pump to injectors)	2: Fuel pressure too low	3, Pressure relief valve failure	Y			Y	?		1	7	10	70	RTF	Diagnose with pressure test. Replace relief valve.	as needed	3	N	N		
4: Oil Pressure Regulator	A: Contain oil in pressurized section of system below X PSI	1: Allows premature flow of oil to sump	1, Valve stuck due to debris				Y	?		1	7	3	21	RTF	replace regulator/relief valve	as needed	3	N	N		
4: Oil Pressure Regulator	A: Contain oil in pressurized section of system below X PSI	1: Allows premature flow of oil to sump	2, Broken/weak spring				Y	?		3	7	3	63	RTF	replace regulator/relief valve	as needed	3	N	N		
4: Oil Pressure Regulator	B: Prevent excess oil pressure	1: Fails to relieve over pressure	1, Valve seized					?		1	4	3	12	RTF	Replace relief valve	as needed	3	N	N		
5: Oil Filter Assembly	A: Contain Oil	1: Rupture of canister	1, Road debris strike			Y	Y	?		1	7	3	21	RTF	replace filter and oil	as needed	3	N	N		
5: Oil Filter Assembly	A: Contain Oil	2: Leaking O-ring	1, Knick in O-ring			Y	Y	?		3	7	3	63	RTF	replace filter/o-ring and add oil	as needed	3	N	N		

System	Function	Functional Failure	Failure Mode	Hidden	Safety Consequences	Environmental	Operational	Non-Operational	Maintenance Category	Occurrence	Severity	Detection	RPN	Task Type	Task Description	Frequency	Level of Maintenance	Proposed Change	Study Required	Comment	CBM Sensor Notes
5: Oil Filter Assembly	A: Contain Oil	2: Leaking O-ring	2, Install problem			Y	Y	?		3	7	3	63	RTF	replace filter/o-ring and add oil	as needed	3	N	N		
5: Oil Filter Assembly	B: Collect and contain dirt and debris	1: Internal relief is actuated	1, Filter is clogged	Y						3	1	10	30	SD	replace filter and oil	x hours or y miles	3	N	N		
6: Cooler Assembly	A: Prevent mixture of oil and coolant	1: Cross contamination of coolant and oil	1, Fatigue failure of the plates	Y			Y	?		3	1	10	30	RTF	Replace oil cooler, change oil filter, replace fluids	as needed	3	N	N		inline oil monitoring, oil & coolant temp
6: Cooler Assembly	B: Contain oil	1: Leaks Oil to engine compartment	1, Gasket failure of outside edge of casting							3	1	3	9	RTF	replace gasket, change fluids and filters	as needed	3	N	N		
6: Cooler Assembly	C: Transfer Heat from oil to cooling system	1: Inefficient removal of heat	1, Debris\sludge inside of fins	Y						3	1	10	30	OC	Replace cooler gaskets etc...	as needed	3	N	N	Monitor oil temp for exceeding X temp, oil breakdown	in line oil analysis/temp sensor
6: Cooler Assembly	C: Transfer Heat from oil to cooling system	1: Inefficient removal of heat	2, Corrosion of fins on coolant side	Y						1	1	10	10	RTF	Replace cooler, flush and change fluids, filter	as needed	3	N	N		
6: Fuel Filter	A: Contain Fuel	1: Rupture of canister	1, Road debris strike				Y	?		1	7	3	21	RTF	Replace filter	as needed.	3	N	N		
6: Fuel Filter	A: Contain Fuel	2: Leaking O ring	1, Knick in O-ring	Y						1	1	7	7	RTF	Replace if found	as needed.	3	N	N		
6: Fuel Filter	A: Contain Fuel	2: Leaking O-ring	2, Install Problem							1	1	7	7	RTF	Remove, inspect and reinstall. Or replace filter.	as needed.	3	N	N		
6: Fuel Filter	B: Collect and contain dirt and debris	1: Inability to supply enough fuel through filter	1, Filter is clogged	Y			Y	?		3	4	10	120	SD	Change fuel filter	as scheduled	3	N	N		

System	Function	Functional Failure	Failure Mode	Hidden	Safety Consequences	Environmental	Operational	Non-Operational	Maintenance Category	Occurrence	Severity	Detection	RPN	Task Type	Task Description	Frequency	Level of Maintenance	Proposed Change	Study Required	Comment	CBM Sensor Notes
6: Fuel Filter	B: Collect and contain dirt and debris	1: Inability to supply enough fuel through filter	1, Filter is clogged	Y			Y	?		3	4	10	120	OC	Differential pressure sensor across filter ports.	Once diff pressure is exceeded.	3	Y	N		
7: Engine Block Assembly	A: Provide pathways for lubrication	1: Restricted or blocked lubrication pathway	1, Clogged oil passageways	Y			Y	?		1	7	5	35	RTF	Replace engine	as needed	3	N	N		
7: Engine Block Assembly	A: Provide pathways for lubrication	1: Restricted or blocked lubrication pathway	2, Clogged oil pickup	Y			Y	?		1	7	3	21	RTF	Replace and rebuild engine	as needed	3	N	N	Detected through low oil pressure	
7: Engine Block Assembly	B: Contain oil for lubrication	1: Major loss of oil (> quart/ 12 hours or 475 miles of operation)	1, Head gasket failure				Y			3	4	5	60	RTF	Replace head gasket (possible engine swap) and flush and change fluids.	As needed	3	N	N		
7: Engine Block Assembly	B: Contain oil for lubrication	1: Major loss of oil (> quart/ 12 hours or 475 miles of operation)	2, Front crank seal failure				Y			3	4	5	60	RTF	Replace seals and top off oil	As needed	3	N	N		
7: Engine Block Assembly	B: Contain oil for lubrication	1: Major loss of oil (> quart/ 12 hours or 475 miles of operation)	3, Front timing cover seal failure				Y			3	4	5	60	RTF	Replace seal and top off oil	as needed	3	N	N		
7: Engine Block Assembly	B: Contain oil for lubrication	1: Major loss of oil (> quart/ 12 hours or 475 miles of operation)	4, Rear main seal failure	Y			Y	?		3	7	3	63	OC	Pull fly wheel housing drain plug. Access for oil.	at each oil change	5	Y	N		
7: Engine Block Assembly	B: Contain oil for lubrication	1: Major loss of oil (> quart/ 12 hours or 475 miles of operation)	5, Turbo oil supply line leak			Y	Y	?		3	7	3	63	RTF	Change out hose. Change turbo if necessary.	as needed	3	N	N		

System	Function	Functional Failure	Failure Mode	Hidden	Safety Consequences	Environmental	Operational	Non-Operational	Maintenance Category	Occurrence	Severity	Detection	RPN	Task Type	Task Description	Frequency	Level of Maintenance	Proposed Change	Study Required	Comment	CBM Sensor Notes
7: Engine Block Assembly	B: Contain oil for lubrication	1: Major loss of oil (> quart/ 12 hours or 475 miles of operation)	6, Turbo oil return line leak				Y	?		3	4	3	36	RTF	Reattach, replace tubing.	as needed	3	N	N		
7: Engine Block Assembly	B: Contain oil for lubrication	1: Major loss of oil (> quart/ 12 hours or 475 miles of operation)	7, Damaged oil pan			Y	Y	?		1	7	1	7	RTF	Replace oil and oil.	As needed	3	N	N		
7: Engine Block Assembly	C: Maintain adequate compression within engine cylinders	1: Loss of Cylinder Pressure	1, Improper Timing	Y	Y		Y	?		1	7	10	70	OTC				N	N		
7: Engine Block Assembly	C: Maintain adequate compression within engine cylinders	1: Loss of Cylinder Pressure	1.1, Gear tooth failure	Y	Y		Y	?		1	7	10	70	RTF	Field swap engine and send core to depot for inspection and rebuild	Upon failure	3	N	N		
7: Engine Block Assembly	C: Maintain adequate compression within engine cylinders	1: Loss of Cylinder Pressure	1.2, Gear retaining bolt back out	Y	Y		Y	?		1	7	10	70	RTF	Replace engine and send core to depot for inspection and rebuild	Upon failure	3	N	N		
7: Engine Block Assembly	C: Maintain adequate compression within engine cylinders	1: Loss of Cylinder Pressure	1.3, Gear keyway breakage	Y	Y		Y	?		1	7	10	70	RTF	Replace engine, send core to depot for inspection and rebuild	Upon failure	3	N	N		

System	Function	Functional Failure	Failure Mode	Hidden	Safety Consequences	Environmental	Operational	Non-Operational	Maintenance Category	Occurrence	Severity	Detection	RPN	Task Type	Task Description	Frequency	Level of Maintenance	Proposed Change	Study Required	Comment	CBM Sensor Notes
7: Engine Block Assembly	C: Maintain adequate compression within engine cylinders	1: Loss of Cylinder Pressure	2, Piston Damage	?	?	?	?	?										N	N		
7: Engine Block Assembly	C: Maintain adequate compression within engine cylinders	1: Loss of Cylinder Pressure	2.1, Crack in piston	Y			Y	?		1	7	3	21	RTF	Engine rebuild	When failed	5	N	N		sound pressure sensor or acoustic emissions, encoder on flywheel
7: Engine Block Assembly	C: Maintain adequate compression within engine cylinders	1: Loss of Cylinder Pressure	2.2, Rod Failure				Y	?		1	7	1	7	RTF	Replace engine	as needed	3	N	Y		Vibration, acoustic
7: Engine Block Assembly	C: Maintain adequate compression within engine cylinders	1: Loss of Cylinder Pressure	3, Valve not sealing	?	?	?	?	?										N	N		
7: Engine Block Assembly	C: Maintain adequate compression within engine cylinders	1: Loss of Cylinder Pressure	3.1, Bent valve				Y	?		1	7	10	70	RTF	Replace engine and send to depot for inspection and rebuild	Upon failure	3	N	N		
7: Engine Block Assembly	C: Maintain adequate compression within engine cylinders	1: Loss of Cylinder Pressure	3.2, Bad return spring	Y			Y	?		3	1	7	21	RTF	Remove and replace valve springs. Inspect.	Failure	3	N	N	Research what happens with valve blow by.	Measure exhaust gas temp. Acoustic sensor.

System	Function	Functional Failure	Failure Mode	Hidden	Safety Consequences	Environmental	Operational	Non-Operational	Maintenance Category	Occurrence	Severity	Detection	RPN	Task Type	Task Description	Frequency	Level of Maintenance	Proposed Change	Study Required	Comment	CBM Sensor Notes
7: Engine Block Assembly	C: Maintain adequate compression within engine cylinders	1: Loss of Cylinder Pressure	3.3, Damaged Valve Seat	Y			Y	?		1	7	10	70	RTF	Replace engine and send to depot for inspection and rebuild	Upon failure	3	N	N		
7: Engine Block Assembly	C: Maintain adequate compression within engine cylinders	1: Loss of Cylinder Pressure	4, Worn Cylinder Wall				Y	?		3	4	5	60	SR	Vehicle Overhaul	6 yrs.	5	N	N		
7: Engine Block Assembly	C: Maintain adequate compression within engine cylinders	1: Loss of Cylinder Pressure	4, Worn Cylinder Wall				Y	?		3	4	5	60	RTF	Sleeve replacement on failure	on failure	3	N	N		
7: Engine Block Assembly	C: Maintain adequate compression within engine cylinders	1: Loss of Cylinder Pressure	5, Worn Piston Ring				Y	?		3	4	5	60	OC	Acoustic monitoring	continuous		N	N		acoustic microphone
7: Engine Block Assembly	C: Maintain adequate compression within engine cylinders	1: Loss of Cylinder Pressure	5, Worn Piston Ring				Y	?		3	4	5	60	OC	Oil monitoring	Continuous or sampling every X month	3	Y	N		Oil Monitoring
7: Engine Block Assembly	C: Maintain adequate compression within engine cylinders	1: Loss of Cylinder Pressure	5, Worn Piston Ring				Y	?		3	4	5	60	SR	Vehicle Overhaul	6 yrs.	5	N	N		

System	Function	Functional Failure	Failure Mode	Hidden	Safety Consequences	Environmental	Operational	Non-Operational	Maintenance Category	Occurrence	Severity	Detection	RPN	Task Type	Task Description	Frequency	Level of Maintenance	Proposed Change	Study Required	Comment	CBM Sensor Notes
7: Engine Block Assembly	D: Contain exhaust	1: Does not provide adequate path to turbo	1, Blockage of pathway	Y			Y	?		3	4	7	84	RTF	Swap out engine	as needed.	3	N	N		
7: Engine Block Assembly	D: Contain exhaust	2: Exhaust gasses not contained	1, Crack in head				Y	?		1	7	1	7	RTF	Replace engine and rebuild	as needed	3	N	N		
7: Engine Block Assembly	D: Contain exhaust	2: Exhaust gasses not contained	2, Manifold gasket leaks				Y	?		1	4	3	12	RTF	Replace gaskets	as needed.	3	N	N		
7: Engine Block Assembly	E: Translate linear piston motion to rotational motion of crankshaft	1: Fails to rotate	1, Head gasket failure	Y			Y	?		3	7	7	147	RTF	Pull engine and rebuild.	As need	3	N	N		
7: Engine Block Assembly	E: Translate linear piston motion to rotational motion of crankshaft	1: Fails to rotate	2, Crack Piston	Y			Y	?		1	7	7	49	RTF	Pull and rebuild engine	as needed	3	N	Y		Accelerometer pick up floating metal parts.
7: Engine Block Assembly	E: Translate linear piston motion to rotational motion of crankshaft	1: Fails to rotate	3, Melt hole in top of piston	Y			Y	?		1	7	7	49	RTF	Pull and rebuild engine	as needed	3	N	N		Temp on exhaust. Acel on engine.

System	Function	Functional Failure	Failure Mode	Hidden	Safety Consequences	Environmental	Operational	Non-Operational	Maintenance Category	Occurrence	Severity	Detection	RPN	Task Type	Task Description	Frequency	Level of Maintenance	Proposed Change	Study Required	Comment	CBM Sensor Notes
7: Engine Block Assembly	E: Translate linear piston motion to rotational motion of crankshaft	2: Fails to rotate at certain efficiency level relative to performance curve	1, Bent Rod	Y			Y	?		1	7	7	49	RTF	pull and rebuild engine	as needed.	3	N	N		
7: Engine Block Assembly	E: Translate linear piston motion to rotational motion of crankshaft	2: Fails to rotate at certain efficiency level relative to performance curve	2, Wrist pin bearing failure	Y						1	1	10	10	RTF	swap/pull and rebuild engine	as needed	3	N	Y		Accel and microphone in oil sump
7: Engine Block Assembly	E: Translate linear piston motion to rotational motion of crankshaft	2: Fails to rotate at certain efficiency level relative to performance curve	3, Rod journal bearing failure	Y						3	1	7	21	RTF	Rebuild engine	as needed	3	N	Y		Accel in oil sump
7: Engine Block Assembly	E: Translate linear piston motion to rotational motion of crankshaft	2: Fails to rotate at certain efficiency level relative to performance curve	4, Crank Journal Bearing failure							3	1	7	21	RTF	Pull engine and rebuild	as needed	3	N	N		accel and microphone in oil sump.
7: Engine Block Assembly	E: Translate linear piston motion to rotational motion of crankshaft	2: Fails to rotate at certain efficiency level relative to performance curve	5, Fuel wash on cylinder liner	Y			Y	?		3	7	7	147	RTF	Pull and rebuild engine	as need	3	N	N		acoustic sensor

System	Function	Functional Failure	Failure Mode	Hidden	Safety Consequences	Environmental	Operational	Non-Operational	Maintenance Category	Occurrence	Severity	Detection	RPN	Task Type	Task Description	Frequency	Level of Maintenance	Proposed Change	Study Required	Comment	CBM Sensor Notes
7: Engine Block Assembly	F: Contain coolant	1: Coolant Leaks	1, Inlet/outlet flange gaskets				Y	?		1	4	3	12	RTF	Replace gasket and refill coolant.	as needed	3	N	N		
7: Engine Block Assembly	F: Contain coolant	1: Coolant Leaks	2, Soft plugs			Y	Y	?		3	4	3	36	OTC	Replace soft plugs during lower end rebuild	upon failure or at scheduled engine rebuild	5	N	Y	Radiator, water pump, and hose failures covered with coolant pressure failure	Coolant Pressure Sensor
7: Engine Block Assembly	F: Contain coolant	1: Coolant Leaks	3, Head gasket failure	Y		Y	Y	?		3	4	5	60	OC	Replace head gasket	Failure	4	N	N		Oil quality, oil temp
7: Engine Block Assembly	G: Provide cooling pathways	1: Blocked Pathway	1, Debris	?	?	?	?	?										N	N		
7: Engine Block Assembly	H: Maintain injector fuel return flow	1: Blocked pathway	1, Varnish/debris build up	?	?	?	?	?										N	N		

8 Appendix B: Additive Repair Abstracts

This appendix provides additional detail on the disseminated work performed under the additive repair assessment portion of this project. The breadth of this work covers three presentations and six publications focusing on aluminum, steel, and cast iron repair. The abstracts from those works are provided below in Sections 2.1 through 2.4, which are organized by subtopic. Appendix D provides references for access to the publications.

8.1 Additive Repair Framework

Development of a Framework for Component Repair Using Additive Manufacturing (TechConnect World Innovation Conference 2021)

Maintenance and sustainment of high value assets, such as vehicles, often relies on replacing damaged components rather than repairing them. In the case of components that no longer have a replacement option, additive manufacturing (AM) technologies are being considered to build these components from scratch through use of 3D printers. For some components this may be feasible; however, replacement using current 3D printing technologies is not always possible due to limited material options and performance considerations. Furthermore, replacement with new or printed components can be more costly than repairing the existing assets. Due to these challenges, the option to repair damaged components using maturing AM repair technologies is enticing to many industry and government practitioners. Within the engineering community there is a knowledge gap in how to efficiently evaluate potential AM repair approaches against the original equipment part performance requirements, especially when original design information is unavailable. The performance and durability of repaired components must meet the requirements of the application, which is highly dependent on the AM technology and material combination used for the repair. Additionally, each damaged component must be evaluated to understand the particular condition that resulted in removal from service. Adoption of AM repair processes for the damaged component is currently limited by complexities associated with material properties and the need for a comprehensive, systemic solution for repair. One approach to this problem is the definition of AM repair solutions based on their technological and functional capabilities. The present work focuses on creation of a framework to determine if components are suitable candidates for additive repair and, if so, recommend an AM repair process and material combination that is best suited for the functions of the part. This task requires an understanding of both the initial performance requirements of the part and the functional failures that caused the need for repair. The decision tool, which recommends an appropriate additive technology, must draw on a database of mechanical properties from a variety of process-material combinations. For an example, this presentation highlights one of the AM repair technologies being investigated, additive friction stir deposition (AFSD), that adds material to a substrate through a thermo-mechanical process. Specifically, AFSD for the deposition of aluminum 6061-T6 to repair similar 6061 plate was used as one of the AM repair options in a case study to demonstrate the framework. Material testing was conducted to populate the as-deposited material properties along with the original substrate properties to be used in the evaluation.

8.2 Additive Friction Stir Deposition

Evaluation of Additive Friction Stir Deposition for the Repair of Cast Al-1.4Si-1.1Cu-1.5Mg-2.1Zn [1] (*Journal* of Manufacturing Science and Engineering)

The deposition of new alloy to replace a worn or damaged surface layer is a common strategy for repairing or remanufacturing structural components. Solid-state methods, such as additive friction stir deposition (AFSD), mitigate the challenges associated with traditional fusion methods by depositing material at temperatures below the melting point. In this study, AFSD of aluminum alloy 6061-T6 was investigated as a means to fill machined grooves in a substrate of cast aluminum alloy Al-1.4Si-1.1Cu-1.5Mg-2.1Zn. The combination of machining and deposition simulate a repair in which damaged material is mechanically removed and then replaced using AFSD. Three groove geometries were evaluated by means of metallographic inspection and tensile and fatigue testing. For the process conditions and groove geometries used in this study, the effective repair depth was limited to 2.3–2.6 mm; below that depth, the interface between the filler and substrate materials exhibited poor bonding associated with insufficient shear deformation. Mechanical test data indicated that, under optimized processing conditions, the strength of the deposited filler alloy may approach that of the cast substrate. In addition, the fatigue life during fully reversed axial fatigue testing was 66% of that predicted from historical data for comparable stress amplitudes. The results suggest that there is potential to utilize AFSD of 6061 as a viable repair process for cast Al-1.4Si-1.1Cu-1.5Mg-2.1Zn and other comparable alloys.

Repair of aluminum 6061 plate by additive friction stir deposition [2] (The International Journal of Advanced Manufacturing Technology)

The deposition of new alloy to replace a worn or damaged surface layer is a common strategy for repairing or remanufacturing structural components. For high-performance aluminum alloys common in the automotive, aerospace, and defense industries, however, traditional fusion-based deposition methods can lead to solidification cracking, void formation, and loss of strength in the heat-affected zone. Solid-state methods, such as additive friction stir deposition (AFSD), mitigate these challenges by depositing material at temperatures below the melting point. In this work, a solid-state volumetric repair was performed using AFSD of aluminum alloy 6061-T6 to fill grooves machined into the surface of a plate of 6061-T651. The groove-filling process is relevant to replacement of cracked or corroded material after removal by localized grinding. Three groove geometries were evaluated by means of metallographic inspection, tensile testing, and fatigue testing. For the process conditions and groove geometries used in this study, effective mixing of the substrate and deposited alloy were achieved to a depth of 3.1–3.5 mm. Below that depth, the interface between the substrate and AFSD alloy exhibited poor bonding associated with insufficient shear deformation. This suggests a practical limitation of approximately 3 mm for the depth of repair by groove filling using the current combination of process parameters, materials, and tool design. The mechanical properties of the filler alloy, the depth of the heat-affected zone, and areas for further optimization are discussed within the context of precipitation hardened aluminum alloys.

Evaluation of Additive Friction Stir Deposition of AISI 316L For Repairing Surface Material Loss in AISI 4340 [3] (The International Journal of Advanced Manufacturing Technology)

Additive technologies provide a means for repair of various failure modes associated with material degradation occurring during use in aggressive environments. Possible repair strategies for AISI 4340 steel using AISI 316L deposited by additive friction stir deposition (AFSD) were evaluated under this research by metallography, microhardness, and wear and mechanical testing. Two repair geometries were investigated: groove-filling and surface cladding. The former represents repair of localized grinding to eliminate cracks, while the latter represents material replacement over a larger area, for example to repair general corrosion or wear. The 316L deposited by AFSD exhibited a refined microstructure with decreased

grain size and plastic strain, lower strength, and lower hardness than the as-received feedstock. Wear testing by both two-body abrasion and erosion by particle impingement both indicated that the wear resistance of the 316L cladding was as good as, or better than, the substrate 4340 material; however, there was some evidence that the resistance to intergranular corrosion was compromised due to the formation of carbides or sigma phase. In both repair geometries, the microstructure of the substrate beneath the deposited material exhibited heat affected zones that appeared to have austenized during the deposition process, and transformed to martensite or bainite during cooling. This report constitutes an initial evaluation of a novel approach to the repair of structural steel components damaged by microcracking, wear, or corrosion.

8.3 Twin-Wire Arc

Investigation of Mechanical Properties of Twin Wire Arc Repair of Cast Iron Components (International Thermal Spray Conference presentation)

Twin wire arc is a commonly used thermal spray technology for application of steel coatings to cast iron components. Hardness and adhesion strength are critical properties of such coatings, and significant research is available reporting these properties. However, residual stresses and the anisotropic structure of the coatings lead to significantly different behavior in bending applications than in the purely tensile loading of the standard adhesion test. In addition, microstructural features that are controlled by certain process parameters during deposition of the coating can have a significant effect on these properties. This work seeks to relate the hardness and pull-off adhesion strength to the coating microstructure, and to assess the related bending strength and failure mode. Comparisons between bend tests and pull-off adhesion tests show significant differences to consider when evaluating twin wire arc coatings.

Mechanical Properties of High Carbon Steel Coatings on Gray Cast Iron Formed by Twin Wire Arc (submitted to Journal of Thermal Spray Technology)

Twin wire arc is a thermal spray technology commonly used for applying coatings to cast iron components. This study relates the microstructure and mechanical properties to the spray parameters used during deposition of high carbon steel coatings on grey cast iron substrates. Directional relationships are established between the spray parameters, including air pressure, traverse speed, standoff distance, and arc current, and the coating properties, such as porosity, hardness, and strength. Bend testing was used to establish the in-plane elastic modulus and strength of the coatings, and adhesion testing was used to determine the out-of-plane (normal) strength. The flexural strength was found to be an order of magnitude greater than the adhesive strength, suggesting orthotropic behavior associated with the lamellar structure of the coatings. The resistance of the coatings to both abrasive and sliding wear was investigated and found to be on the same order of magnitude as cast iron substrate. This report is an initial evaluation of twin wire arc repair of cast iron components damaged by wear or corrosion, with relevance to a wide range of automotive and heavy industrial applications.

Investigation of Mechanical Properties of Twin Wire Arc Repair of Cast Iron Components [4] (Journal of Thermal Spray Technology)

Twin wire arc is a commonly used thermal spray technology for application of steel coatings to cast iron components. Hardness and adhesion strength are critical properties of such coatings, and significant research is available reporting these properties. However, the lamellar structure of the coatings and residual stresses induced during the coating process leads to significantly different behavior in bending

applications than in purely tensile applications which are evaluated by the standard adhesion test. In addition, microstructural features that are controlled by certain process parameters during deposition of the coating can have a significant effect on these properties. This work relates the hardness, adhesion strength, and wear resistance to the coating microstructure, and assesses the related bending strength and failure mode. Comparisons between bend tests and pull-off adhesion tests show significant differences to consider when designing a twin wire arc coating.

8.4 Cold Spray

Adhesion Test Method and Material Properties for High-strength High-pressure Cold Spray Coatings on Hardened 4340 Steel (Cold Spray Action Team Conference)

Evaluation of a modified adhesion strength pull test methodology and apparatus for high-strength high-pressure cold spray (HPCS) coatings. The modified adhesion test is intended for coatings that exceed the 10 ksi limitation of conventional epoxy based adhesion tests. The modified adhesion test is evaluated through both finite element simulation and comparison to ASTM D4541 test results. Cold spray process parameters and adhesion results for HPCS of WIP-C1 coatings onto hardened 4340 steel (HRC>50) using a VRC Gen III system are presented along with other material properties.

9 Appendix C: Supplemental Unpublished Works

This appendix provides information on work performed under the additive repair assessment portion of this project that was not disseminated through publications or conferences. Two additive repair processes, Directed Energy Deposition and Low Pressure Cold Spray, are discussed to relay information this is not currently readily available in open literature.

9.1 Directed Energy Deposition

9.1.1 Abstract

Laser-based Directed Energy Deposition (DED) of metal is an emerging additive manufacturing method with applications across many industries. Cladding of high-alloy stainless and tool steels onto existing parts is a particular area of interest in the remanufacturing of wear surfaces in critical components. As this is a relatively new technology, there are many different applications and materials that have yet to be fully researched and developed into robust processes. The primary focus of this work is on cladding hardened steel substrates with 420 stainless, H13 tool, and M2 tool steels. Process optimization was performed to obtain satisfactory cladding results before creating samples to test abrasion resistance and bending strength. Abrasion results showed the benefits of these clad materials in wear related applications compared to the substrate material. Similarly, bend test results showed that comparable material properties were achieved in surface clad parts.

Keywords: Laser cladding, direct metal deposition, 420 stainless steel, H13 tool steel, M2 tool steel.

9.1.2 Introduction

Laser-based Additive Manufacturing (AM) processes are known by several different names depending on the company associated with the manufacturing of the system, these terms including: laser engineered net shape (LENS®) from Optomec, laser powder fusion from Huffman Corporation, directed light fabrication from Los Alamos National Laboratories, and direct metal deposition from the University of Michigan[5]. All of these processes follow the same basic principles for powder deposition and laser melt pool creation; however, these different methods cover a wide range of applications from simple crack repairs to complex geometric builds similar to that of a 3D printer. The DED process is a versatile tool in the repair of wear surfaces, where the damaged material can be clad over with harder metals that are more resistant to abrasion. If the damage is significant, some material may need to be ground away prior to cladding. After cladding, parts are machined back to the original specifications and can be put back into use.

The DED process used in this study applied metal powders to substrates by forming a melt pool with a high-power laser then directing powdered metal into the localized molten substrate. The laser head was configured to co-axially distribute the metal powder around the laser spot in order to achieve even distribution into the melt pool. The powder is propelled through this system by argon gas that also acted as a shielding gas for the melt pool as it cooled and solidified, similar to that of a conventional welding process. This DED system was integrated with a computer-numeric-control (CNC) machining system to precisely control the laser path, allowing complex build geometries through importation of computer-aided design (CAD) files and g-code programming.

The goal of this work was to apply a DED process in a representative remanufacturing application of industrial components using tool steel materials that have not been studied intensively in academic laboratory settings. Testing was performed to evaluate the material properties created in this cladding process compared to the original substrate material properties. The main testing methods were abrasion wear testing and bend testing. Abrasion testing was done on flat, surface-clad parts, while bend testing was done on both flat-clad and crack fill cladding configurations that are discussed later. Post-clad heat treatment (PCHT) was also experimented with during the bend testing in order to examine the effects of internal stresses on the bending strength of the cladding.

9.1.3 MATERIALS AND METHODS

The DED system used to clad the samples discussed in this work was a modified version of a LENS® Print Engine from Optomec. This system was integrated into a vertical CNC mill, refer to .

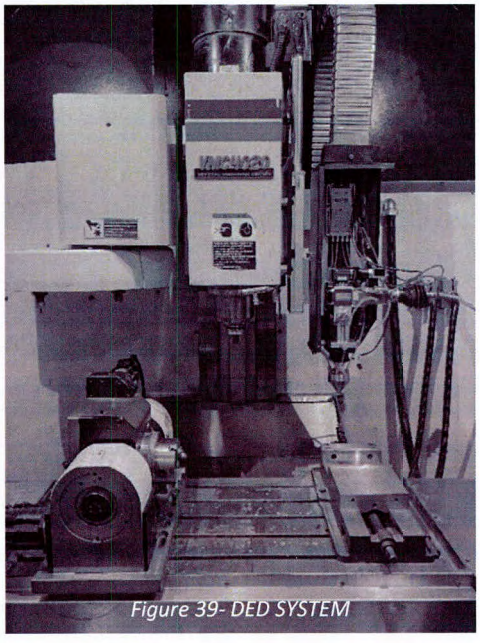

Figure 39- DED SYSTEM

The DED system consisted of a Fraunhofer COAX14 laser head, IPG optics, a 1000W IPG Photonics laser controller (Model YLR-1000-MM-W C-Y11), an Optomec SteadyFlow™ dual powder feeder, and the associated motion control and tool path software. The cladding powder materials evaluated were 420 stainless steel[6], H13 tool steel [7], and M2 tool steel. The 420 stainless steel by Reade Advanced Materials had a powder size distribution of 22-53 µm. The H13 powder and M2 powders were both of size -75+20 µm and supplied by Sandvik Osprey. The base metal for final testing included both 4140 [8] in the annealed condition and a version tempered to ~43 Rockwell C Hardness (245 Vickers). This material was supplied by EMJ Metals in 5 x 1 x 0.25 inch blanks. In order to test a representative crack-fill configuration, a U-shaped groove was milled into a number of the 4140 blanks. Refer to Figure 40 for a model of the blank dimensions and alloy compositions for all materials used.

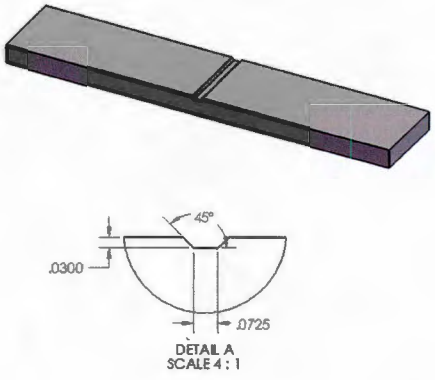

Alloy Specifications, [% comp.]	Fe	C	Cr	Ni	Mo	Si	Mn	W	V	S	P
4140 Base Metal*	Bal	0.38-0.43	0.80-1.1	-	0.15-0.25	0.15-0.30	0.75-1.0	-	-	<=0.040	<=0.035
420 SS Powder*	Bal	>=0.15	12-14	-	-	<=1	<=1	-	-	<=0.030	<=0.040
H13 TS Powder	Bal	0.32-0.45	4.75-5.50	0.3	1.10-1.75	0.80-1.20	0.20-0.50	-	0.8-1.2	-	-
M2 TS Powder	Bal	0.78-1.05	3.75-4.50	0.3	4.5-5.5	0.2-0.45	0.15-0.40	5.5-6.75	1.75-2.20	-	-

*AISI Specifications for these alloys from Matweb.

Figure 40 - ALLOY COMPOSITIONS AND MODEL OF U-GROOVE

DED type systems are capable of cladding many alloys that are normally difficult to work with like titanium (Ti-6Al-4V), other stainless and tool steels (316, 304L, 309, P20, P21, S7, D2) copper and its alloys, and nickel-based alloys (Inconel 600, 625, 690, 719) [9]. The materials for this project were selected in order to best replicate the materials used to make shafts and housings for industrial vehicles and heavy-duty machines. Screening tests were first performed on alloy 420 and H13 in order to narrow down process parameters. Once acceptable results were achieved using H13 powder, the associated powder feeder was switched over to M2. With parameters and information gathered from the 420 and H13 testing, only a small screening test was needed to find acceptable operating parameters for the M2. The initial tests were conducted on low-carbon steel substrates for supply reasons. Later, final testing was conducted on the blank 5 x 1 x 0.25 inch 4140 steel substrates. Based on final project results, there was negligible observed impact of using the inexpensive, readily available material on the cladding process parameter definition during screening tests.

Before cladding was performed, the substrate was sandblasted with an aluminum oxide abrasive to remove any surface contaminants. Then the part was mounted into a fixture and zeroed on the DED machine. A pre-defined cladding tool path program initiated the powder flow several seconds before activating the laser to ensure there was full powder flow when the laser formed the initial melt pool. Cladding experiments were performed in two different configurations to mimic two common applications for this process: surface cladding and crack fill cladding, refer to Figure 41. The parts were air cooled post-cladding.

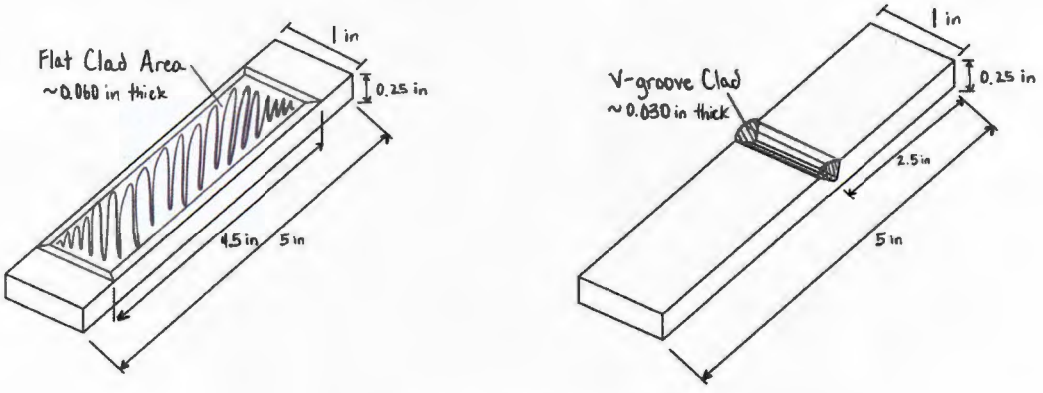

Figure 41 - CLAD BAR AND U-GROOVE FILL

The g-code programming was primarily coded manually to create the toolpaths with better control of bead placement for the complex crack fill geometries to minimize creation of voids between beads. In many of the early tests, beads would not bond properly in the corners and along the edges of the U-groove as shown in Figure 42. This ultimately caused weak cladding and could cause stress concentrations where cracks formed during testing. The solution to this was manually programming the bead positions to get closer to a 50% offset between layers. The original CAM-generated programs opted to space beads evenly across the given width, while manual programming allowed a 0.015 inch step-over constant between each layer. This also allowed beads to be positioned in direct contact to the side surfaces of the U-groove to account for the material that diluted into the sidewall.

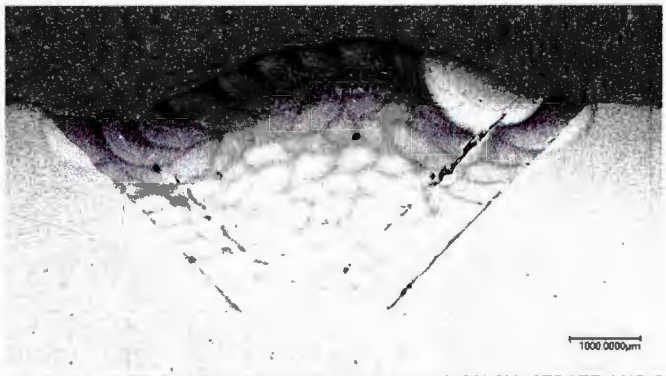

Figure 42 - EARLY U-GROOVE TEST SHOWING LACK OF BONDING ON SUBSTRATE AND BETWEEN LAYERS

9.1.4 Cladding Analysis

In order to analyze the tests and look for porosity in the cladding, each test was individually sectioned and mounted in epoxy mounts in accordance with metallographic sample preparation procedures outlined in ASTM E3 [5]. These mounts were ground and polished where the final finishing was performed with a 3µm diamond abrasive. This level of polishing was sufficient to make large pores, voids, and cracks visible during microscopy. Many of the tests showed these major defects after polishing and did not need any further analysis. Some of the samples were randomly selected to perform hardness maps on using a LECO LM248AT micro indentation hardness tester. Analysis indicated heat was dissipated away from the surface of the material, slightly heat treating the lower layers of cladding as well as the top surface of the base

metal. The hardness points around 300-400 HV in Figure 43 showed an interaction zone where there mixing of the hard 420 stainless steel and the softer 4140 substrate occurred.

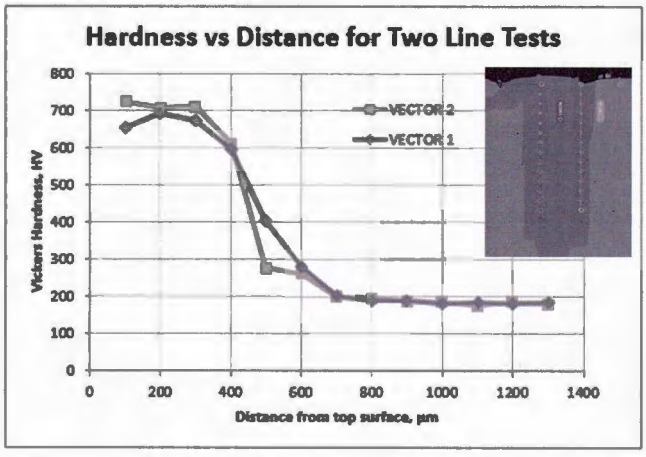

Figure 43 - HARDNESS TEST FROM TOP SURFACE CLAD WITH 420 STAINLESS STEEL INTO 4140 STEEL SUBSTRATE

Chemical etching, per ASTM E407 [10], was applied to aid in interrogation of the clad and substrate materials after hardness testing to not influence the impact results. Two different etchants were used in order to highlight different areas of each part. Both etchants were simply swabbed on for about 10-15 seconds or until etching became visibly dark, before being rinsed in water to stop the etching reaction. The first etchant used was for the base metal was a 10% nital (nitric acid and alcohol) etchant mix. This etchant was used when analyzing the Heat Affected Zone (HAZ) as the etch darkened the harder portions of the base metal thereby contrasting the approximate outline of the HAZ. To examine the clad material structure a Vilella's reagent was used to aid in identifying potential bead geometry positioning issues, refer to Figure 44.

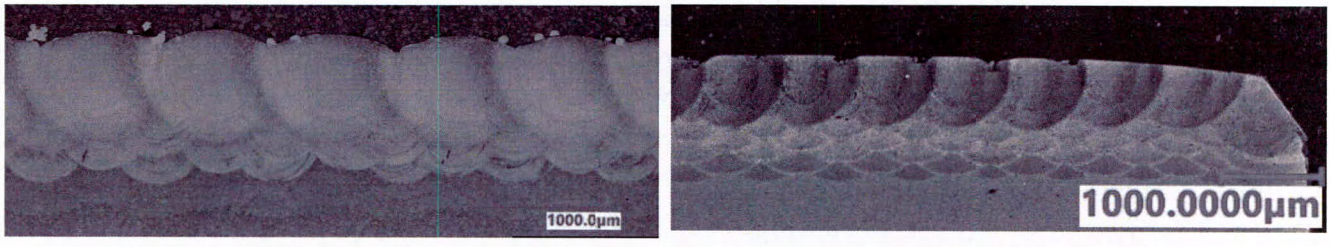

Figure 44 – LEFT: 420 STAINLESS ON 4140 STEEL SAMPLE ETCHED WITH NITAL, HAZ IS DISCOLORED AREA AT BASE OF CLADDING. RIGHT: 420 STAINLESS ON 4140 STEEL SAMPLE ETCHED WITH VILLELA'S REAGENT

A simple design of experiment (DOE) was created with four initial parameters to optimize the clad process for each material. Parameter included as factors in the experiment were: laser power, laser speed, powder feed rate, and nozzle standoff height. The first test was done with only 420 stainless steel and focused on finding the range of parameters that clad smoothly. After this first test, a standoff height of 0.6 inches showed the best results and was fixed for the rest of testing. Argon was supplied at 10 lpm and 40 psi for all testing. After the process parameter studies, further testing was performed to optimize the geometry parameters such as bead step over for multi-bead cladding and layer height for multi-layer cladding. These parameters were also fixed and independent of cladding material. The final process parameters used for each cladding material were defined as shown in Table 16.

Table 16 - TABLE OF CLADDING PARAMETERS FOR EACH CLADDING MATERIAL

Test Parameter	420 SS	H13 TS	M2 TS
Laser Power	400 W	450 W	450 W
Laser Speed	40 ipm	40 ipm	40 ipm
Powder Feed Rate	1.4 g/min	1.15 g/min	1.16 g/min
Horizontal Step	0.030"	0.030"	0.030"
Vertical Step	0.010"	0.010"	0.010"

Following cladding process optimization, abrasive wear testing was performed to evaluate the viability of this process for repairing of wear surfaces. Abrasion testing was conducted by Bud Labs in Rochester, New York in accordance with ASTM G174 Type C [11]. Two clad samples of each material, as well as two blank 4140 bars for a total of 16 samples, were provided for sectioning into 0.25 inch wide test specimens[12]. Test parameters included a 100-gram loading mass, 30-micron aluminum oxide tape, and 75 belt passes. Scar width was measured to quantify the material removal results of abrasion process by employing (Equation 1.

$$V_w = \frac{D^2 t}{8}\left[2sin^{-1}\frac{b}{D} - \sin\left(2sin^{-1}\frac{b}{D}\right)\right] \qquad \text{(Equation 1)}$$

Where V_W = wear volume (mm^3), b = width of the wear scar (mm), and D = diameter of the ring specimen [13].

9.1.4.1 Post-Clad Heat Treat (PCHT) Testing

Heat treating was applied to a portion of the parts after cladding to elucidate the impact on bend test results. The goal of the heat treating procedure was to stress relieve the cladding, releasing residual stresses left from the heat effects of laser cladding. This stress was very apparent in parts directly after cladding, as most of the parts experienced warping. The heat treating process was performed on flat clad samples of both H13 and M2, as well as flat 4140 control bars. These two materials were selected for PCHT evaluation because tool steels are known to have stress and cracking issues, and both alloys required similar temperatures and procedures for stress relieving. The PCHT process brought the specimens up to 600 °C, held there for 2 hours, and then allowed them to furnace cool overnight.

9.1.4.2 Bend Testing

In order to avoid issues with the bend test setup, post-process milling was applied to reduce the severity of warping caused by the cladding process. The parts with the worst warpage were first measured to determine the minimum amount of material removal to return the back surface of each specimen to a flat state. A schematic of this milling procedure is shown in Figure 45. A fixture was used to align each part in the vice, referencing each end of the part to get the warped portion centered. In order to get the parts with the worst warpage flat, 0.025 inches was milled off the back of the part. Then, to keep testing consistent between all parts, the 0.025 inches was milled off of all samples, keeping the nominal thickness of 4140 base material being tested consistent between clad and unclad parts. As-clad parts were also given a quick polish with a flap disc angle grinder. This took off the top rough as-clad layer to create a smooth, low-friction surface for the part to move across the bend testing dies. For post-clad heat treated parts, these steps were performed after the heat treat process. While this process aiding in the test setup there was an unquantified effect on the residual stress in the process.

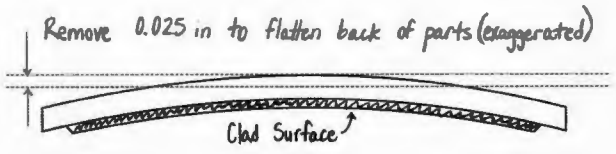

Figure 45- SCHEMATIC OF MILLING PROCEDURE

Three-point bend testing was executed on an Instron 8801 test machine to measure the ultimate strength of each specimen. Data collected included the ultimate load, extension difference at the ultimate load, specimen dimensions, and the Young's Modulus for each sample. This testing followed section 8.3 of ASTM Standard E290-14 for guidance [14]. A schematic of the test setup is provided in Figure 46. The dies used had a radius, r, of inches and center spacing, C, of 3.5 inches.

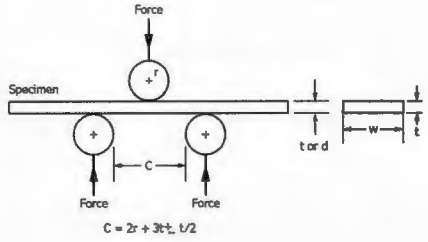

NOTE 1: C=distance between lower supports,
r=radius of the end of the mandrel or plunger,
t=sheet specimen thickness,
d=round specimen diameter, and
w=sheet specimen width.

Figure 46 - SCHEMATIC OF BEND TESTING SETUP (ASTM E290) [14]

After bend testing was completed, the data was analyzed to correct calculations from the Instron. Load vs. displacement data from the Instron was plotted to produce a curve to identify and parse the elastic region of the data set. The slope was then taken from the modified data and used in Equation 2. The measurements used for the width and depth of the part were measured individually for each part.

$$E = \frac{dP}{d\omega_0} * \frac{L^3}{48I}$$

Equation 2

Where: *E* is the Young's Modulus of the material, P is the load, ω_0 is the linear displacement in bending, $\frac{dP}{d\omega_0}$ is the slope of the load vs. displacement curve, *L* is the bottom die separation, and *I* is the second moment of area of the part.

9.1.5 Experimental Results and Analysis

Results from the experiments on M2 and H13 tool steel included wear, bend and hardness testing.

9.1.5.1 *Wear Test Results*

Results from the abrasive wear testing were summarized by the average scar volume for each material, refer to Figure 47. The data on the abrasion-resistance for the three additive materials and 4140 substrate revealed M2 had the smallest wear volume at 0.945 mm^3. The wear volume of the deposited H13 tool steel was the highest compared to the 420 and M2 cladding. The control, 4140 steel, had the highest wear volume at 1.495 mm^3 of all the specimens. These results indicate all of the proposed cladding materials may yield a benefit for remanufactured parts containing wear surfaces that are subject to abrasion.

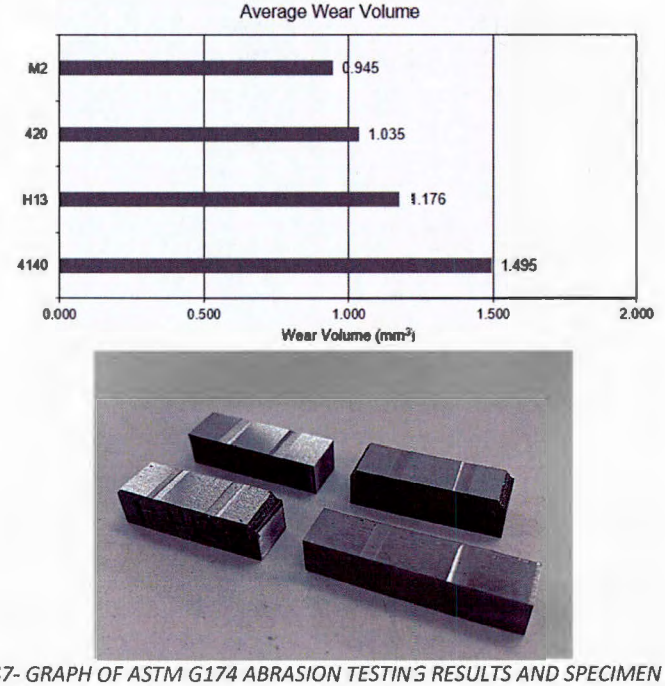

Figure 47- GRAPH OF ASTM G174 ABRASION TESTING RESULTS AND SPECIMEN IMAGES

9.1.5.2 *Bend Testing Results*

Results were obtained for 3-point bend test specimens including: the baseline 4140, H13 clad, and M2 clad specimens in both the as-clad (no heat treatment) and PCHT conditions. The average Young's Moduli were calculated for each test specimen type, refer to Figure 48. In all cases, the post-process heat treating procedure influenced the specimens to bring the measured modulus of elasticity near the value of the original 4140 material due to relieving residual stress. The average ultimate bending strengths calculated for each specimen were summarized in Figure 49. The heat treated 4140 showed a 5% increase in elasticity and a 37% decrease in strength in comparison to the untreated 4140. By contrast, the H13 as-clad samples showed a 15% decrease in elasticity and a 9% decrease in strength compared to the baseline 4140 specimens. The heat treat process brought the measured elasticity of the H13 samples to within 1% of the baseline 4140, but decreased the strength by 32%. The M2 as-clad samples showed a slight 4% increase in elasticity, but had a massive 57% decrease in strength compared to the 4140. This is likely due to the brittleness of the M2 material, causing these parts to fail prematurely with cracking on the clad surface. In contrast, the heat treating had a minimal effect on the M2 with only a 2% increase in elasticity and a 3% decrease in strength over the as-clad M2 samples. These figures show that the cladding process used in conjunction with a post clad heat treatment allowed the material to return to a state of similar

measured elasticity, minimizing the risk of failures due to non-uniform deformation within the elastic deformation region of the material.

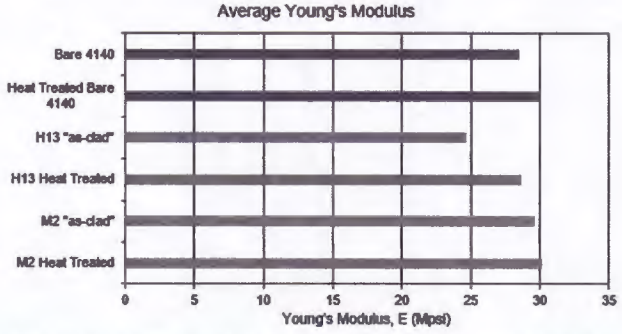

Figure 48 -CALCULATED AVERAGE ELASTIC MODULI FOR EACH SPECIMEN TYPE

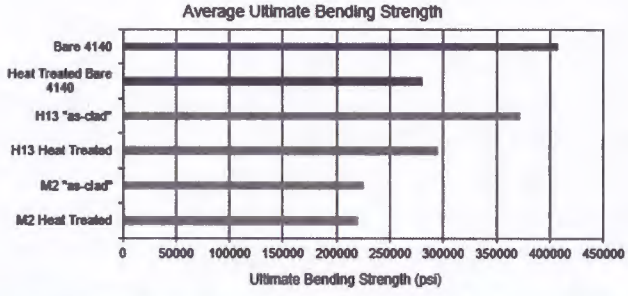

Figure 49 - AVERAGE ULTIMATE BENDNG STRESS FOR EACH SPECIMEN TYPE

Additional bend tests were performed on the U-groove filled specimens; however, the modulus of elasticity results were substantially far from expected values likely due to stress concentrations caused by voids in the fill geometry. Further testing would be needed to truly understand the structural properties of these U-groove repair processes, especially in gap filling applications.

9.1.5.3 Hardness Testing Results

Hardness testing was performed throughout the testing process to ensure the material properties were within expectations. Average hardness for each material were measured with an automated microhardness system, results shown in Table 17. The values were averaged within a single layer of cladding as shown in Figure 50. The HAZ hardness was the average hardness within the transition zone between the clad metal and the 4140 substrate. There was little variation in hardness in the PCHT samples, as the process was only a stress-relieving process, not annealing or hardening the material.

Sample Type	Average Hardness	Average HAZ Hardness
4140	43 HRC	(-)
420 SS	52 HRC	39 HRC
H13 TS	53 HRC	41 HRC
M2 TS	59 HRC	41 HRC

Table 17 - AVERAGE SURFACE HARDNESS FOR EACH MATERIAL AND IN THE HAZ OF EACH CLAD SAMPLE

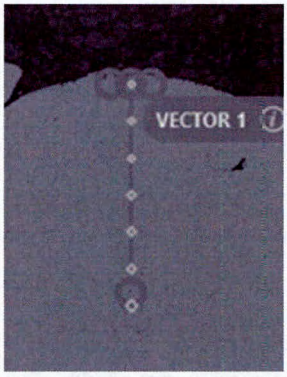

Figure 50 - SINGLE LAYER HARDNESS TEST ON M2 TOOL STEEL SAMPLE

9.1.6 Summary

Two tool steel and one stainless steel surface claddings were applied to 4140 steel using laser directed energy deposition to evaluate the viability of the process for a repair technique of wear surfaces on critical components. The evaluation of the H13, M2, and 420 alloy additive depositions included tests of wear resistance, bending strength, and hardness. Abrasive wear test results showed as-clad M2 tool steel outperformed of materials, followed by 420, H13, and the baseline 4140 substrate. A post-heat treatment was performed to relieve residual stresses induced during the cladding process to understand the effect on strength and modulus. The baseline 4140 steel had the greatest bending strength followed by as-clad H13, stress relieved H13, stress relieved 4140 substrate material, and the M2 tool steel specimens. The measured elastic modulus of the as-clad H13 specimens were 20% lower than the stress relieved specimens due to the residual stresses resulting from the cladding process. Surface harness of M2 reached 59 HRC, while H13 was 53 HRC and 420 was 52 HRC, all of which were greater than the 4140 substrate that measured 43 HRC. In summary, the application of tool steel as an option to repair chromoly steel proved to be feasible with H13 proving higher hardness, greater wear resistance, and a bending strength approaching that of the substrate.

9.2 Investigation of an Alternative Substrate to 5083-H for Low Pressure Cold Spray Experiments

9.2.1 Introduction

5083-H116 is a hardened aluminum alloy used in ballistic armor plating applications[15] and is a prime candidate for repair using portable additive manufacturing processes. Low pressure cold spray (LPCS) presents an opportunity to repair cracked or corroded 5083-H116 components to recover some of the original material properties required for various applications. LPCS is a relatively low cost process that allows greater flexibility than other additive manufacturing processes, including portability, ease of use, and inexpensive equipment investment. In previous work, 5083-H116 proved difficult to procure for lab testing so alternative substrates were investigated under this project to allow for future LPCS material property studies. Alca 5, a widely available cast aluminum plate, possesses a similar chemical composition and corrosion resistance as 5083-H116; therefore, it was evaluated to determine if the cast material behaves similarly to 5083-H116 for LPCS process development. Ultimately, Alca 5 appears to behave generally similarly to 5083-H116 in the cold spray process with adhesion strengths exceeding 10,000psi, but differences in substrate hardness do lead to small differences in mechanical performance.

9.2.2 Materials

5083 is a 5000 series non-heat treatable aluminum-magnesium alloy with high strength and good corrosion resistance. Due to its high strength and resistance to attack by seawater, 5083 is commonly used in ship building and other applications involving seawater exposure. The high strength of 5083 makes it an attractive choice for armor plating of aquatic and amphibious vehicles, which is the application of interest for this study. 5083-H is a strain hardened variant that is commonly available in two tempers: H116 and H131. In contrast, Alca 5 is a widely available cast aluminum-magnesium a loy with a similar chemical composition to 5083-H. Alca 5 is available in the O3 temper and cannot be hardened. The chemical compositions of each alloy are similar, as provided in Table 18.

Table 18. Chemical Composition of 5083 and Alca 5

	Al	Mg	Mn	Cr	Zn	Other (Cu, Fe, Si)
5083[16]	93	5	1	.25	.25	<.5
Alca 5[17]	95	4	.5	.1	Trace	Trace

Based on previous experience with the low pressure cold spray process, a powder mixture of 55% aluminum, 30% aluminum oxide, and 15% zinc was selected for the deposition mater al to evaluate the feasibility of cold spray repair on these materials and to compare the response of the substrates to LPCS. The chemical composition of each material sprayed was measured using energy dispersive X-ray spectroscopy analysis and is given in Table 19. All feedstock materials were nominally sized -32 µm with the aluminum and zinc powders spherical in shape, and the Al_2O_3 irregularly shaped.

Table 19. Cold Spray Feedstock Powder Chemical Composition

	Al	O	Zn	Other
Al	100	-	-	Trace
Al_2O_3	75	25	-	Trace
Zn	-	3	96	Trace

The powder mixture was selected to match previously explored, high quality cold spray coatings. The powder was mixed at 55% Al + 30% Al_2O_3 + 15% Zn by volume, which is equivalent to 40% Al + 31% Al_2O_3 + 29% Zn by mass. The powder size distribution is summarized by *Table 20*.

Table 20. Powder PSD

Percentile [%]	Diameter [μm]
10	9.1
50	17.9
90	34.8

Prior to the cold spray process, all substrates were roughened using a grit blast process. Grit blasting utilized #36 Silicon Carbide grit and 60 psi blasting pressure. This provided a surface roughness of 200 – 250 μin R_a, which past experiments have determined to be beneficial to improving adhesion strength and coating repeatability.

9.2.3 Setup

Deposition was performed with a K-205/407R low pressure cold spray system manufactured by RS Technologies Inc. This system utilizes a DeLaval nozzle geometry (converging-throat-diverging) to accelerate the gas and particles. The accelerating gas temperature, gas pressure, and powder feed rate are controlled by the cold spray system. Compressed air was used as the accelerating gas for all experiments. The LPCS system employs a shock wave formed in the outlet tube to create a low pressure zone at the outlet of the nozzle that draws in the powder. Past experiments with this integrated suction-based powder feed system revealed powder flow rate inconsistencies and difficulty in feeding powders above 110 psi accelerating gas pressure. To solve the powder feeder limitations, an external powder feeder was utilized to maintain a steady powder mass flow rate. A Uniquecoat G5 gravimetric powder feeder (G5 feeder) with a single 1.9L hopper was used for these experiments. The G5 feeder utilizes a pressurized hopper and a metering blade to feed powders into the LPCS stream at a constant rate. A custom weighted metering blade was fabricated to prevent the blade from lifting during operation with this powder blend that previously caused interference with the housing.

9.2.4 Test Methods:

Prior to any cold spray processing, the substrates were tested for micro and macro indentation hardness. As Alca 5 is not hardened and 5083-H is strain hardened, it was expected that the 5083-H would display significantly harder behavior than the Alca 5. Vickers micro-indentation hardness, Rockwell B, and Brinell hardness readings were all recorded. Vickers micro-indentation hardness was tested using a LECO automatic indenter. The reported Vickers measurements are an average of 18 indentations. Rockwell hardness was tested using a Struers manual indenter with a Rockwell B tip under a 100 kgf load. Reported Rockwell measurements are an average of eight measurements. Brinell testing was performed on a Detroit Testing HRB 3000A test apparatus and each sample was only tested once due to the destructive nature of the test. An Olympus IX50 microscope was used to evaluate coating microstructure.

The LPCS process used an ABB IRB1600 robot to apply the coatings. For all samples, the robot was programmed to maintain a constant stand-off distance of 15 mm and a constant traverse speed of 10 mm/s. The accelerating gas pressure was varied from 75 to 100 psi. Accelerating gas temperature was not controlled directly, instead it is set by using a dial increment, 1 through 5, with each setting correlating to an approximate 120°C increase in temperature, e.g. heat setting 1 = 120°C, heat setting 2 = 240°C etc.

The accelerating gas temperature also impacts the static gas pressure. To monitor the static pressure changes due to accelerating gas temperature changes, a pressure gage and Type K thermocouple apparatus was designed, built, and integrated with the cold spray system gun adjacent to the converging section of the DeLaval nozzle. The static pressure and temperature were measured using this apparatus for all experiments after a warm-up period of one minute. The accelerating gas was compressed air and powder flow was maintained at a constant 6 g/min for all experiments.

ASTM standard D4541 was followed as a guideline when measuring the adhesion of the coatings. FM1000 epoxy was used to adhere the dollies to the coating. A Defelsko PosiTest AT-M adhesion tester was applied to exert and measure the load to failure. When using standard 10 mm dollies the maximum applied stress was 10,000 psi; however, the cold spray coatings were expected to have strength >10,000 psi, so the dollies were modified to 8 mm diameter in order to apply a greater stress.

Deposition efficiency (D.E.) was measured by recording the mass of powder in the powder feeder and the substrate mass before and after each run of the experiment. The D.E. was calculated using:

$$D.E. = \frac{\Delta Sample\ Mass}{\Delta Powder\ Mass}$$

9.2.5 Results

9.2.5.1 Base material hardness evaluation

Prior to any analysis of cold spray deposits, the substrate materials were compared on the basis of hardness. Nominal Brinell hardness values for Alca 5 and the two most common tempers of 5083-H are shown in Table 21. Based upon the material distributor's recommendation, Vickers micro-indentation hardness and Brinell hardness testing were performed to determine the tempers as Rockwell B testing is improper for this material.

Table 21: Alca 5, 5083H-116, and 5083H-131 hardness specification from manufacturer data sheets. Rockwell B values are converted to approximate Brinell values using ASTM E140

Material	Brinell Hardness Spec
Alca 5 [17]	70
5083-H116 [16]	85
5083-H131	110

Micro-indentation hardness mapping of two thickness of ALCA 5, 0.250 inch and 1.500 inch, produced nearly identical results, with an average Vickers hardness of 82 for all samples. Brinell testing produced an average of 69 HB, which matched the manufacturer specification of 70 HB for Alca 5.

Table 22. Alca 5 Hardness Comparison

Alca 5 Substrate Thickness (in)	Average Vickers Hardness	Average Brinell Hardness
0.250	82	69
1.500	82	74

This additional hardness testing led to the conclusion that the hardness of the Alca 5 material did not have a dependency on the thickness of the samples, and confirmed the material distributor information that the Rockwell B test was improper for this material. Ultimately, it was concluded that the Alca 5 hardness was as expected. A commercially available 5083-H116 was procured from MTS LLC for testing. This material behaved as expected in Brinell and Vickers testing.

Table 23. Comparison of Measured Hardness for each material

Substrate	Brinell Hardness (HB)	Vickers Hardness (HV 0.2)
Alca 5 (purchased)	69	82
5083-H116 (purchased from MTS)	89	95

9.2.5.2 Evaluation of the impact of base material type on cold spray coatings performance

A 2^3 full factorial experimental design was devised to understand whether cold spray coatings deposited on Alca 5 or 5083-H116 displayed similar mechanical performance through a range of coating conditions. The accelerating gas pressure was varied between 75 and 100 psi while the heater was varied between setting 2 and 3. Each combination of process settings was used with each of the two substrate materials to create eight specimens. A single 28 mm x 28 mm deposit was applied for each specimen, which allowed for two adhesion specimens and hardness measurements. The number of spray layers was varied in order

to achieve a coating thickness of approximately 0.050 inch. The experimental design s shown in Table 24.

Table 24. Cold spray processing parameters utilizing a 2^3 full factorial design

Specimen #	Substrate Material	Accelerating Gas Pressure [psi]	Heater Setting	Number of Layers
1	Alca 5	100	3	6
2	5083-H116	75	2	6
3	Alca 5	100	2	6
4	5083-H116	100	2	6
5	Alca 5	75	2	8
6	Alca 5	75	3	8
7	5083-H116	75	3	8
8	5083-H116	100	3	6

The process and substrate surface conditions after grit blast were monitored for each specimen and were recorded in *Table 25*, see below:

Table 25. Conditions measured during coating process

Trial #	Gas Temperature [°C]	Air flow rate [g/s]	Surface roughness (before coat ng) [µin]
1	382	7.66	281
2	290	6.55	282
3	290	7.93	289
4	290	7.75	272
5	289	6.00	288
6	380	5.79	254
7	380	5.78	284
8	381	7.47	302

Deposition efficiency was calculated for each deposit and is shown in Figure 51. The deposition efficiency for each parameter set is slightly higher with Alca 5 substrates than with 5083-H116. In every parameter set, the deposition efficiency was measured to be 0.5 percentage points higher when using Alca 5. Additionally, it is noted that the deposition efficiencies increase with both increasing heat and increasing accelerating pressure. This is consistent with past observations and literature that deposition efficiency generally increases with particle velocity, which is governed by both pressure and heat. It should be noted

that increasing particle velocity will only increase deposition efficiency up to a point, beyond that limit the deposition efficiency will begin to decrease due to erosion.

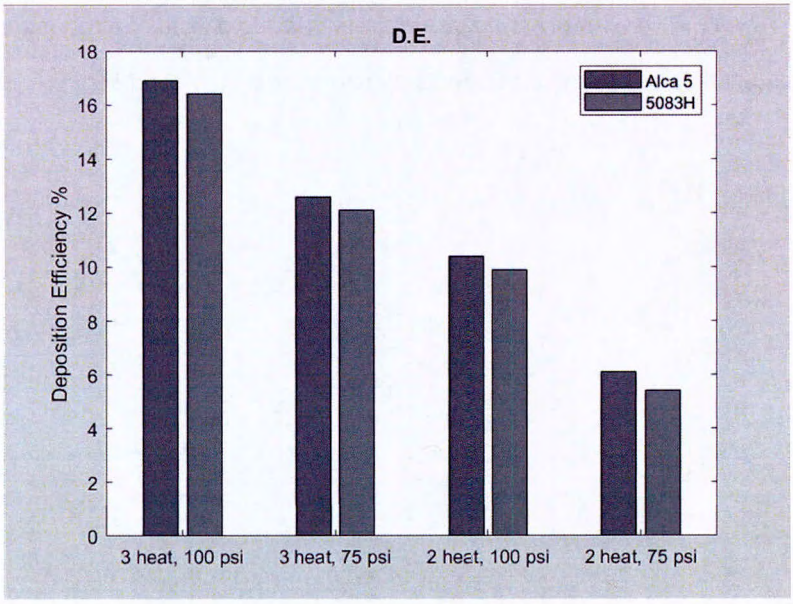

Figure 51. Deposition Efficiency Comparison (all values ±.2%)

Each deposit's adhesion strength was measured twice. The rated breaking strength of the FM1000 adhesive was 10,000 psi and failures were occurring in some cases below 5,000 psi. Figure 52 shows the results from the samples with new adhesive. Even with properly functioning adhesive, most of the failures were epoxy failures, indicating that the true adhesion strength of the deposits was greater than the reported values. No direct conclusions can be drawn regarding similarities or differences between the two substrates from this data. What can be determined is that cold spray produces coatings with high adhesion strength on both substrates.

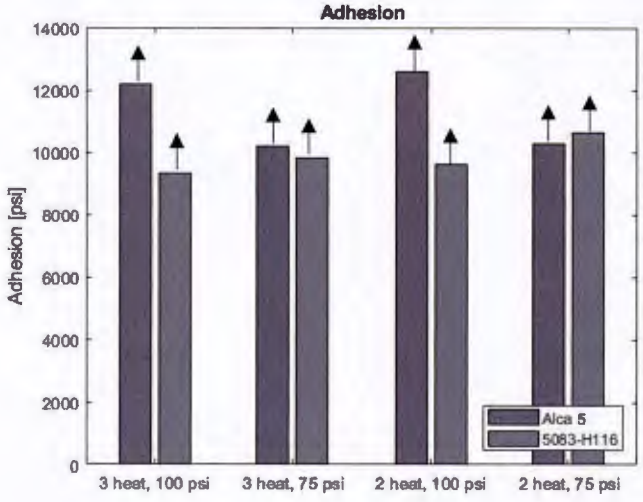

Figure 52. Adhesion Test Results comparing Alca 5 and 5083-H116 at varying spray conditions. Epoxy failures for each indicate true strength exceeds reported values

A comparison of the micro hardness of each LPCS deposit is shown in Figure 53. Each deposit was tested near the substrate/coating interface, in the middle of the coating, and near the surface. These localized values were both analyzed independently and were averaged to determine a mean micro hardness for each deposit. There are no discernable differences between deposits on the Alca 5 and on the 5083-H116. Further scrutiny of the localized values shows that the deposit was generally harder closer to the interface than at the surface.

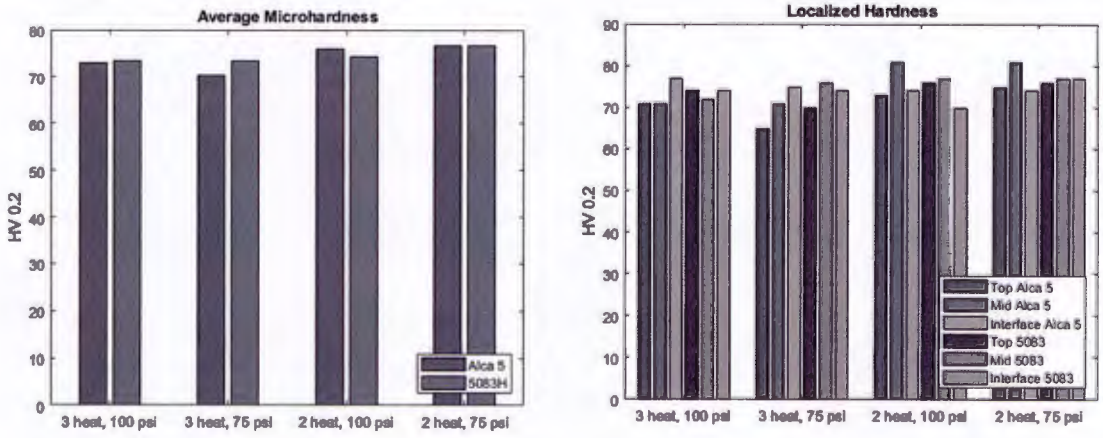

Figure 53. Micro-indentation hardness results of the coating

9.2.6 Conclusion

Based on a review of the properties of the cold spray deposits, it was concluded that the two substrate materials imparted an insignificant difference on the performance of the cold spray process. While there was a significant difference in the hardness of the base metals, results indicate the difference had minimal

impact on the cold spray process. The deposition efficiency of deposits on Alca 5 were approximately 0.5 percentage points higher than for 5083-H116; however, an uncertainty analysis of the deposition efficiency calculation reveals that deposition efficiency measurements have a systematic uncertainty of ±0.2 percentage points. Further testing with more data points would be needed to understand the random uncertainty of deposition efficiency. Adhesion testing showed that low pressure cold spray was able to deposit coatings with adhesion strength in excess of 10,000 psi for both substrate materials, but limitations of the test method prevented absolute comparisons between the substrates. Hardness values of approximately 75HV were measured for the coatings of both substrates. Ultimately, Alca 5 appears to behave similarly to 5083-H116 in the cold spray process, but differences in substrate hardness lead to small differences in mechanical performance.

10 Appendix D: References

[1] L. P. Martin, A. Luccitti, and M. Walluk, "Evaluation of Additive Friction Stir Deposition for the Repair of Cast Al-1.4Si-1.1Cu-1.5Mg-2.1Zn," *J. Manuf. Sci. Eng. Trans. ASME*, vol. 144, no. 6, Jun. 2022, doi: 10.1115/1.4052759/1121897.

[2] L. P. Martin, A. Luccitti, and M. Walluk, "Repair of aluminum 6061 plate by additive friction stir deposition," *Int. J. Adv. Manuf. Technol.*, vol. 118, no. 3–4, pp. 759–773, Jan. 2022, doi: 10.1007/S00170-021-07953-Z/FIGURES/14.

[3] L. P. Martin, A. Luccitti, and M. Walluk, "Evaluation of additive friction stir deposition of AISI 316L for repairing surface material loss in AISI 4340," *Int. J. Adv. Manuf. Technol.*, vol 121, no. 3–4, pp. 2365–2381, Jul. 2022, doi: 10.1007/S00170-022-09507-3/TABLES/8.

[4] K. DePalma, M. Walluk, L. P. Martin, and K. Sisak, "Investigation of Mechanical Properties of Twin Wire Arc Repair of Cast Iron Components," *J. Therm. Spray Technol.*, vol. 31, no. 1–2, pp. 315–328, Jan. 2022, doi: 10.1007/S11666-021-01304-W/FIGURES/17.

[5] "Optomec LENS® Print Engine." https://staging25.optomec.com/3d-printed-metals/LENS®-printers/hybrid-cnc-machine-tool-and-3d-printer/.

[6] "AK Steel 420 Martensitic Stainless steel." https://www.matweb.com/search/DataSheet.aspx?MatGUID=4c543f6cc59b48859eac0ff7f2302b9a (accessed Oct. 25, 2022).

[7] J. Brooks, C. Robino, T. Headley, S. Goods, and M. Griffith, "Microstructure and Property Optimization of LENS Deposited H13 Tool Steel," 1999, doi: 10.26153/TSW/830.

[8] "AISI 4140 Steel, normalized at 870°C (1600°F), air cooled, 13 mm (0.5 in.) round." https://www.matweb.com/search/datasheet.aspx?matguid=42f0179c4d5d4d43b20feb5ad9370f08&ckck=1 (accessed Oct. 25, 2022).

[9] S. Kumar, A. K. S. Choudhary, A. Kishore, S. Amit, K. Gupta, and U. G. Student, "A Comparison of Additive Manufacturing Technologies," *IJIRST-International J. Innov. Res. Sci. Technol.*, vol. 3, 2016, Accessed: Oct. 25, 2022. [Online]. Available: www.ijirst.org.

[10] "Standard Practice for Microetching Metals and Alloys." https://www.astm.org/e0407-07r15e01.html (accessed Oct. 25, 2022).

[11] "Standard Test Method for Measuring Abrasion Resistance of Materials by Abrasive Loop Contact." https://www.astm.org/g0174-04r17.html (accessed Oct. 25, 2022).

[12] "ASTM E3-11 Standard Guide for Preparation of Metallographic Specimens," ASTM Interational, West Conshohocken, PA, 2011.

[13] P. J. Blau, "For the ASTM Journal af Testing a d Evaluation and to be presented at thc ASTM Symposium on Precision WwrMeasuremenxr andMonitoring Needs and Challenges in Precision Wear Measurement," 1996.

[14] "Standard Test Methods for Bend Testing of Material for Ductility." https://www.astm.org/e0290-14.html (accessed Oct. 25, 2022).

[15] A. V. Jebaraj, K. V. V. Aditya, T. S. Kumar, L. Ajaykumar, and C. R. Deepak, "Mechanical and corrosion behaviour of aluminum alloy 5083 and its weldment for marine applications," *Mater.*

Today Proc., vol. 22, pp. 1470–1478, Jan. 2020, doi: 10.1016/J.MATPR.2020.01.505.

[16] "Aluminium 5083: Properties, Fabrication and Applications." https://www.azom.com/article.aspx?ArticleID=2804 (accessed Oct. 25, 2022).

[17] "Discover our product ALCA5 (AA5083) - PCP Aluminium." https://pcpaluminium.com/alca5/ (accessed Oct. 25, 2022).

REPORT DOCUMENTATION PAGE

1. REPORT DATE	2. REPORT TYPE	3. DATES COVERED	
		START DATE	END DATE
20221028	Final	20180701	20220630

4. TITLE AND SUBTITLE

Impacts of Technology Advancements on CBM+

5a. CONTRACT NUMBER	5b. GRANT NUMBER	5c. PROGRAM ELEMENT NUMBER
	N00014-18-1-2339	
5d. PROJECT NUMBER	**5e. TASK NUMBER**	**5f. WORK UNIT NUMBER**

6. AUTHOR(S)

Thurston, Michael, G; McConky, Sean, P; Walluk, Mark, R; Nenadic, Nenad, G; Hurley, Gerald, M; DePalma, Kyle, P; Sullivan, Matthew, R; Amerine, W. Evan;

7. PERFORMING ORGANIZATION NAME(S) AND ADDRESS(ES)

ROCHESTER INSTITUTE OF TECHNOLOGY
1 LOMB MEMORIAL DRIVE
ROCHESTER, NY 14623-5603

8. PERFORMING ORGANIZATION REPORT NUMBER

9. SPONSORING/MONITORING AGENCY NAME(S) AND ADDRESS(ES)	10. SPONSOR/MONITOR'S ACRONYM(S)	11. SPONSOR/MONITOR'S REPORT NUMBER(S)
Office of Naval Research 875 North Randolph Street Arlington, VA 22203-1995	ONR	

12. DISTRIBUTION/AVAILABILITY STATEMENT

Approved for Public Release; Distribution is Unlimited.

13. SUPPLEMENTARY NOTES

14. ABSTRACT

This project consisted of three sub-projects related to CBM+ and maintenance strategies, particularly Vehicle CBM Research, Gear Prognostics Research, and Additive Manufacturing Research. The Vehicle CBM research evaluated low cost acoustic and vibration sensing technologies, as well as mobile GPUs for edge processing of high speed waveform data. The gear prognostics research focused on the fusion of vibration and oil quality monitoring data to enhance the detection horizon of existing gear prognostics. The additive manufacturing research focused on closing the knowledge gaps relating to additive repair material properties and advancing the state of technology to facilitate the adoption of additive manufacturing repair processes.

15. SUBJECT TERMS

Condition Based Maintenance, low cost vibration sensors, vibration processing at the edge, mobile GPUs, prognostics, diesel fuel injector fault detection, gear vibration, oil quality monitoring, gear crack propagation, neural networks, machine learning, feature fusion, additive manufacturing, additive repair, friction stir, Laser Engineered Net Shaping, lased cladding, twin wire arc, cold spray

16. SECURITY CLASSIFICATION OF:			17. LIMITATION OF ABSTRACT	18. NUMBER OF PAGES
a. REPORT	b. ABSTRACT	C. THIS PAGE		
U	U	U	UU	150